2012

Complex-valued Adaptive Digital Signal Enhancement For Applications In Wireless Communication Systems

Ying Liu
University of Central Florida

COMPLEX-VALUED ADAPTIVE DIGITAL SIGNAL ENHANCEMENT FOR APPLICATIONS IN WIRELESS COMMUNICATION SYSTEMS

by

YING LIU
B.S. Huazhong University of Science and Technology, China, 2007
M.S. University of Central Florida, 2011

A dissertation submitted in partial fulfillment of the requirements
for the degree of Doctor of Philosophy
in the Department of Electrical Engineering and Computer Science
in the College of Engineering and Computer Science
at the University of Central Florida
Orlando, Florida

Fall Term
2012

Major Professor: Wasfy B. Mikhael

ABSTRACT

In recent decades, the wireless communication industry has attracted a great deal of research efforts to satisfy rigorous performance requirements and preserve high spectral efficiency. Along with this trend, I/Q modulation is frequently applied in modern wireless communications to develop high performance and high data rate systems. This has necessitated the need for applying efficient complex-valued signal processing techniques to highly-integrated, multi-standard receiver devices.

In this dissertation, novel techniques for complex-valued digital signal enhancement are presented and analyzed for various applications in wireless communications.

The first technique is a unified block processing approach to generate the complex-valued conjugate gradient Least Mean Square (LMS) techniques with optimal adaptations. The proposed algorithms exploit the concept of the complex conjugate gradients to find the orthogonal directions for updating the adaptive filter coefficients at each iteration. Along each orthogonal direction, the presented algorithms employ the complex Taylor series expansion to calculate time-varying convergence factors tailored for the adaptive filter coefficients. The performance of the developed technique is tested in the applications of channel estimation, channel equalization, and adaptive array beamforming. Comparing with the state of the art methods, the proposed techniques demonstrate improved performance and exhibit desirable characteristics for practical use.

The second complex-valued signal processing technique is a novel Optimal Block Adaptive algorithm based on Circularity, OBA-C. The proposed OBA-C method compensates for a complex imbalanced signal by restoring its circularity. In addition, by utilizing the complex

Taylor series expansion, the OBA-C method optimally updates the adaptive filter coefficients at each iteration. This algorithm can be applied to mitigate the frequency-dependent I/Q mismatch effects in analog front-end. Simulation results indicate that comparing with the existing methods, OBA-C exhibits superior convergence speed while maintaining excellent accuracy.

The third technique is regarding interference rejection in communication systems. The research on both LMS and Independent Component Analysis (ICA) based techniques continues to receive significant attention in the area of interference cancellation. The performance of the LMS and ICA based approaches is studied for signals with different probabilistic distributions. Our research indicates that the ICA-based approach works better for super-Gaussian signals, while the LMS-based method is preferable for sub-Gaussian signals. Therefore, an appropriate choice of interference suppression algorithms can be made to satisfy the ever-increasing demand for better performance in modern receiver design.

This work is dedicated to my parents, far away in China.

ACKNOWLEDGMENTS

Firstly, I would like to express my sincere respect and gratitude to my dissertation advisor, Dr. Wasfy B. Mikhael, for his many suggestions and constant support during this research. His great wisdom and timely encouragement helped me overcome various obstacles, both academically and personally.

I am thankful to Dr. Matthew T. Hunter and Dr. Thomas T. Yang for their continuous help. I would also like to express my appreciation to Dr. Raghuram Ranganathan for his valuable comments and guidance through the early years of chaos and confusion.

I should give thanks to the members of my dissertation committee as well.

In addition, I would like to thank Astronics DME Corporation and ZTEC Instruments for supporting this work.

I am indebted to my wonderful parents for their patience and unconditional love. Without them, this work would never have come into existence.

TABLE OF CONTENTS

LIST OF FIGURES

LIST OF TABLES

LIST OF ACRONYMS/ABBREVIATIONS

ACI	Adjacent Channel Interference
ADC	Analog to Digital Converter
AM	Amplitude Modulation
AOA	Angle Of Arrival
BLMS	Block Least Mean Square
BPSK	Binary Phase Shift Keying
BSS	Blind Source Separation
CBC-LMS	Complex Block Conjugate based Least Mean Square
CBCI-LMS	Complex Block Conjugate based Least Mean Square with Individual adaptation
CCI	Co-Channel Interference
CG	Conjugate Gradient
CMA	Constant Modulus Algorithm
DAC	Digital to Analog Converter
DSP	Digital Signal Processor
DTFT	Discrete-Time Fourier Transform
FIR	Finite Impose Response
FE	Front-End
FM	Frequency Modulation
FT	Fourier Transform
HA	Homogeneous Adaptive

IA	Individual Adaptive
I/Q	In-phase/Quadrature-phase
ICA	Independent Component Analysis
IF	Intermediate Frequency
IRR	Image Rejection Ratio
LMS	Least Mean Square
LO	Local Oscillator
LPF	Low Pass Filter
ML	Maximum Likelihood
MPI	Multiplications Per Iteration
MSE	Mean Square Error
NEE	Normalized Error Energy
NLMS	Normalized Least Mean Square
OFDM	Orthogonal Frequency Division Multiplexing
OBA-C	Optimal Block Adaptive algorithm based on Circularity
OBA	Optimal Block Adaptive method
OBAI	Optimal Block Adaptive method with Individual adaptation
pdf	probability density function
PAM	Pulse Amplitude Modulation
PLL	Phase Locked Loop
PSK	Phase Shift Keying
QAM	Quadrature Amplitude Modulation

QoS	Quality of Service
QPSK	Quadrature Phase Shifting Keying
RF	Radio Frequency
SDR	Software Defined Radio
SER	Symbol Error Rate
SIR	Signal to Interference Ratio
SNR	Signal to Noise Ratio
WLAN	Wireless Local Area Network

CHAPTER 1 INTRODUCTION

Since the end of the 20th century, wireless communication has become one of the most successful and profitable market in industry. Even during the late-2000s recession, the number of the wireless subscribers still grew steadily both within U.S. and worldwide. The International Telecommunication Union[1] reported that at the end of 2011, there were 6.0 billion mobile subscriptions [1], which is equivalent to 86.7 percent of the world population. That is a huge increase from 5.4 billion in 2010 and 4.7 billion mobile subscriptions in 2009. Table 1 shows more detailed statistics [1] from World Telecommunication Service at the end of 2011.

The Portio Mobile Factbook 2012 [2] predicts that the number of worldwide mobile subscribers will reach 6.5 billion by the end of 2012, 6.9 billion by the end of 2013 and 8 billion by the end of 2016. This recent forecast indicates that there is still a steady growth during 2012 to 2016 in the global wireless communication market, driven mainly by emerging market growth and a shift toward the next generation of mobile networks. This shift will offer consumers not only higher data rates and more efficient systems, but also broadband Internet access to support innovative multimedia services and applications.

[1] The International Telecommunication Union (Union internationale des télécommunications, in French), previously the International Telegraph Union, is the specialized agency of the United Nations which is responsible for information and communication technologies. ITU coordinates the shared global use of the radio spectrum, promotes international cooperation in assigning satellite orbits, works to improve telecommunication infrastructure in the developing world and establishes worldwide standards.

Table 1 Global Telecom Indicators for the World Telecommunication Service in 2011

	Global	Developed nations	Developing nations	Asia & Pacific	Europe	The Americas
Mobile cellular subscriptions (millions)	5,981	1,461	4,520	2,897	741	969
Per 100 people	86.7%	117.8%	78.8%	73.9%	119.5%	103.3%
Fixed telephone lines (millions)	1,159	494	665	511	242	268
Per 100 people	16.6%	39.8%	11.6%	13.0%	39.1%	28.5%
Active mobile broadband subscriptions (millions)	1,186	701	484	421	336	286
Per 100 people	17.0%	56.5%	8.5%	10.7%	54.1%	30.5%
Fixed broadband subscriptions (millions)	591	319	272	243	160	145
per 100 people	8.5%	25.7%	4.8%	6.2%	25.8%	15.5%

In order to keep up with this rapid growth of the wireless communication market, the design of wireless systems satisfying rigorous constraints and diversified specifications is becoming increasingly important. The past decade has seen a surge of research activities in this area. Research efforts concentrate on schemes that are capable of increasing the system capacity, providing reconfigurability/reprogrammability, and reducing the hardware complexity [3]–[6].

By the strong push towards flexible and software-configurable receiver structures, high-performance signal processing techniques in the digital domain are highly desirable. As a result, it can reduce the size of the implementation and the cost of the Front-End (FE). As the computational power of Digital Signal Processor (DSP) is increasing rapidly, implementing radio

functionalities digitally is becoming more feasible, leading to the long-term transceiver design objective-*Software Defined Radio* (SDR).

This chapter is organized as follows. 1.1 introduces different applications of complex signal processing in wireless communications. The concept of SDR is briefly reviewed in 1.2. Two challenges in wireless communications, channel fading and interference suppression are described in 1.3 and 1.4, respectively. 1.5 illustrates the motivation and scope of this dissertation, followed by the mathematical notation and preliminaries in 1.6. The organization of the dissertation is given in 1.7.

1.1 Applications of Complex Signal Processing in Wireless Communications

Low cost, low power dissipation and small size are important implementation requirements for wireless receiver design. The flexibility to support different types of waveforms and various air interface technologies of existing and emerging wireless systems is another important receiver design objective. The requirements for implementation on one side and the demand for flexibility on the other side often pose significant challenges. In this regard, the quadrature concept is frequently adopted due to its potential to support the development of new systems which can achieve these design objectives [7]–[8]. The understanding of the quadrature concept is often simplified by considering both the signal and the system transfer function as ‘complex’ quantities.

A complex signal is the combination of two real-valued independent components, the real/In-phase (I) and the imaginary/Quadrature-phase (Q) components. A complex system employs two independent channels to generate the I and Q components of the signal. Many high-

bit-rate modulation schemes are based on complex signal concepts, such as Phase Shift Keying (PSK), Quadrature Amplitude Modulation (QAM), Orthogonal Frequency Division Multiplexing (OFDM), [9], [10].

The application of complex signal processing in wireless systems has blossomed in the past decade [11]–[23]. This is especially true for high-bit-rate standards, such as Wireless Local Area Network (WLAN) [11], and for highly-integrated multi-standard transceivers [12]–[13]. Employing complex signal processing in wireless communications can limit the use of narrow-band fixed-coefficient filters at high frequencies (including Radio Frequency or RF, and high Intermediate Frequency or IF). This advantage leads to the development of new systems with highly integrated receivers using less power and requiring less physical space.

1.1.1 Complex Filters

Among various wireless applications of complex signal processing, complex filters are important and ubiquitous in modern wireless receiver design [14]–[17]. From an implementation point of view, cross-coupling between the real and imaginary signal paths is utilized to realize asymmetrical filters, which implies that the filter has complex coefficients. The realization of complex filters includes the basic operations of addition, multiplication, and the delay operator for digital filters or the integrator operator for analog filters.

Traditionally, complex analog filters are used to perform complex signal processing in wireless transceivers [18]–[21]. However, the non-ideality of analog components causes all kinds of distortions, e.g., unexpected image signal aliasing into the desired signal band [22], [23]. Furthermore, analog filters do not permit a high degree of integration, which is crucial for the

development of modern wireless systems. In this regard, complex-valued filters implemented digitally have been developed and become essential in the design of highly-integrated multi-standard wireless receivers.

1.1.2 Low-IF and Zero-IF Quadrature Receivers

In wireless receiver design, increased integration level with fewer external components is the trend to reduce product cost. This demand has led to the popularity of low-IF and zero-IF receiver structures.

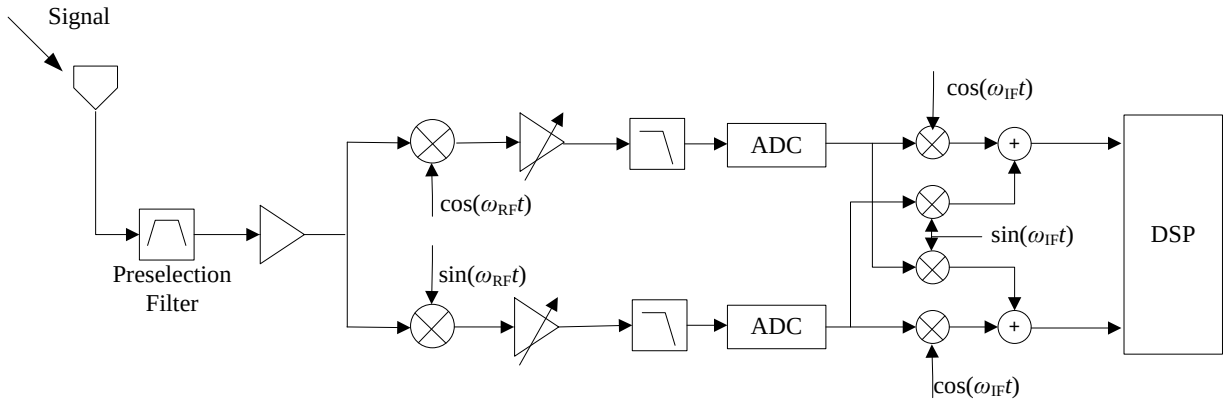

Figure 1 Low-IF Receiver Architecture

Low-IF architecture, shown in Fig. 1, is currently a popular architecture for designing highly-integrated wide-band wireless receivers [24], [25]. In a low-IF receiver, the RF signal is demodulated in two stages. The first stage employs two analog multipliers to translate the RF input signal down to a low-IF frequency. The second stage shifts the IF signal to baseband complex signal using four real-valued multipliers. Both stages can be implemented by analog components before the analog to digital conversion [26]. Alternatively, the analog to digital conversion can be done at the IF stage as shown in Fig. 1, and then the second frequency shift

can be realized in the digital domain. This digital demodulation alternative is always preferred for two reasons. First, this scheme implements the second complex modulation in the digital domain, and thus the imperfection can be minimized. Second, if the analog to digital sampling frequency is chosen properly, the second mix can be significantly simplified.

Low-IF architecture is especially suitable for multi-standard receivers when the channel-selection filter is realized using digital circuits after the Analog to Digital Converter (ADC). In this way, programmable digital devices can be applied to accommodate the requirements of different standards, so as to avoid rebuilding the analog circuits. The major drawback of low-IF architectures is image interference, but it can be significantly minimized by using digital filters, which will be mainly discussed in Chapter 6.

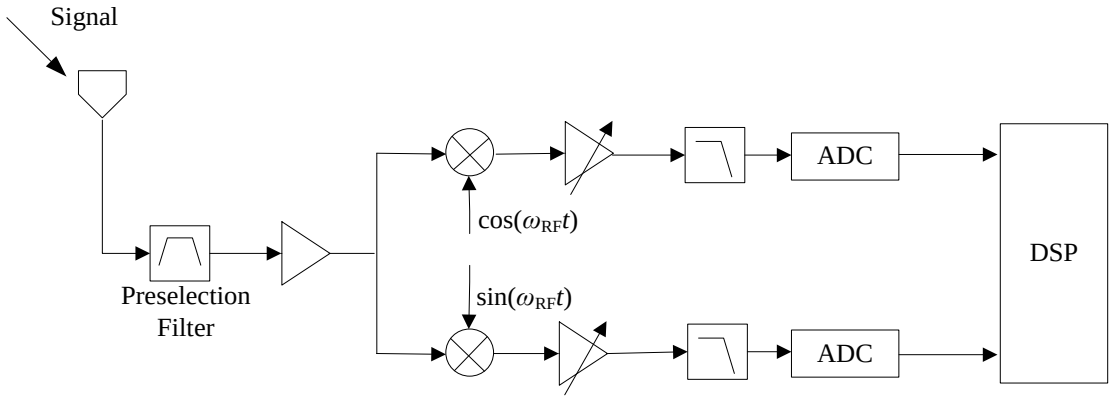

Figure 2 Zero-IF Receiver Architecture

A zero-IF receiver [27], [28], shown in Fig. 2, is also known as direct-conversion receiver. As explained by its name, this architecture demodulates the incoming RF signal to a baseband signal using a Local Oscillator (LO) whose frequency is identical or very close to the signal's carrier frequency. This is in contrast to the standard low-IF receiver, in which this step is accomplished after an initial conversion to an IF signal.

The simplification of performing a single frequency conversion reduces the circuit complexity. However, other issues arise. For example, in the original form, a zero-IF receiver is incapable to receive Amplitude Modulation (AM) and Frequency Modulation (FM) signals without implementing an elaborate Phase Locked Loop (PLL). Although there are technical challenges in the implementations of the zero-IF receiver, today's advanced technology, SDR in particular, has revived the use of zero-IF receivers in various areas, including consumer electronic products.

1.1.3 Beamforming

In recent years, antenna array becomes a key component in various wireless applications, such as radar, sonar and cellular mobile communications [29]. It increases the detection range of radar and sonar systems, and improves the capacity of mobile communication systems. Modern antenna technology in conjunction with beamforming offers a promising solution to reduce interference levels and improve the system capacity. This is achieved by maximizing the signal reception from the desired direction, and suppressing the reception from other directions. Conventional beamformer uses a fixed set of weights to combine a sequence of the array signals with time delays. This scheme primarily uses the information regarding the sensor locations and the waveform directions. In contrast, adaptive beamformers combine this information with the properties of the received signals, to improve rejection of unwanted signals from other directions. The adaptive array beamforming can be considered as a spatial form of an adaptive filtering process. The output of the antenna elements is adapted so as to produce a desired radiation pattern which is optimized to receive the target signal from the desired direction. In this manner,

the spatial separation of different user signals is exploited to retrieve the desired signal from the interfering signals at the same transmission band.

1.2 Software Defined Radio

The development of programmable DSPs [30]–[31] has enabled signal processing operations (e.g., image rejection, channel equalization, signal estimation, and interference suppression) to be performed in the digital domain using adaptive techniques [32]–[35]. In this regard, SDR system has been developed. SDR is a radio communication system where components typically implemented in hardware are replaced by software executed on a computer or embedded computing devices [36]–[37]. Today's rapidly evolving capabilities of digital electronics are making practical many operations that were once only theoretically feasible [38].

In order to achieve SDR, two primary tasks have to be accomplished. Firstly, the Analog-to-Digital Converter or ADC (at the receiver side) and Digital-to-Analog Converter or DAC (at the transmitter side) have to be moved near the antenna, thus more signal processing tasks can be performed in digital domain. Secondly, delicate hardware needs to be replaced by DSPs.

The main desirable feature of SDR is that, software controls and programs the transceiver devices to flexibly achieve the capability of reconfiguration. Furthermore, SDR supports multiple modes and multiple standards. Therefore, SDR is crucial in the development of *cognitive radio*, which is considered as a fully reconfigurable wireless transceiver capable to automatically adapt its communication parameters according to the network and user demands. In the long term, SDR is expected to become one of the dominant technologies in radio communication systems.

1.3 Fading Channels

In most wireless communication channels, fading is caused by two major reasons. The first is the multipath propagation, which refers to multiple reflective paths from a transmitter to a receiver for a signal to travel. The second is shadowing, in which the wave propagation is affected by obstacles. Both of them cause fluctuations in the received signal's amplitude, phase, and angle of arrival. These factors should be taken into account when describing the channel behavior or predicting the system performance.

1.3.1 Slow vs. Fast Fading

Channel fading can be categorized into two types: *slow fading* and *fast fading*. Before the definitions are given, an important term, *coherence time* is defined here. Coherence time is the minimum time required for the magnitude change of the channel to become uncorrelated from its previous value.

Slow fading occurs when the coherence time of the channel is greater than the channel delay constraint. In this scenario, the amplitude and phase changes imposed by the channel can be considered roughly constant. In other words, the characteristics of the channel remain approximately the same over the period of use. Therefore, a slow fading channel is usually considered as a *time-invariant fading* channel.

Fast fading arises when the coherence time of the channel is less than the delay constraint of the channel. In this scenario, the amplitude and phase change imposed by the channel varies considerably over the period of use. Therefore, a fast fading channel is usually considered as a *time-variant fading* channel. The time variation can be small-scale effect due to the multipath

fading, or the larger-scale effect due to the path loss via distance attenuation as well as shadowing by obstacles.

1.3.2 Flat vs. Frequency-selective Fading

Channel fading can also be categorized into *flat fading* and *frequency-selective fading*. As the carrier frequency of a signal varies, the change in amplitude may be different. *Coherence bandwidth* is defined here as the statistical measurement of the frequency range over which two frequencies of a signal are likely to experience comparable or correlated amplitude fading.

In flat fading, the coherence bandwidth of the channel is greater than the bandwidth of the signal. In this scenario, all frequency components of the signal experience the same fading effects.

In frequency-selective fading, the coherence bandwidth of the channel is smaller than the bandwidth of the signal. In this scenario, different frequency components of the signal experience different fading parameters. Frequency-selective fading channel brings big challenges to the area of wireless communications. In this scenario, the signal energy associated with each symbol is spread out in time, which causes the adjacent transmitted symbols to interfere with each other. To satisfy the performance requirements, equalizers are often deployed to compensate for the effects of this intersymbol interference [39].

1.4 Interference in Wireless Communications

In a telecommunication system, interference is any effect that distorts a signal as it travels between a transmitter and a receiver. In contrast to the wired communications where each transmitter-receiver pair can be considered as an isolated point-to-point link, wireless users

communicate over the air and thus there is inevitable interference. The interference can be between different user signals transmitted to a common receiver (e.g., uplink of a cellular system), between signals from the same transmitter to multiple receivers (e.g., downlink of a cellular system), or between different transmitter-receiver pairs (e.g., interference between users in different cells). In the following, three important types of interference are introduced–Co-Channel Interference (CCI), Adjacent Channel Interference (ACI) and image interference.

1.4.1 Co-Channel Interference

Co-Channel Interference or CCI is the crosstalk from two different users occupying the same frequency band. In cellular communications, CCI is caused by the phenomenon of frequency reuse after certain geographical distance. When the cell size is decreased due to the increasingly hectic cell phone business, this problem will become more severe. Since CCI significantly affects the system capacity, a good suppression technology becomes critical. In practice, CCI is hardly attenuated by analog filters.

1.4.2 Adjacent Channel Interference

Adjacent Channel Interference or ACI is caused by extraneous power from a signal in an adjacent channel. ACI is typically caused by nonideal filtering in either the reference or interference channel, such as inadequate filtering of unwanted modulation products in FM systems, improper tuning, or poor frequency control.

1.4.3 Image Interference

The problem of image interference arises from out-of-band users due to the adoption of IF stage as mentioned in 1.1.2. In low-IF receivers, after the frequency translation from the first down-conversion mixer, the unwanted image signal and wanted RF signal both lie in the IF band and cannot be distinguished. The image signal may have higher power than the desired signal and thus it can significantly degrade the system performance. Ideally, the image signal band can be totally attenuated in I/Q signal processing. However, perfect image rejection is realized only if the I and Q branches of such a system are completely matched (with equal amplitudes and a phase difference of 90), which is impossible in practical analog circuits [40]. Particularly, if the analog I/Q processing is applied to a wideband multichannel signal, the effect of the image interference becomes extremely severe.

1.5 Motivation and Scope of the Dissertation

This dissertation deals with two fundamental aspects, which cause challenging yet interesting problems in wireless communications [41]. The first is channel fading introduced in 1.3, and the second is the interference discussed in 1.4. How to deal with channel fading and interference is essential to the design of wireless communication systems and will be the theme of this dissertation.

The scope of this work is to investigate novel complex signal processing algorithms to enhance the signal after it is corrupted by the fading effects or interferences. This work concentrates on complex adaptive Finite Impose Response (FIR) filtering techniques.

To solve channel fading problems, the complex Least Mean Square (LMS) algorithm has been frequently applied in channel identification and equalization. However, the choice of the learning rate or convergence factor in the complex LMS method is made empirically, resulting in the inefficiency in utilizing the degrees of freedom of the adaptive system. In this research, attempts have been made to develop more efficient algorithms by using complex conjugate gradients. In addition, a time-varying step size is applied instead of the constant step size. Intuitively, greater values are chosen at the start point of the adaption to achieve rapid convergence. When the adaptation is approaching the solution, smaller values are chosen to minimize misadjustment.

To suppress the interference in a wireless system, there are two typical ways. If the network loading is relatively low, incorporating interference measurements in resource management helps to provide interference avoidance. However, if the network loading is high, avoidance technique is no longer effective. Therefore, to maintain high level of Quality of Service (QoS), it is necessary to reduce interference after it has already occurred.

To suppress CCI in an adaptive array beamforming application, LMS based algorithms can be employed. As mentioned before, the LMS technique is easy to implement but the performance is limited, especially when the power of the interference is comparatively large. To improve the performance, the proposed complex conjugate gradient block LMS techniques can also be applied in adaptive beamforming.

Besides the LMS based methods, Independent Component Analysis (ICA) is recently applied to suppress CCI in a general receiver. In this dissertation, the effect of signals' probabilistic distributions on the performance of both LMS and ICA based adaptive interference

canceling algorithms is studied. The conclusion is made that if the prior information of the signals' probabilistic distributions is known, a proper choice can be made between the LMS and ICA algorithms to achieve better performance.

The image interference is another important interference in wireless receivers. The image interference is unavoidable for practical quadrature receivers and can be frequency-dependent in nature. In this dissertation, a novel Optimal Block Adaptive algorithm based on the Circularity (OBA-C) is presented for frequency-dependent image interference suppression. The proposed OBA-C technique is based on the assumption that the received signal deviates from circularity in the presence of the image interference. The OBA-C method uses the complex Taylor series expansion to optimally update the adaptive filter coefficients at each iteration, until the circularity of the signal is restored.

1.6 Mathematical Notations and Preliminaries

To avoid the ambiguity of mathematical notations in the algorithm formulation, notational conventions are given in Table 2. In this dissertation, scalar variables appear in lower case, vectors in bold lower case, and matrices in bold upper case.

Table 2 Mathematical Notations

j	Square root of –1, $\sqrt{-1}$
$(.)^T$	Transposition
$(.)^H$	Conjugate Transposition
$(.)^*$	Conjugation
$(.)^{-1}$	Inverse of a matrix
$(.)^+$	Pseudo inverse of a matrix or vector
$E\{.\}$	Expectation
$*$	Convolution
I	Identity matrix

1.7 Organization of the Dissertation

The dissertation is organized as follows.

Chapter 2 develops the formulations of the Complex Block Conjugate based LMS (CBC-LMS) and Complex Block Conjugate based LMS with Individual adaptation (CBCI-LMS).

Chapter 3 applies the proposed CBCI-LMS and CBC-LMS algorithms to channel estimation and equalization. Besides, the implementation issues are discussed.

Chapter 4 presents an adaptive array beamforming application employing the proposed CBCI-LMS and CBC-LMS methods.

Chapter 5 proposes a novel non-data-aided block adaptive technique with optimal adaptations, OBA-C, to restore the circularity of a distorted complex signal.

Chapter 6 applies the proposed OBA-C technique to solve the frequency-dependent I/Q mismatch problem.

Chapter 7 studies the effect of signals' probabilistic distributions on performance of adaptive interference cancelling problem.

Chapter 8 summarizes the contributions of the presented research and suggests future research directions.

CHAPTER 2 CONJUGATE GRADIENT BASED COMPLEX BLOCK LMS ALGORITHMS WITH OPTIMAL ADAPTATION

The LMS algorithm has become a widely used adaptive digital filtering technique since the pioneering work of Bernard Widrow [42]–[45]. Various LMS based algorithms for adaptive digital FIR filters have been studied [43]–[53]. These algorithms can be categorized into two types: the sequential processing methods [43]-[49], and the block processing methods [50]–[53]. The sequential processing method calculates the output values sequentially from the preceding inputs, and thus it is a direct implementation of convolution or a difference equation. The Block LMS (BLMS) method calculates a block or a finite set of output values from a block of input samples. An important advantage of the block processing method is that it yields smooth convergence curve. Although the block method has higher computational complexity, it can achieve the same convergence speed as the sequential method by efficient use of parallel devices. In addition, block formulation lends itself to efficient implementation by employing the matrix inversion lemma [54] and transform methods [55]–[56]. Therefore, block processing algorithms are intensively applied to modern adaptive systems. Both the sequential and block processing LMS algorithms can be developed for complex signals and systems [57]–[59].

The performance of the LMS method depends on a crucial factor, namely, the convergence factor or step size. Conventional LMS techniques apply a time-invariant step size which is the same for all the adaptive filter coefficients. It is difficult to choose a common convergence factor that guarantees the stability of the algorithm for all conditions [60]. Since the step size controls the speed, accuracy, and stability of the adaptive system, properly selecting the

step size is important. The complex LMS algorithm has this inherent limitation of the real-valued LMS method: the performance is dependent on the proper choice of the step size.

The concept of using time-varying convergence factors has been investigated by several researchers [48]–[51], [61]–[64]. A widely used technique is the Normalized LMS (NLMS) method, which normalizes the step size by the signal power in either the time-domain [61], or the frequency-domain [62]. However, most of the previously proposed variable step size algorithms require a priori knowledge or estimates of the input signal power or the eigenvalues of the input autocorrelation matrix [61]–[64]. On the contrary, without any priori information, the Homogeneous Adaptive (HA), and Individual Adaptive (IA) methods [48] were proposed for sequential processing, while the Optimal Block Adaptive method (OBA), Optimal Block Adaptive method with Individual adaptation (OBAI) [50], were proposed for block processing. These optimal methods were extended to the complex domain in [49], [51].

The LMS based algorithms employ the steepest descent method, in which the update of the weight vector is proportional to the negative gradient. As a result, it always takes more than one step in the same direction, which causes the redundancy in adaptation and thus slows down the convergence. To improve the convergence performance, the Conjugate Gradient (CG) concept [65]–[68] can be applied. The main advantage of the CG is that it achieves rapid convergence by employing conjugate gradients instead of using the negative gradients as in the LMS method. This improvement is achieved at the expense of a relatively modest increase in the number of computations per iteration. This unique combination of convergence speed and computational complexity gives CG desirable properties for applications in numerous mathematical optimization problems.

In this chapter, a general formulation is given for developing two fast-converging complex block conjugate LMS adaptive algorithms, CBC-LMS and CBCI-LMS. The presented unified approach employs the concept of complex conjugate gradients and calculates time-varying convergence factors at each iteration. The optimal step sizes are computed from the available input signals to adjust the adaptive filter coefficients without trial and error. The difference between these two methods is that CBC-LMS uses a common step size for all the adaptive filter coefficients while CBCI-LMS computes individual step size for each filter coefficient. The formulation shows that the CBCI-LMS algorithm achieves faster adaptation than CBC-LMS at the expense of increase in the number of computations per iteration.

This chapter is organized as follows. The derivation of complex conjugate gradients is given in 2.1. In 2.2, the most general form of the algorithm, CBCI-LMS, is developed, which utilizes all the available degrees of freedom of the system. In 2.3, another class of algorithms, CBC-LMS is derived, which uses fewer computations with sacrifice in performance. In 2.4, the computational complexity of the proposed algorithms is analyzed, followed by the conclusion in 2.5.

2.1 Complex Conjugate Gradients

In this section, the complex conjugate gradient directions are derived for the adaptive filter coefficients. In 2.1.1, the block implementation of the Complex LMS algorithm is briefly reviewed. In 2.1.2, the formulation of complex conjugate gradients is given.

2.1.1 Complex BLMS

In this subsection, the BLMS is developed in the complex domain as the Complex BLMS.

Table 3 Defined Variables

k	Iteration index
l	Sample index within a block
N	Number of the FIR filter coefficients
L	Block Size
$\mathbf{w}(k)$	Filter coefficient vector at iteration index k, size $N\times 1$
$w_n(k)$	The n^{th} coefficient of $\mathbf{w}(k)$, $1 \le n \le N$
$\mathbf{X}(k)$	Filter input matrix at the time index k, size $L \times N$
$\mathbf{x}_l(k)$	The l^{th} column of $\mathbf{X}^T(k)$, size $N \times 1$
$x(k)$	Current input signal at the time index k
$\mathbf{y}(k)$	Filter output vector at iteration index k, size $N\times 1$
$y_l(k)$	The lth variable in $\mathbf{y}(k)$, $1 \le l \le L$
$\mathbf{d}(k)$	Desired signal vector at iteration index k, size $N\times 1$
$d_l(k)$	The lth variable in $\mathbf{d}(k)$, $1 \le l \le L$
$\mathbf{e}(k)$	The error signal vector at iteration index k, size $N\times 1$
$e_l(k)$	The lth error signal at iteration index k, $1 \le l \le L$
μ	Convergence factor of the Complex BLMS method

Fig. 3 gives the block diagram of a complex adaptive FIR filter. All signals are assumed to be complex. The formulation starts by defining the variables in Table 3.

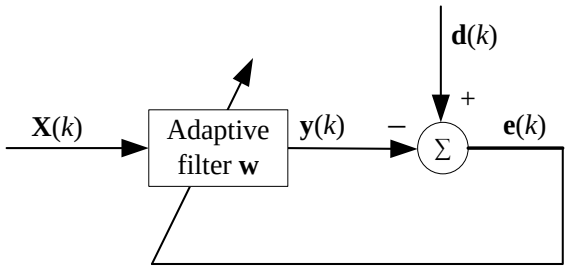

Figure 3 Adaptive FIR Filter

As defined above, the weight vector **w**(k) is an $N\times 1$ vector, given by,

$$\mathbf{w}(k) = [w_1(k), w_2(k), ...w_N(k)]^T \tag{2.1}$$

The FIR input vector $\mathbf{x}_l(k)$ is also an $N\times 1$ vector, as follows,

$$\mathbf{x}_l(k) = [x(k+l-1), x(k+l-2), ...x(k+l-N)]^T \tag{2.2}$$

At the iteration index k, the l^{th} FIR filter output $y_l(k)$, the l^{th} desired signal $d_l(k)$, and the l^{th} error signal $e_l(k)$ are formulated as follows, respectively,

$$y_l(k) = \mathbf{w}^T(k)\mathbf{x}_l(k) \tag{2.3}$$

$$d_l(k) = d(k+l-1) \tag{2.4}$$

$$e_l(k) = d_l(k) - y_l(k) \tag{2.5}$$

In a block algorithm, **e**(k) can be written in a matrix-vector expression, given by,

$$\mathbf{e}(k) = \mathbf{d}(k) - \mathbf{y}(k) = \mathbf{d}(k) - \mathbf{X}(k)\mathbf{w}(k) \tag{2.6}$$

where the vectors and matrices are listed below,

$$\mathbf{X}(k) = [\mathbf{x}_1(k), \mathbf{x}_2(k), ...\mathbf{x}_L(k)]^T \tag{2.7}$$

$$\mathbf{y}(k) = [y_1(k), y_2(k), ...y_L(k)]^T \tag{2.8}$$

$$\mathbf{d}(k) = [d_1(k), d_2(k), ...d_L(k)]^T \tag{2.9}$$

$$\mathbf{e}(k) = [e_1(k), e_2(k), ... e_L(k)]^T \tag{2.10}$$

The objective is to minimize the Mean Square Error (MSE) of the adaptation block by adjusting the filter coefficients at each iteration. The MSE function, $f_{\text{MSE}}(k)$, is defined as,

$$f_{\text{MSE}}(k) = E[e(k)e(k)^*] \approx \frac{1}{L}\mathbf{e}^H(k)\mathbf{e}(k) \tag{2.11}$$

In the block implementation of the Complex LMS, the real and imaginary components of the complex weight vector **w**, namely $\mathbf{w}_{\text{R}}$ and $\mathbf{w}_{\text{I}}$ respectively, are updated by the following equations,

$$\mathbf{w}_{\text{R}}(k+1) = \mathbf{w}_{\text{R}}(k) - \mu \cdot \mathbf{g}_{\text{R}}(k) \tag{2.12}$$

$$\mathbf{w}_{\text{I}}(k+1) = \mathbf{w}_{\text{I}}(k) - \mu \cdot \mathbf{g}_{\text{I}}(k) \tag{2.13}$$

where μ is the fixed step size, and $\mathbf{g}_{\text{R}}(k)$ and $\mathbf{g}_{\text{I}}(k)$ are the gradients of the real and the imaginary components, which can be calculated respectively, as follows,

$$\mathbf{g}_{\text{R}}(k) = \frac{\partial f_{\text{MSE}}(k)}{\partial \mathbf{w}_{\text{R}}(k)} = \frac{1}{L}[-\mathbf{X}^T(k)\mathbf{e}^*(k) - \mathbf{X}^H(k)\mathbf{e}(k)]$$

$$= \text{Re}\{-\frac{2}{L}\mathbf{X}^H(k)\mathbf{e}(k)\} \tag{2.14}$$

$$\mathbf{g}_{\text{I}}(k) = \frac{\partial f_{\text{MSE}}(k)}{\partial \mathbf{w}_{\text{I}}(k)} = \frac{1}{L}[-j\mathbf{X}^T(k)\mathbf{e}^*(k) + j\mathbf{X}^H(k)\mathbf{e}(k)]$$

$$= j \cdot \text{Im}\{\frac{2}{L}\mathbf{X}^H(k)\mathbf{e}(k)\} \tag{2.15}$$

Substituting (2.14) and (2.15) into (2.12) and (2.13), respectively, the following is obtained,

$$\mathbf{w}(k+1) = \mathbf{w}_{\text{R}}(k+1) + j \cdot \mathbf{w}_{\text{I}}(k+1)$$

$$= \mathbf{w}(k) + 2\frac{\mu}{L}\mathbf{X}^H(k)\mathbf{e}(k) \tag{2.16}$$

Similar as in the real domain, the update of the complex weight vector can be formulated in terms of complex gradient vector **g**(*k*), as follows,

$$\mathbf{w}(k+1) = \mathbf{w}(k) - \mu \cdot \mathbf{g}(k) \tag{2.17}$$

From (2.16) and (2.17), **g**(*k*) can be computed as,

$$\mathbf{g}(k) = \frac{\partial f_{\text{MSE}}(k)}{\partial \mathbf{w}(k)} \approx -\frac{2}{L}\mathbf{X}^H(k)\mathbf{e}(k) \tag{2.18}$$

The main drawback of the Complex BLMS is that the choice of the learning rate μ is made empirically, depending on the type of the application and the input signal. Moreover, a small step size results in slow convergence, and a large step size may cause unstable gradient descent, leading to divergence.

2.1.2 Formulation of Complex Conjugate Gradients

The CG principle [65] is a prominent method for solving unconstrained optimization problems such as energy minimization and adaptive filtering [66]–[68]. Compared to the two widely-used optimization approaches, the LMS method and the Newton's method, the CG principle has its unique features. In comparison with the LMS method, CG achieves more rapid convergence by employing orthogonal search directions instead of using the steepest descent method [69]. In comparison with the Newton's iteration approach which involves matrix inversion and approximation to the second-order derivative of the objective function, CG has lower computational complexity. This unique combination of convergence speed and

computational complexity gives CG desirable properties for applications in numerous mathematical optimization problems.

In implementation, CG picks a set of orthogonal search directions {**q**(0), **q**(1), … **q**(*k*), …}. When the performance function is the MSE defined in (2.11), which is a quadratic function of the weights, the performance surface is *bowl-shaped*. In this case, the adaptation will adjust the filter weights iteratively, searching for the bottom of the bowl.

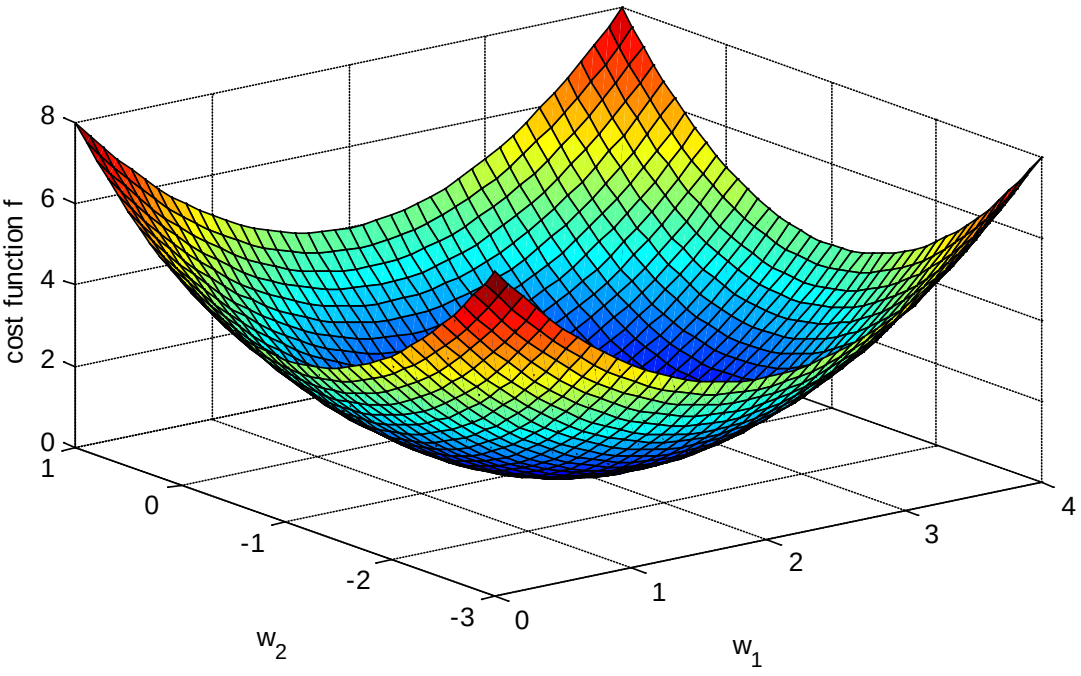

Figure 4 Performance Surface of MSE

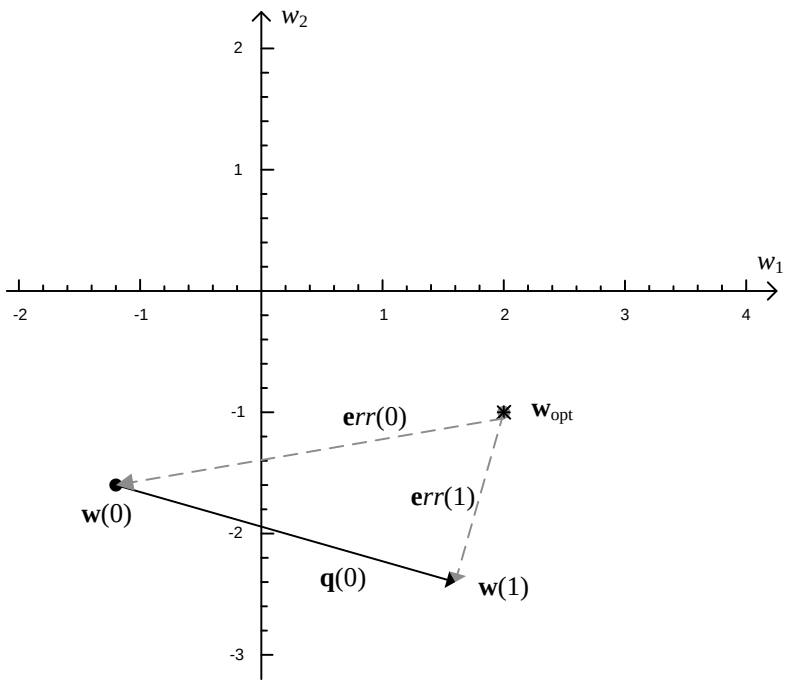

Figure 5 CG Searching Directions

Figs 4 and 5 illustrate this idea with an example of a 2×1 filter weight vector, $\mathbf{w}(k) = [w_1(k), w_2(k)]^T$. Fig. 4 shows the performance surface of MSE and Fig. 5 is the weight searching process. In Fig. 4, $\mathbf{w}(0)$ is the starting point and $\mathbf{w}_{opt}$ is the searching destination, which is the optimal filter weight to yield the least MSE. As long as the searching directions $\mathbf{q}(k)$'s are orthogonal with each other, and the step sizes $\alpha(k)$'s are properly chosen, the second step can always achieve the optimal solution $\mathbf{w}_{opt}$, regardless of the coordinates of the starting point $\mathbf{w}(0)$ and the initial direction $\mathbf{q}(0)$.

In general, **w** is updated as follows,

$$\mathbf{w}(k+1) = \mathbf{w}(k) + \alpha(k)\mathbf{q}(k) \tag{2.19}$$

The error **err** is updated as,

$$\mathbf{err}(k+1) = \mathbf{err}(k) + \alpha(k)\mathbf{q}(k) \tag{2.20}$$

To find the optimal value of $\alpha(k)$, $\mathbf{err}(k+1)$ should be orthogonal to $\mathbf{q}(k)$, so that the searching process will never again step in the direction of $\mathbf{q}(k)$. In the real domain, the mathematical relation of orthogonality between $\mathbf{q}(k)$ and $\mathbf{err}(k+1)$ is expressed as $\mathbf{q}^T(k)\mathbf{err}(k+1) = 0$, where T is the transpose. In the complex domain, the difference is that the Hermitian or conjugate transpose H is used instead of T. Thus, the orthogonal relationship is expressed as,

$$\mathbf{q}^H(k)\mathbf{err}(k+1) = 0 \tag{2.21}$$

Substituting (2.20) into (2.21), the following equation is obtained,

$$\mathbf{q}^H(k)[\mathbf{err}(k) + \alpha(k)\mathbf{q}(k)] = 0 \tag{2.22}$$

From (2.22), the step size $\alpha(k)$ is computed as:

$$\alpha(k) = -\frac{\mathbf{q}^H(k)\mathbf{err}(k)}{\mathbf{q}^H(k)\mathbf{q}(k)} \tag{2.23}$$

Unfortunately, nothing is accomplished, because $\alpha(k)$ cannot be solved without knowing $\mathbf{err}(k)$.

The solution is to replace the orthogonal relationship of the search directions with A-orthogonal. $\mathbf{q}(k)$ and $\mathbf{err}(k+1)$ are defined to be A-orthogonal if

$$\mathbf{q}^H(k) \cdot \mathbf{A} \cdot \mathbf{err}(k+1) = 0 \tag{2.24}$$

where $\mathbf{A}$ is a positive definite symmetric matrix, which in turn guarantees that the left side of (2.24) can be regarded as some form of the inner product of the vectors $\mathbf{q}(k)$ and $\mathbf{err}(k+1)$, with the usual properties in a projective plane. In other words, two vectors in A-orthogonal relationship are orthogonal in a projective plane, but not in the current plane.

Fortunately, there is a simple way to generate the A-orthogonal directions, {$\mathbf{q}(0)$, $\mathbf{q}(1)$, … $\mathbf{q}(k)$, …}, namely, conjugate Gram-Schmidt process. Here, a set of linear independent vectors

are defined as {**u**(0), **u**(1), … **u**(*k*), …}. To construct **q**(*k*), take **u**(*k*) and subtract out any components that are not A-orthogonal to the previous **q** vectors. In other words, the process to generate **q**(*k*) is as follows. First, initialize with **q**(0) = **u**(0). Second, for *k* > 0, set

$$\mathbf{q}(k) = \mathbf{u}(k) + \sum_{i=0}^{k-1} \beta_{ki} \mathbf{q}(i) \tag{2.25}$$

In fact, CG is simply the method of conjugate directions where the search directions are constructed by conjugation of the residuals. (that is, **u**(*k*) = **r**(*k*)). Therefore, following the same procedure as in the real domain in [66], β_{ki} can be simplified and derived as,

$$\beta_{ki} = \begin{cases} \dfrac{r_{(k)}^H r_{(k)}}{r_{(k-1)}^H r_{(k-1)}} & k = i+1 \\ 0 & k > i+1 \end{cases} \tag{2.26}$$

Equation (2.26) indicates that it is no longer necessary to store old search vectors to ensure the A-orthogonality of the new search vector. This major advance is significant reduction of both space complexity and computational complexity at each iteration, which is desirable in real-world applications. Henceforth, the abbreviation $\beta(k)$ is used instead of $\beta_{k,k-1}$, which can be simplified further as follows,

$$\beta(k) = \beta_{k,k-1} = \frac{\mathbf{r}^H(k)\mathbf{r}(k)}{\mathbf{r}^H(k-1)\mathbf{r}(k-1)} \tag{2.27}$$

By substituting the residue by the negative of the gradient estimate (that is, $\mathbf{r}(k) = -\mathbf{g}(k)$), the method of complex conjugate gradient directions can be summarized by the following equations,

$$\mathbf{q}(0) = \mathbf{r}(0) = -\mathbf{g}(0) \tag{2.28}$$

$$\beta(k) = \frac{\mathbf{r}^H(k)\mathbf{r}(k)}{\mathbf{r}^H(k-1)\mathbf{r}(k-1)} = \frac{\mathbf{g}^H(k)\mathbf{g}(k)}{\mathbf{g}^H(k-1)\mathbf{g}(k-1)} \tag{2.29}$$

$$\mathbf{q}(k) = \mathbf{r}(k) + \beta(k)\mathbf{q}(k-1) = -\mathbf{g}(k) + \beta(k)\mathbf{q}(k-1) \tag{2.30}$$

It is worthwhile to mention that $\beta(k)$ is a real value.

Assuming $\mathbf{w}(k)$ is a $N\times 1$ vector, the degree of freedom of the direction searching space is N. Theoretically, to achieve $\mathbf{w}_{opt}$, the number of required A-orthogonal search directions is equal to or less than N. In other words, practically $\mathbf{q}(k)$ needs to be reset to the negative gradient every D iterations, where $D \leq N$. D is called the search dimension parameter.

2.2 Formulation of the CBCI-LMS Algorithm

In this subsection, the most general form of generating the complex block conjugate algorithms with optimal step sizes is developed, using all the available degrees of freedom of the system. The convergence factor, which is unique for each coefficient of the adaptive filter, is derived at each iteration. This yields the CBCI-LMS method [70]–[71].

As mentioned previously, the proposed CBCI-LMS algorithm employs the individual convergence factor for each weight of the adaptive filter. In a block formulation using the method of the conjugate gradients, the coefficient update formula of $\mathbf{w}(k)$ can be written as

$$\mathbf{w}(k+1) = \mathbf{w}(k) + \boldsymbol{\alpha}\boldsymbol{\alpha}(k)\mathbf{q}(k) \tag{2.31}$$

where the step size matrix $\boldsymbol{\alpha}\boldsymbol{\alpha}(k)$ is a diagonal matrix of order N, whose diagonal elements are the convergence factors for the components of $\mathbf{w}(k)$, i.e.,

$$\boldsymbol{\alpha\alpha}(k)=\begin{bmatrix}\alpha_1(k) & 0 & 0 & \cdots & 0\\ 0 & \alpha_2(k) & 0 & \cdots & 0\\ 0 & 0 & \alpha_3(k) & \cdots & 0\\ \vdots & \vdots & \vdots & \ddots & \vdots\\ 0 & 0 & 0 & \cdots & \alpha_N(k)\end{bmatrix} \tag{2.32}$$

Its diagonal elements construct the step size vector $\boldsymbol{\alpha}(k)$, defined as

$$\boldsymbol{\alpha}(k)=[\alpha_1(k),\alpha_2(k),...\alpha_N(k)]^T \tag{2.33}$$

The objective is searching for the appropriate step sizes, $\boldsymbol{\alpha}(k)$ or $\boldsymbol{\alpha\alpha}(k)$, such that the MSE at next iteration, $\{\mathbf{e}^H(k+1)\mathbf{e}(k+1)/L\}$, is minimized. This is achieved by considering the performance surface of the MSE function in an N+1 dimensional space where the convergence factors of the adaptive filter are N independent variables. Taking the complex Taylor series expansion [72], the error at the $(k+1)^{\text{th}}$ iteration, $\mathbf{e}(k+1)$, can be expressed in terms of $\mathbf{e}(k)$, and the derivatives of $\mathbf{e}(k)$ with respect to the current filter weights $\mathbf{w}(k)$, as follows,

$$\mathbf{e}(k+1)=\mathbf{e}(k)+\sum_{n=1}^{N}\frac{\partial\mathbf{e}(k)}{\partial w_n(k)}\Delta w_n(k)+\frac{1}{2!}\sum_{l=1}^{N}\sum_{m=1}^{N}\frac{\partial^2\mathbf{e}(k)}{\partial w_l(k)\partial w_m(k)}\Delta w_l(k)\Delta w_m(k)+... \tag{2.34}$$

where

$$\Delta w_n(k)=w_n(k+1)-w_n(k),\ n=1,2,\ldots,N. \tag{2.35}$$

Since the error vector $\mathbf{e}(k)$ given by (2.6) is linear to the weight vector $\mathbf{w}(k)$, the derivatives higher than the first order in (2.34) are equal to zero. Thus, (2.34) becomes

$$\mathbf{e}(k+1)=\mathbf{e}(k)+\sum_{n=1}^{N}\frac{\partial\mathbf{e}(k)}{\partial w_n(k)}\Delta w_n(k) \tag{2.36}$$

Substituting (2.6) and (2.31) into (2.36), the following is obtained,

$$\mathbf{e}(k+1)=\mathbf{e}(k)-\mathbf{X}(k)\boldsymbol{\alpha\alpha}(k)\mathbf{q}(k) \tag{2.37}$$

The next step is to choose an optimal value for each convergence factor such that the approximation of MSE at next iteration is minimized. In other words, the following condition must be satisfied,

$$\frac{\partial\{f_{\mathrm{MSE}}(k+1)\}}{\partial\boldsymbol{\alpha}(k)} = \frac{\partial\{E[e(k+1)e(k+1)^*]\}}{\partial\boldsymbol{\alpha}(k)} \approx \frac{\partial\{\mathbf{e}^H(k+1)\mathbf{e}(k+1)/L\}}{\partial\boldsymbol{\alpha}(k)}$$

$$= \left[\frac{\partial\{\mathbf{e}^H(k+1)\mathbf{e}(k+1)/L\}}{\partial\alpha_1(k)} \quad \ldots \quad \frac{\partial\{\mathbf{e}^H(k+1)\mathbf{e}(k+1)/L\}}{\partial\alpha_N(k)}\right]^T = 0 \tag{2.38}$$

The MSE at next iteration can be rewritten as

$$\mathbf{e}^H(k+1)\mathbf{e}(k+1) = S_1 + S_2 + S_3 \tag{2.39}$$

where

$$S_1 = \mathbf{e}^H(k)\mathbf{e}(k) \tag{2.40}$$

$$S_2 = -[\mathbf{e}^H(k)\mathbf{X}(k)\boldsymbol{\alpha}\boldsymbol{\alpha}(k)\mathbf{q}(k) + \mathbf{q}^H(k)\boldsymbol{\alpha}\boldsymbol{\alpha}(k)\mathbf{X}^H(k)\mathbf{e}(k)]$$

$$= -[\mathbf{e}^H(k)\mathbf{X}(k)\mathbf{Q}(k)\boldsymbol{\alpha}(k) + \boldsymbol{\alpha}^T(k)\mathbf{Q}(k)\mathbf{X}^H(k)\mathbf{e}(k)] \tag{2.41}$$

$$S_3 = \mathbf{q}^H(k)\boldsymbol{\alpha}\boldsymbol{\alpha}(k)\mathbf{X}^H(k)\mathbf{X}(k)\boldsymbol{\alpha}\boldsymbol{\alpha}(k)\mathbf{q}(k)$$

$$= \boldsymbol{\alpha}^T(k)\mathbf{Q}^H(k)\mathbf{X}^H(k)\mathbf{X}(k)\mathbf{Q}(k)\boldsymbol{\alpha}(k) \tag{2.42}$$

where the diagonal matrix of the search direction, $\mathbf{Q}(k)$, is given by,

$$\mathbf{Q}(k) = \begin{bmatrix} q_1(k) & 0 & 0 & \cdots & 0 \\ 0 & q_2(k) & 0 & \cdots & 0 \\ 0 & 0 & q_3(k) & \cdots & 0 \\ \vdots & \vdots & \vdots & \ddots & \vdots \\ 0 & 0 & 0 & \cdots & q_N(k) \end{bmatrix} \tag{2.43}$$

By straightforward matrix and vector manipulations,

$$\frac{\partial S_1}{\partial \boldsymbol{\alpha}(k)} = 0 \tag{2.44}$$

$$\begin{aligned}\frac{\partial S_2}{\partial \boldsymbol{\alpha}(k)} &= -[(\mathbf{e}^H(k)\mathbf{X}(k)\mathbf{Q}(k))^T + \mathbf{Q}^H(k)\mathbf{X}^H(k)\mathbf{e}(k)] \\ &= [\mathbf{Q}^T(k)\mathbf{X}^T(k)\mathbf{e}^*(k) + \mathbf{Q}^H(k)\mathbf{X}^H(k)\mathbf{e}(k)] \\ &= -\mathrm{Re}[\mathbf{Q}^H(k)\mathbf{X}^H(k)\mathbf{e}(k)]\end{aligned} \tag{2.45}$$

$$\frac{\partial S_3}{\partial \boldsymbol{\alpha}(k)} = \mathbf{Q}^H(k)\mathbf{X}^H(k)\mathbf{X}(k)\mathbf{Q}(k)\boldsymbol{\alpha}(k) \tag{2.46}$$

Combing (2.38) and (2.39) yields

$$\frac{\partial S_1}{\partial \boldsymbol{\alpha}(k)} + \frac{\partial S_2}{\partial \boldsymbol{\alpha}(k)} + \frac{\partial S_3}{\partial \boldsymbol{\alpha}(k)} = 0 \tag{2.47}$$

Evaluating (2.47), the following is obtained,

$$\mathbf{Q}^H(k)\mathbf{X}^H(k)\mathbf{X}(k)\mathbf{Q}(k)\boldsymbol{\alpha}(k) = \mathrm{Re}[\mathbf{Q}^H(k)\mathbf{X}^H(k)\mathbf{e}(k)] \tag{2.48}$$

Assume

$$\mathbf{C}(k) = \mathbf{Q}^H(k)\mathbf{X}^H(k)\mathbf{X}(k)\mathbf{Q}(k) \tag{2.49}$$

It is easy to prove that $\mathbf{C}(k)$ shown in (2.49) is positive definite. Then the final formula of the step size vector $\boldsymbol{\alpha}(k)$ is derived as follows,

$$\boldsymbol{\alpha}(k) = \mathbf{C}^{-1}\,\mathrm{Re}[\mathbf{Q}^H(k)\mathbf{X}^H(k)\mathbf{e}(k)] \tag{2.50}$$

where the notation $[.]^{-1}$ denotes the inverse of a square matrix. Then, the step size matrix $\boldsymbol{\alpha}\boldsymbol{\alpha}(k)$ can be obtained from $\boldsymbol{\alpha}(k)$ according to (2.32).

Since the proposed technique tries to achieve convergence in one step, an optional scaling factor γ can be introduced to ensure the stability of convergence. Equation (2.31) can thus be modified as

$$\mathbf{w}(k+1) = \mathbf{w}(k) + \gamma \cdot \boldsymbol{\alpha}\boldsymbol{\alpha}(k)\mathbf{q}(k) \tag{2.51}$$

In summary, the CBCI-LMS algorithm can be described in steps as follows.

1) Initialize

Start with $k = 0$; $\mathbf{w}(k) = 0$.

2) Calculate the Error Vector, $\mathbf{e}(k)$

$$\mathbf{e}(k) = \mathbf{d}(k) - \mathbf{X}(k)\mathbf{w}(k).$$

3) Compute the Gradient Vector, $\mathbf{g}(k)$

$$\mathbf{g}(k) \approx -\frac{2}{L}\mathbf{X}^H(k)\mathbf{e}(k).$$

4) Search for the Conjugate Gradient Direction, $\mathbf{q}(k)$

$$\mathbf{q}(k) = [q_1(k), q_2(k), \ldots q_N(k)]^T.$$

If k/D is an integer, then do the following,

$$\mathbf{q}(k) = -\mathbf{g}(k)$$

otherwise,

$$\mathbf{q}(k) = -\mathbf{g}(k) + \frac{\mathbf{g}^H(k)\mathbf{g}(k)}{\mathbf{g}^H(k-1)\mathbf{g}(k-1)}\mathbf{q}(k-1), k \geq 1.$$

The diagonal matrix of the search direction, **Q**(k), is given by,

$$\mathbf{Q}(k)=\begin{bmatrix} q_1(k) & 0 & 0 & \cdots & 0 \\ 0 & q_2(k) & 0 & \cdots & 0 \\ 0 & 0 & q_3(k) & \cdots & 0 \\ \vdots & \vdots & \vdots & \ddots & \vdots \\ 0 & 0 & 0 & \cdots & q_N(k) \end{bmatrix}.$$

5) Derive the Optimal Step Size Vector **α***(k)*

α(*k*) is the optimal step size vector to update the weight vector w(k), given by

$\boldsymbol{\alpha}(k)=[\alpha_1(k),\alpha_2(k),...\alpha_N(k)]^T$.

α(*k*) is derived as

$\boldsymbol{\alpha}(k)=[\mathbf{Q}^H(k)\mathbf{X}^H(k)\mathbf{X}(k)\mathbf{Q}(k)]^{-1}\cdot[\mathbf{Q}^T(k)\mathbf{X}^T(k)\mathbf{e}^*(k)+\mathbf{Q}^H(k)\mathbf{X}^H(k)\mathbf{e}(k)]$.

Then the step size matrix **αα**(*k*) is given by

$$\boldsymbol{\alpha\alpha}(k)=\begin{bmatrix} \alpha_1(k) & 0 & 0 & \cdots & 0 \\ 0 & \alpha_2(k) & 0 & \cdots & 0 \\ 0 & 0 & \alpha_3(k) & \cdots & 0 \\ \vdots & \vdots & \vdots & \ddots & \vdots \\ 0 & 0 & 0 & \cdots & \alpha_N(k) \end{bmatrix}.$$

6) Update **w**(*k*)

$\mathbf{w}(k+1)=\mathbf{w}(k)+\gamma\cdot\boldsymbol{\alpha\alpha}(k)\mathbf{q}(k)$.

7) Check the convergence of the algorithm

Calculate the Euclidean distance of the performance measurement at iterations *k* and *k*+1. If this distance is less than a threshold value *ε*, terminate the adaptation; otherwise, *k* = *k*+1, and go back to Step *2*.

2.3 Formulation of the CBC-LMS Algorithm

In the CBC-LMS algorithm developed in [72]–[74], the time-varying convergence factor, $\alpha(k)$, although updated at each iteration, is assumed to be the same for all the filter coefficients. Thus, the convergence factors given in (2.32) are now modified as

$$\alpha_1(k) = \alpha_2(k) = ... = \alpha_N(k) = \alpha(k) \tag{2.52}$$

Thus, the formula for updating the CBC-LMS filter coefficients is given by

$$\mathbf{w}(k+1) = \mathbf{w}(k) + \alpha(k)\mathbf{q}(k) \tag{2.53}$$

The convergence factor, $\alpha(k)$, is also optimized in the LMS sense defined by (2.38) which, in the CBC-LMS method, becomes

$$\frac{\partial\{\mathbf{e}^H(k+1)\mathbf{e}(k+1)/L\}}{\partial\alpha(k)} = 0 \tag{2.54}$$

In this case, (2.47) becomes

$$\frac{\partial S_1}{\partial\alpha(k)} + \frac{\partial S_2}{\partial\alpha(k)} + \frac{\partial S_3}{\partial\alpha(k)} = 0 \tag{2.55}$$

By replacing $\boldsymbol{\alpha}\boldsymbol{\alpha}(k)$ with $\alpha(k)\cdot I$ (I is the $N\times N$ identity matrix) in (2.40)–(2.42), the following derivatives are obtained,

$$\frac{\partial S_1}{\partial\alpha(k)} = 0 \tag{2.56}$$

$$\frac{\partial S_2}{\partial\alpha(k)} = -[\mathbf{e}^H(k)\cdot\mathbf{X}(k)\cdot\mathbf{q}(k) + \mathbf{q}^H(k)\cdot\mathbf{X}^H(k)\cdot\mathbf{e}(k)] \tag{2.57}$$

$$\frac{\partial S_3}{\partial\alpha(k)} = \mathbf{q}^H(k)\cdot\mathbf{X}^H(k)\cdot\mathbf{X}(k)\cdot\mathbf{q}(k)\cdot\alpha(k) \tag{2.58}$$

Substituting the above resulting expressions (2.56)–(2.58) into (2.55), the optimal convergence factor $\alpha(k)$ is calculated as,

$$\alpha(k) = \frac{\mathbf{e}^H(k)\mathbf{X}(k)\mathbf{q}(k) + \mathbf{q}^H(k)\mathbf{X}^H(k)\mathbf{e}(k)}{2 \cdot \mathbf{q}^H(k)\mathbf{X}^H(k)\mathbf{X}(k)\mathbf{q}(k)} \tag{2.59}$$

Similar to the CBCI-LMS algorithm, an optional scaling factor γ can be introduced to the final formulation. Equation (2.53) is modified as

$$\mathbf{w}(k+1) = \mathbf{w}(k) + \gamma \cdot \alpha(k) \cdot \mathbf{q}(k) \tag{2.60}$$

Finally, the Complex Block algorithm can be analyzed in steps as follows.

1) Initialize

Start with $k = 0$, $\mathbf{w}(k) = 0$.

2) Calculate the Error Vector, $\mathbf{e}(k)$

$\mathbf{e}(k) = \mathbf{d}(k) - \mathbf{X}(k)\mathbf{w}(k)$.

3) Compute the Gradient Vector, $\mathbf{g}(k)$

$$\mathbf{g}(k) \approx -\frac{2}{L} \cdot \mathbf{X}^H(k)\mathbf{e}(k).$$

4) Search for the Conjugate Gradient Direction, $\mathbf{q}(k)$

If k/D is an integer, then do the following,

$\mathbf{q}(k) = -\mathbf{g}(k)$

otherwise,

$$\mathbf{q}(k) = -\mathbf{g}(k) + \frac{\mathbf{g}^H(k)\mathbf{g}(k)}{\mathbf{g}^H(k-1)\mathbf{g}(k-1)}\mathbf{q}(k-1), k \geq 1.$$

5) Derive the Optimal Step Size Vector α(k)

$\alpha(k)$ is the optimal step size vector to update the weight vector $\mathbf{w}(k)$, derived as

$$\alpha(k) = \frac{\mathbf{e}^H(k)\mathbf{X}(k)\mathbf{q}(k) + \mathbf{q}^H(k)\mathbf{X}^H(k)\mathbf{e}(k)}{2 \cdot \mathbf{q}^H(k)\mathbf{X}^H(k)\mathbf{X}(k)\mathbf{q}(k)}.$$

6) Update the weight vector, $\mathbf{w}(k)$

$$\mathbf{w}(k+1) = \mathbf{w}(k) + \gamma \cdot \alpha(k)\mathbf{q}(k).$$

7) Check the Convergence of the Algorithm

Calculate the Euclidean distance of the performance measurement at iterations k and k+1. If this distance is less than a threshold value ε, terminate the adaptation. Otherwise, $k = k$+1, and go to step *2*.

2.4 Computational Complexity

In this subsection, the computational complexities of the CBCI-LMS and CBC-LMS algorithms are studied and compared to the Complex BLMS technique.

Table 4 Computational Complexities

MPI	Complex BLMS	CBC-LMS	CBCI-LMS
Error Computation	$4LN$	$4LN$	$4LN$
Gradient Computation	$4LN$	$4LN$	$4LN$
Direction Search	–	$4N$	$4N$
Step Size and Weight Update	$2N$	$4LN+6N+2L$	$24N^2+4LN-10N+4L$
Total	$8LN+2N$	$12LN+2L+10N$	$12LN+24N^2-6N+4L$

The weight update equation (2.51) for the CBCI-LMS involves matrix inversion, which is computationally intensive and impractical, especially for high-order adaptive systems. However, the matrix inversion can be significantly simplified in two ways [74].

The first way is introducing the matrix inversion lemma given in APPENDIX. As a result, the computational complexity of the CBCI-LMS algorithm is considerably reduced to $O(LN)$ per iteration, which is comparable to the other methods. Employing the matrix inversion lemma will not degrade the convergence speed and accuracy, which are confirmed in the simulation results given in Chapter 3. With the use of the matrix inversion lemma, the CBCI-LMS algorithm requires only one matrix inversion, which happens at the first iteration of the adaptation process.

The second way is replacing the matrix $\mathbf{C}$ in (2.49) at the first iteration with a diagonal matrix $\mathbf{C}_d$, which contains only the diagonal elements of $\mathbf{C}$. Therefore, the objective matrix for inversion is $\mathbf{C}_d$ instead of $\mathbf{C}$, and thus the computations for matrix inversion is reduced from $O(N^3)$ to $O(N)$, which is a substantial saving in the number of required computations. It is worthwhile to mention that it is possible to estimate $\mathbf{C}$ with an identity matrix I. However, it was found from the computer simulations that using $\mathbf{C}_d$ at $k = 1$ results in much faster adaptation than using the identity matrix.

From the discussion above, there are two implementations of the matrix inversion in the CBCI-LMS algorithm. In CBCI-LMS(1), $\mathbf{C}$ is inverted directly in the first iteration and the matrix inversion lemma is applied when $k > 1$. In CBCI-LMS(2), $\mathbf{C}$ is estimated as a diagonal matrix $\mathbf{C}_d$ at $k = 1$ and then the lemma is applied. It is worthwhile to mention that, CBCI-LMS(1), in comparison with CBCI-LMS(2), requires a large number of computations only at the first iteration. In the cost of the increased computations, CBCI-LMS(1) converges faster and uses

fewer samples to achieve convergence. After the first iteration, CBCI-LMS(1) and CBCI-LMS(2) are identical.

The real-valued Multiplications Per Iteration (MPI) for these methods are summarized in Table 4. Table 4 clearly indicates that the calculation of the optimal step size and weight update results in more computations at each iteration for the CBCI-LMS method.

However, the algorithms with more MPI usually converge in much fewer iterations than the other methods. Thus, it is not sufficient to compare the computational complexity only by employing the criterion of MPI. Hence, the overall real Multiplications required for convergence is adopted as a measure of computational complexity, which is defined as follows:

$$\text{Multiplications} = \text{MPI} \times N_c \tag{2.61}$$

where N_c denotes the number of iterations for convergence.

For example, with regards to the CBC-LMS and the Complex BLMS, it can be seen that the MPI of CBC-LMS is approximately 1.5 times the MPI of Complex BLMS. However, the experimental results in Chapter 3 show that the N_c for Complex BLMS is more than 1.5 times the N_c of CBC-LMS. As a result, the CBC-LMS requires less overall computations or Multiplications.

Besides, even in the situation that more Multiplications are required for convergence, if the number of operations needed per iteration is within the capability of DSP, the proposed algorithms still converge faster in real time by requiring fewer samples. Recent advances in digital signal processing hardware are making high performance algorithms desirable, even at the expense of increased computations.

2.5 Conclusion

In this chapter, the general formulation is given which leads to two classes of adaptive algorithms: the CBCI-LMS and the CBC-LMS algorithms. It is shown that the CBC-LMS is obtained from the CBCI-LMS, with a simple trade-off between adaptation performance and computational complexity. Both algorithms apply the CG theory to find the orthogonal directions of the adaptive filter coefficients. Besides, the convergence factors are generated using the complex Taylor series approximation at each iteration to minimize the next iteration's MSE between the adaptive filter output and the desired signal. Computational complexities of the proposed methods are analyzed and compared to the Complex BLMS method.

CHAPTER 3 CHANNEL ESTIMATION AND EQUALIZATION BASED ON PROPOSED CBCI-LMS AND CBC-LMS

The performance of the generated optimal conjugate gradient algorithms using time-varying convergence factors, CBCI-LMS and CBC-LMS, are evaluated by means of computer simulations as well as laboratory experiment. The experiments include channel identification as well as channel equalization. In addition, the implementation aspects are discussed, including block shifting, block size selection, search dimension parameter, and optional scaling factor. Also, the proposed algorithms are compared with three other algorithms, namely, the Complex BLMS, the Complex OBAI-LMS, and the Complex OBA-LMS, It is demonstrated that the major attractive feature of the CBC-LMS and the CBCI-LMS algorithms are the considerable reduction in the number of required iterations for convergence.

This chapter is organized as follows. Two applications in wireless communications are simulated: channel estimation in 3.1 and channel equalization in 3.2. Implementation issues are discussed in 3.3. Subsection 3.4 compares the proposed algorithms with the state of the art methods, followed by the conclusion in 3.5.

3.1 Channel Estimates

The unknown fading channel can be modeled as a complex FIR filter $F(z)$ shown in Fig. 6.

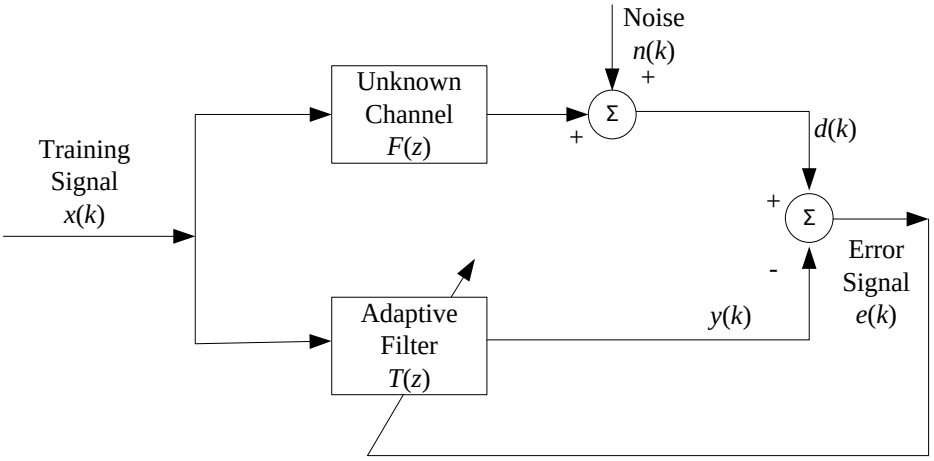

Figure 6 Signal Model for Estimating an Unknown Complex Channel

Both the unknown channel and the adaptive filter are driven by the same input signal, $x(k)$. Practically, noise is uncorrelated with the channel input, which can be represented at the channel output as an additive component. To reduce the error signal $e(k)$, the adaptive filter $T(z)$ tries to emulate the channel's transfer characteristics. After adaptation, the unknown channel is "identified" in the sense that its transfer function can be specified as essentially the same as that of the adaptive filter. Adaptive system identification is used to model an unknown channel when the training signal is available.

The performance of the proposed methods is measured in terms of the Normalized Error Energy (NEE), which is defined as the ratio of the estimated error energy to the energy of the unknown transfer function, as follows

$$\text{NEE} = \int_{\omega=0}^{\omega=\pi} |F(e^{j\omega}) - T(e^{j\omega})|^2 d\omega \Big/ \int_{\omega=0}^{\omega=\pi} |F(e^{j\omega})|^2 d\omega \tag{3.1}$$

where $F(e^{j\omega})$ and $T(e^{j\omega})$ are the transfer functions of the unknown complex channel and the adaptive filter, respectively. Since NEE is independent of the input signal, it is a more reliable performance measurement than the energy of the error signal.

To study the performance of the proposed CBC-LMS and CBCI-LMS algorithms, two series of simulations are carried out: time-invariant fading and time-variant fading. In 3.1.1, time-invariant fading is assumed, while in 3.1.2, time-variant fading is assumed.

3.1.1 Computer Simulation for Time-invariant Channel Estimation

In this subsection, time-invariant channel is simulated. The simulation parameters are set up as follows. The search dimension parameter D = 5 for the CBCI-LMS and CBC-LMS methods. The adaptive filter has N = 10 coefficients and L = 2N = 20 for all the simulated algorithms. The coefficients of $T(z)$ are initialized to zero before adaptation. Two different noise conditions are simulated: no additive noise and zero mean complex white Gaussian noise with the Signal to Noise Ratio (SNR) equal to 35dB. The unknown channel $F(z)$ is defined as follows,

$$F(z) = \sum_{i=0}^{I} a_i z^{-i} \tag{3.2}$$

with the coefficients of $F(z)$ listed in Table 5.

Table 5 Coefficients of $F(z)$ for Time-invariant Channel

i	a_i
0	$-0.8777 + j\cdot 1.1746$
1	$-1.3014 - j\cdot 0.8775$
2	$-0.5138 - j\cdot 0.6327$
3	$1.2437 - j\cdot 1.9955$
4	$2.1850 - j\cdot 0.3038$
5	$1.0560 + j\cdot 1.6765$
6	$-0.3915 - j\cdot 0.4673$
7	$-0.5491 - j\cdot 0.2086$
8	$0.0431 - j\cdot 0.4020$

The input signal, $x(k)$, is a zero-mean complex white Gaussian sequence. The values of the fixed step size μ used in the BLMS algorithm is 0.1. The value of μ has been verified by the equation below,

$$0 < \mu < \frac{1}{\lambda_{\max}} \tag{3.3}$$

where $\lambda_{\max}$ is the largest eigenvalue of the input correlation matrix. The selected values of μ are approximately $\frac{1}{2\lambda_{\max}}$ for this simulation.

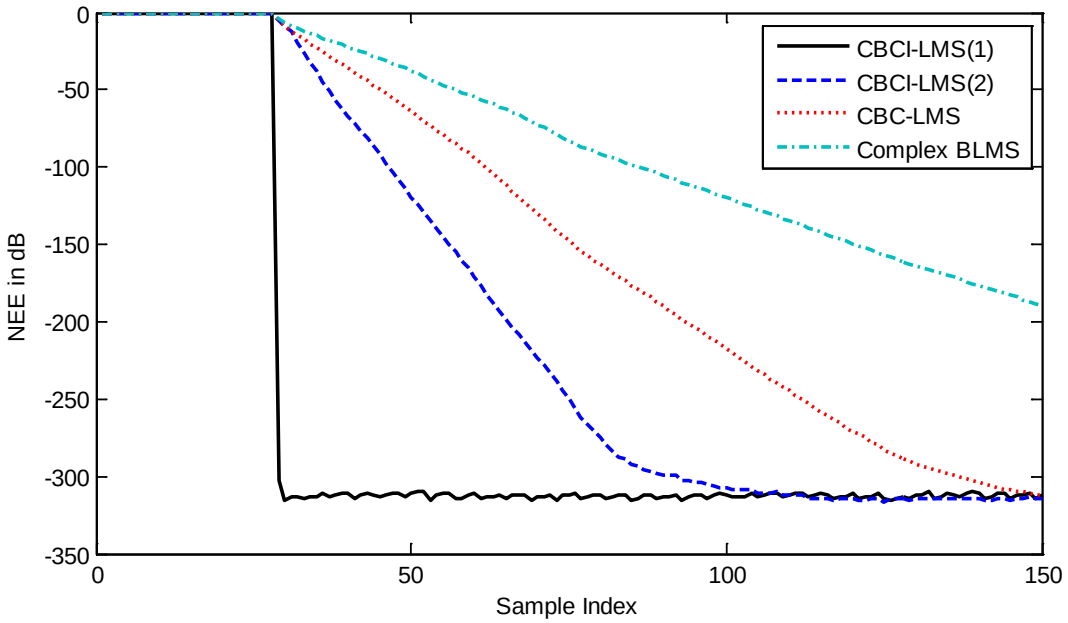

Figure 7 NEE vs. Sample Index when Input Signal $x(k)$ is White Gaussian Signal without Additive Noise $n(k)$

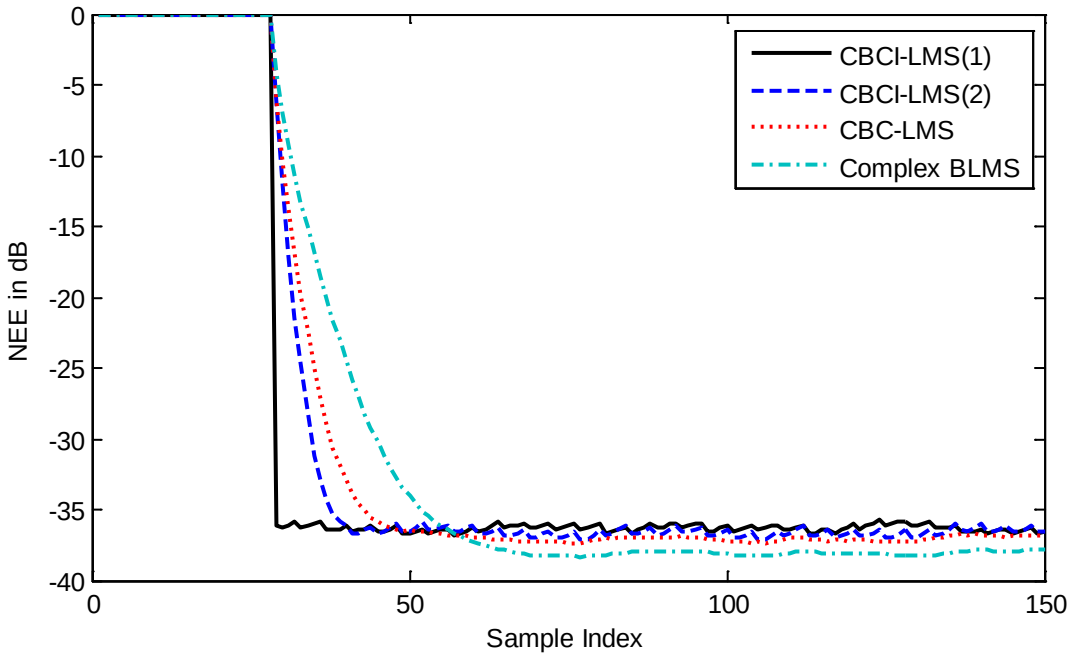

Figure 8 NEE vs. Sample Index when Input Signal $x(k)$ and Additive Noise $n(k)$ are both White Gaussian Signals with SNR=35dB.

Figs. 7–8 show that the CBCI-LMS(1) outperforms the CBCI-LMS(2), and the CBCI-LMS(2) outperforms the CBC-LMS, while all of them outperform Complex BLMS regardless of the additive noise. This has been found true from extensive simulations using other unknown channels in our experiments.

Fig. 7–8 indicates that with or without noise, all the algorithms can estimate the channel properties accurately, with numerical error left only. From Fig. 8, it is worthwhile to mention that the residual NEE upon convergence are equivalent to the input SNR for all these algorithms. Fig. 8 also illustrates the relationship between the convergence speed and the residual NEE. The algorithm with faster convergence has higher level of residual NEE. This reveals the fact that larger residual error is the inevitable cost for the significant improvement of convergence speed.

3.1.2 Computer Simulation for Time-variant Channel Estimation

There are two important types of time-variant changes in wireless channels: Linear change and abrupt change. Two examples in cellular mobile communications are given to illustrate these two types of changes as follows. The frequent channel change due to relative motion between the user and base station is a continuous linear change in the channel coefficients. The change by handoff between two towers or shadowing phenomenon when the mobile user entering a building or tunnel causes an abrupt change in the channel coefficients. In this subsection, the performance of the proposed algorithms is studied in both linearly and abruptly changing channels.

The simulation parameters are set up as follows. The search dimension parameter $D = 5$ for the CBCI-LMS and CBC-LMS methods. The adaptive filter has $N = 10$ coefficients and the

block size $L = 2N = 20$ for all the simulated algorithms. The coefficients of $T(z)$ are initialized to zero before adaptation.

In the first series of simulations, linear time-variant channel is modeled as $F(z, k)$, which is defined as follows,

$$F(z,k) = \sum_{i=0}^{I} (a_i + b_i \cdot k) z^{-i} \tag{3.4}$$

where a_i's are listed in Table 5 and b_i's are normally distributed variables with zero mean and variance equal to 10^{-6}. The input signal is complex white Gaussian signal as in 3.1.1. Complex white Gaussian noise of SNR=35dB is simulated.

The NEE vs. sample index when the step size μ of the Complex BLMS equals to 0.1 and 0.25 are plotted in Figs 9 and 10, respectively. Fig. 10 shows that in a time-variant environment, a relatively large step size leads to divergence for the Complex BLMS. The presented results clearly indicate that in order to guarantee convergence and achieve acceptable convergence speed, the value of μ for the Complex BLMS method has to be set up manually, according to different source signals, environmental parameters and simulation conditions.

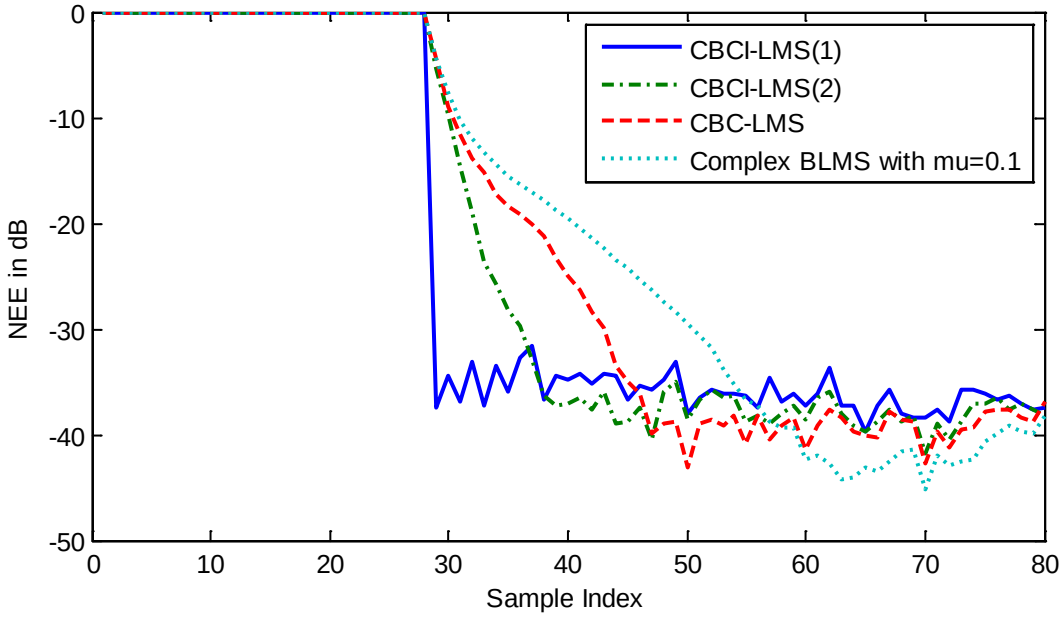

Figure 9 NEE vs. Sample Index when the Complex BLMS converges with SNR=35dB in Linearly Changing Channel

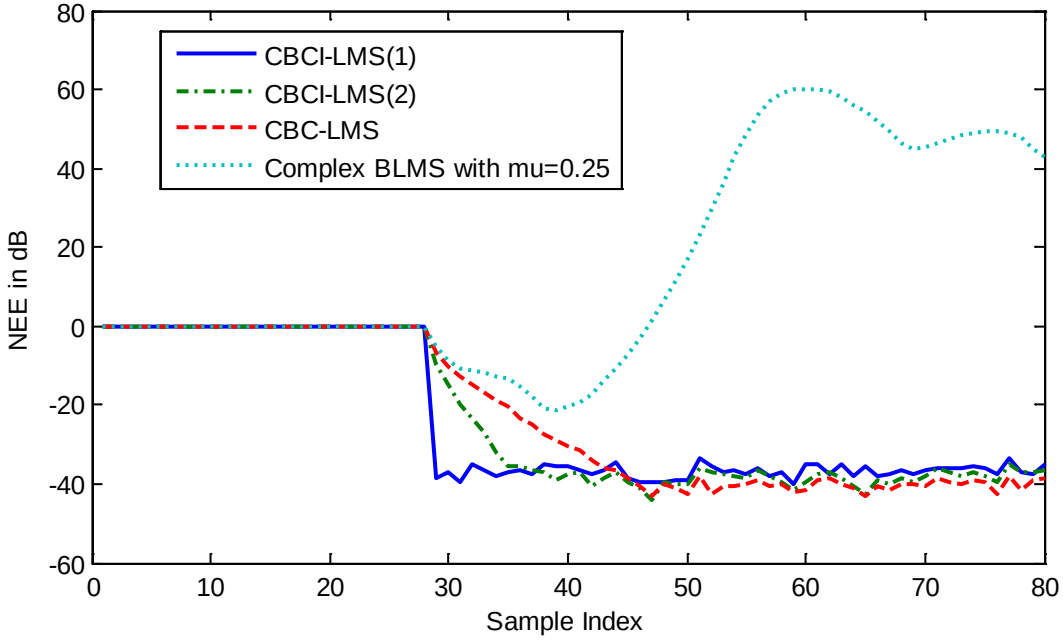

Figure 10 NEE vs. Sample Index when the Complex BLMS diverges with SNR=35dB in Linearly Changing Channel

In the second series of simulations, an abruptly fading channel is modeled by simulating an instantaneous change in channel coefficients during the processing period. When this happens, the applied algorithm has to quickly recover from this variation and reconverge to achieve a new steady state. The coefficients of $F(z)$ before abrupt change are listed in Table 5, while the coefficients of $F(z)$ after abrupt change are listed in Table 6 below.

Table 6 Coefficients of $F(z)$ for Abrupt Changing Channel

i	a_i
0	$0.0883 + j \cdot 0.234$
1	$0.3895 + j \cdot 0.1123$
2	$0.4823 + j\ 0.6574$
3	$-0.3132 - j\ 0.1645$
4	$0.6007 + j\ 0.3245$
5	$0.2538 + j\ 0.4356$
6	$-0.5267 + j \cdot 0.2156$
7	$-0.0552 + j\ 0.123$
8	$0.5530 + j \cdot 0.5612$

Same as the first series of simulation, the input signal is a complex white Gaussian signal. The performance of the algorithms are simulated with no additive noise and white Gaussian noise with SNR=35dB, respectively, in Figs 11 and 12.

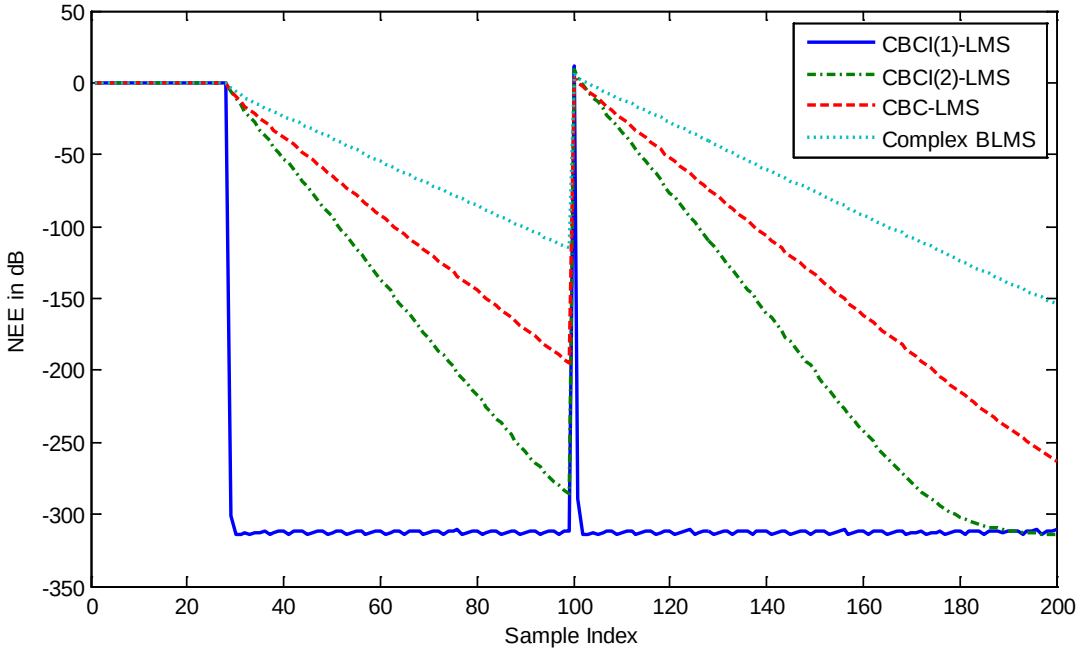

Figure 11 NEE vs. Sample Index when Input Signal *x*(*k*) is white Gaussian Noise without Additive Noise *n*(*k*) in Abruptly Changing Channel

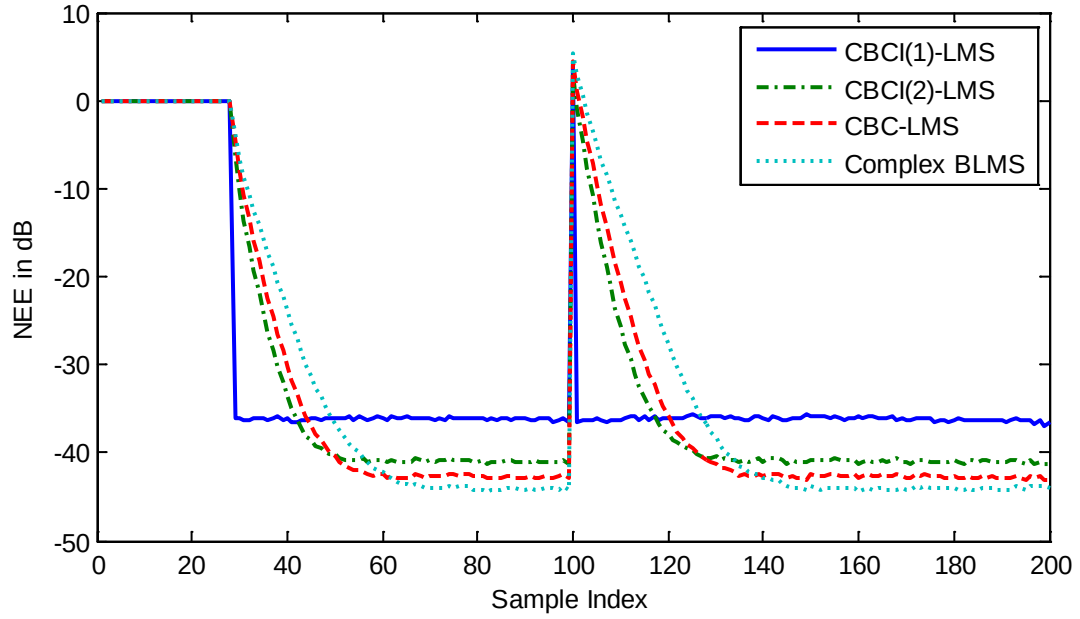

Figure 12 NEE vs. Sample Index when Input Signal *x*(*k*) and the Additive Noise *n*(*k*) are both White Gaussian Signal with SNR=35dB in Abruptly Changing Channel

Figs 9–12 further confirm that the algorithms in the order of decreasing convergence speed are CBCI-LMS(1), CBCI-LMS(2), CBC-LMS, Complex BLMS, for both linear and abrupt time variations. The superiority of the proposed algorithms will be further confirmed in our simulations under different settings. In contract, the Complex BLMS is inefficient in adapting to rapid changes in the channel.

3.2 Channel Equalization

In this section, the novel complex adaptive filtering algorithms, CBCI-LMS and CBC-LMS are applied to complex channel equalization through computer simulations as well as laboratory experiments.

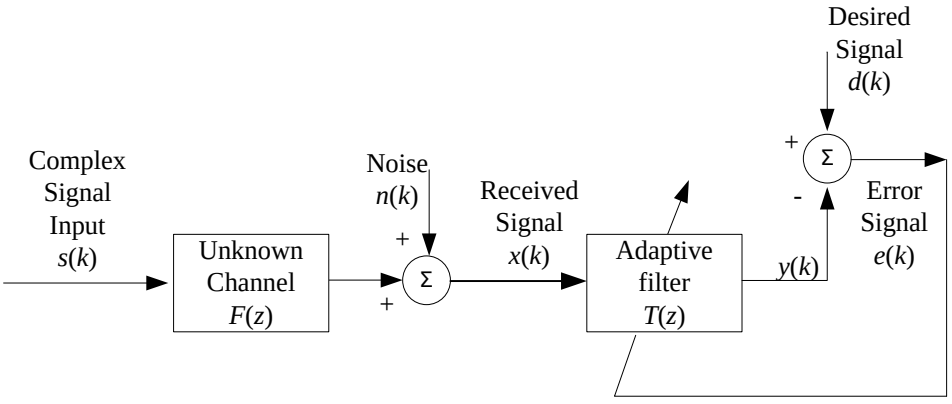

Figure 13 Signal Model for Complex Channel Equalization

A block diagram of channel equalization is shown in Fig. 13. Similar to the channel identification model in 3.1, the unknown wireless channel can be modeled as an complex FIR filter $F(z)$. In this application, the adaptive processor attempts to recover the received signal $x(k)$, which is assumed to be altered by the unknown channel $F(z)$, and to contain additive noise $n(k)$.

This noise is generally uncorrelated with the channel input. After convergence, the adaptive filter output $y(k)$ is the best match to the channel input $s(k)$, and the adaptive filter $T(z)$ becomes an inverse model of the unknown channel $F(z)$. In this sense, the adaptive system equalizes the unknown channel.

Simulations have been performed with different values of SNR. The convergence accuracy is expressed in terms of the NEE, defined as

$$\mathrm{NEE}(k) = \frac{\mathbf{e}^H(k)\mathbf{e}(k)}{\mathbf{s}^H(k)\mathbf{s}(k)} \tag{3.5}$$

3.2.1 Computer Simulation for Channel Equalization

In this subsection, the performance of the CBCI-LMS and CBC-LMS algorithm are tested to equalize a complex channel in computer simulations. The results are compared to those obtained from the Complex Block LMS. The input to the unknown channel, $s(k)$, is a 64QAM signal. The search dimension parameter $D = 5$ for the CBCI-LMS and CBC-LMS methods. The adaptive filter has $N = 10$ coefficients and $L = 2N = 20$ for all the simulated algorithms. The coefficients of $T(z)$ are initialized to zero before adaptation. Two different noise conditions are simulated: no additive noise and zero mean white Gaussian noise with the SNR equal to 35dB. In the simulations, μ is chosen to be 0.05 and 0.03 for the Complex Block LMS. The unknown channel $F(z)$ is defined as in (3.2), with the coefficients of $F(z)$ listed in Table 7.

Table 7 Coefficients of $F(z)$ in Simulation of Channel Equalization

i	a_i
0	$-0.8324 + j\,0.9238$
1	$0.0388 + j\,0.1498$
2	$-0.0227 - 0.0280$

Figs 14 and 15 plot the NEE vs. sample index under different noise conditions for CBCI-LMS(1), CBCI-LMS(2), CBC-LMS, and Complex BLMS with μ equal to 0.005 and 0.003. It is clearly shown from both plots that the Complex Block LMS algorithm is at the divergent boundary when the value of the fixed step size μ is 0.005. The input and output signal constellations of the adaptive filter employing the CBCI-LMS(1) technique are plotted in Figs 16 and 17, respectively. It can be easily inferred from Fig. 16 that the channel distortion destroyed the signal. From Fig. 17, it is clearly shown that the CBCI-LMS(1) effectively equalized the unknown channel and recovered the signal. The residual error left after the equalization is from the additive noise.

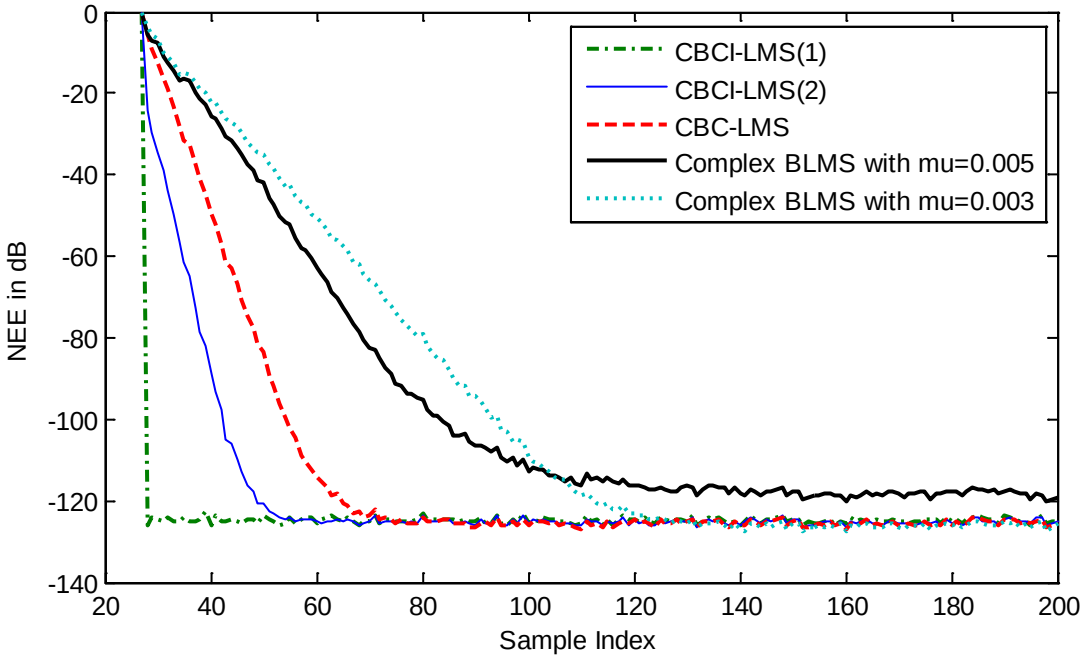

Figure 14 NEE vs. Sample Index without Additive Noise *n*(*k*)

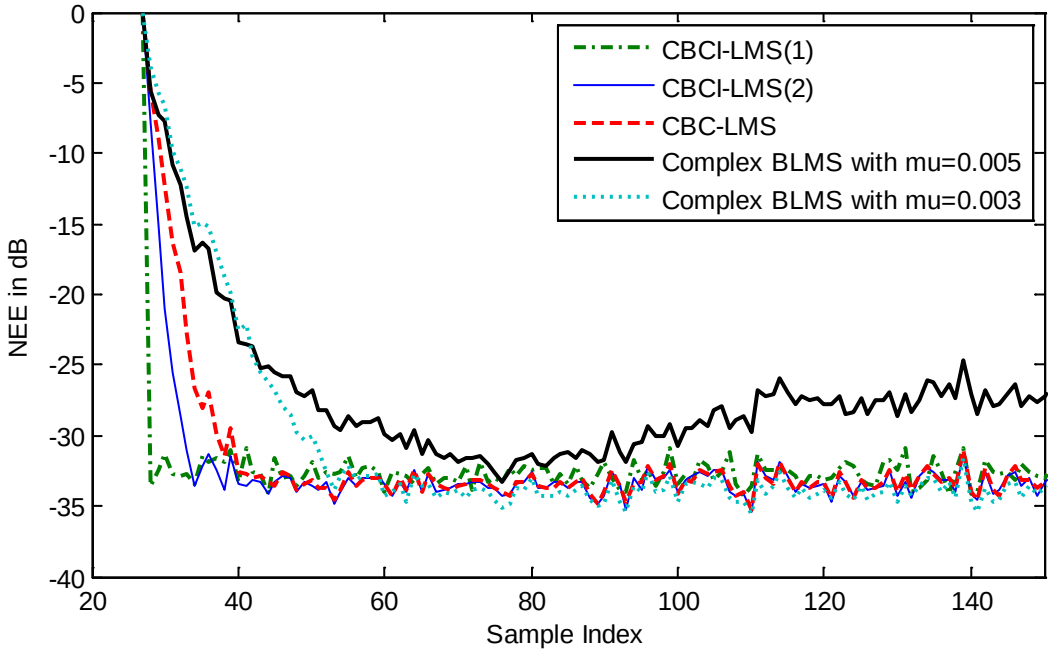

Figure 15 NEE vs. Sample Index when Additive Noise *n*(*k*) is White Gaussian Signal with SNR=35dB

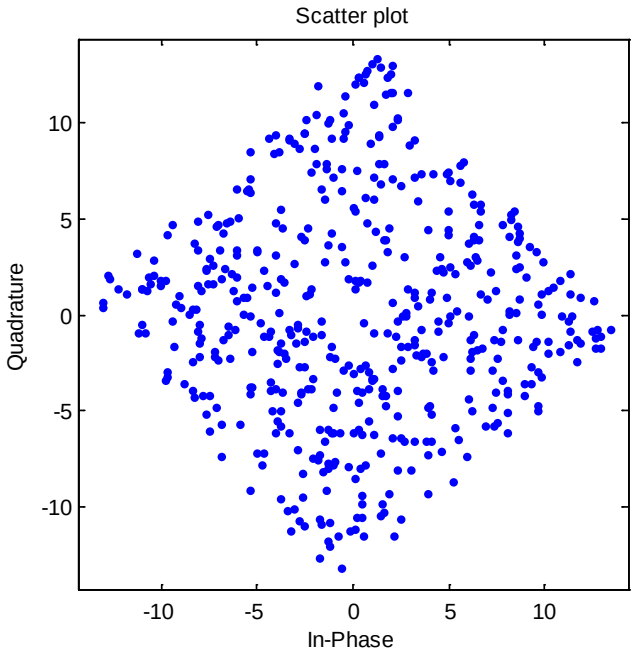

Figure 16 Constellation of Unknown Channel Output

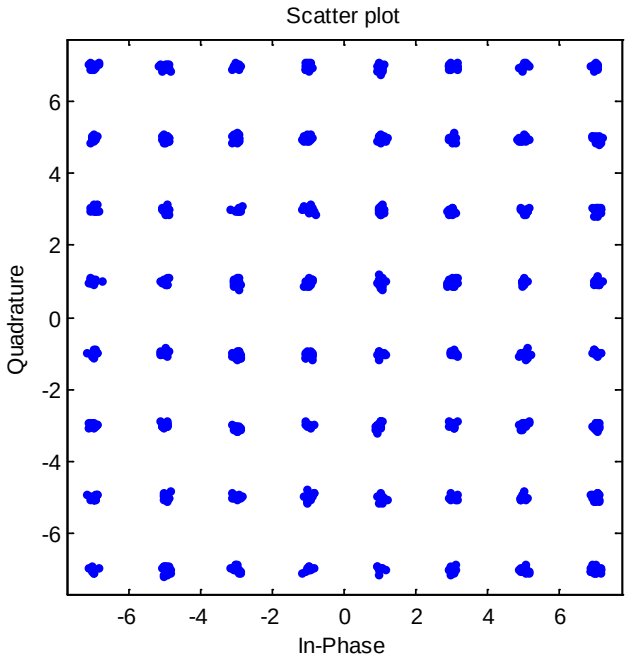

Figure 17 Constellation of Recovered Signal

3.2.2 Laboratory Experiment for Channel Equalization

In this subsection, laboratory experiments have been carried out to examine the performance of the proposed CBCI-LMS and CBC-LMS in an equalization model. The real-world signal generation and processing diagram is illustrated in Fig. 18. Firstly, an Agilent ESG Vector Signal Generator generates the source signal $s(k)$, which is a QPSK signal, 50% roll-off raised-cosine pulse-shaping, centered at 70MHz. The symbol rate is 5 MHz, yielding roughly a $5\times(1+0.5) = 7.5$ MHz signal bandwidth. The signal then passes through a 70 MHz bandpass filter channel. The amplitude response and group delay of the bandpass filter is analyzed with an Agilent E5071C Network Analyzer, and is shown in Fig. 19, along with the input signal spectrum. As can be seen from Fig. 19, the bandpass filter causes significant distortion of the input signal. This is also illustrated in Fig. 20, which shows the NEE of the unequalized signal is close to –10dB. Subsequently, the signal is received and digitized by a ZTEC Instruments ZT8441 IF Digitizer. The ZT8441 samples and digitally downconverts the input bandpass signal, creating the baseband I/Q components which are then loaded into a computer. Finally, Matlab is used to process and recover the symbols. This real-world experimentation is carried out in a low noise environment with SNR ≈ 60dB, which can be proved by the residual error shown in Fig. 20. 300 symbols are collected to test the performance of both the proposed methods and Complex BLMS. The order of the adaptive filter is set to 15 and the block size is 18. Experiments show that the best fixed step size for the Complex BLMS is 0.035 based on trial and error. The performance accuracy is measured by the error signal $e(k)$ in dB.

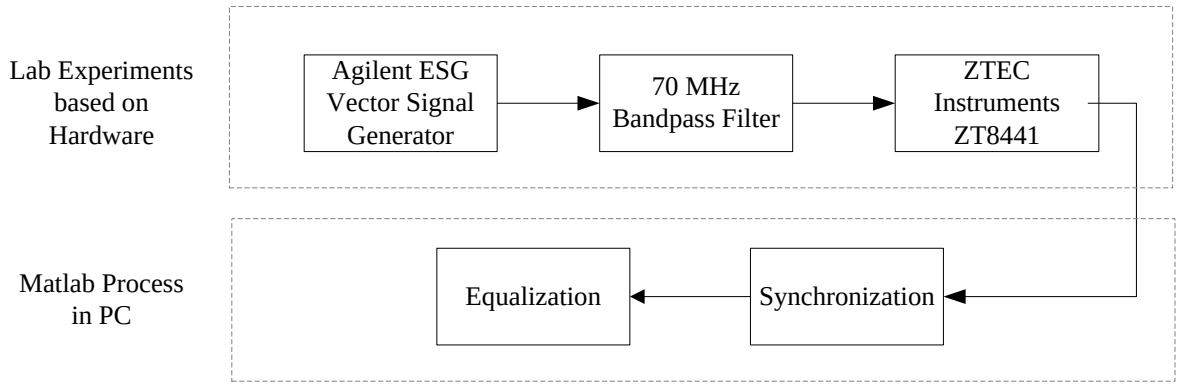

Figure 18 Block Diagram of the Real-world Laboratory Data Experiment

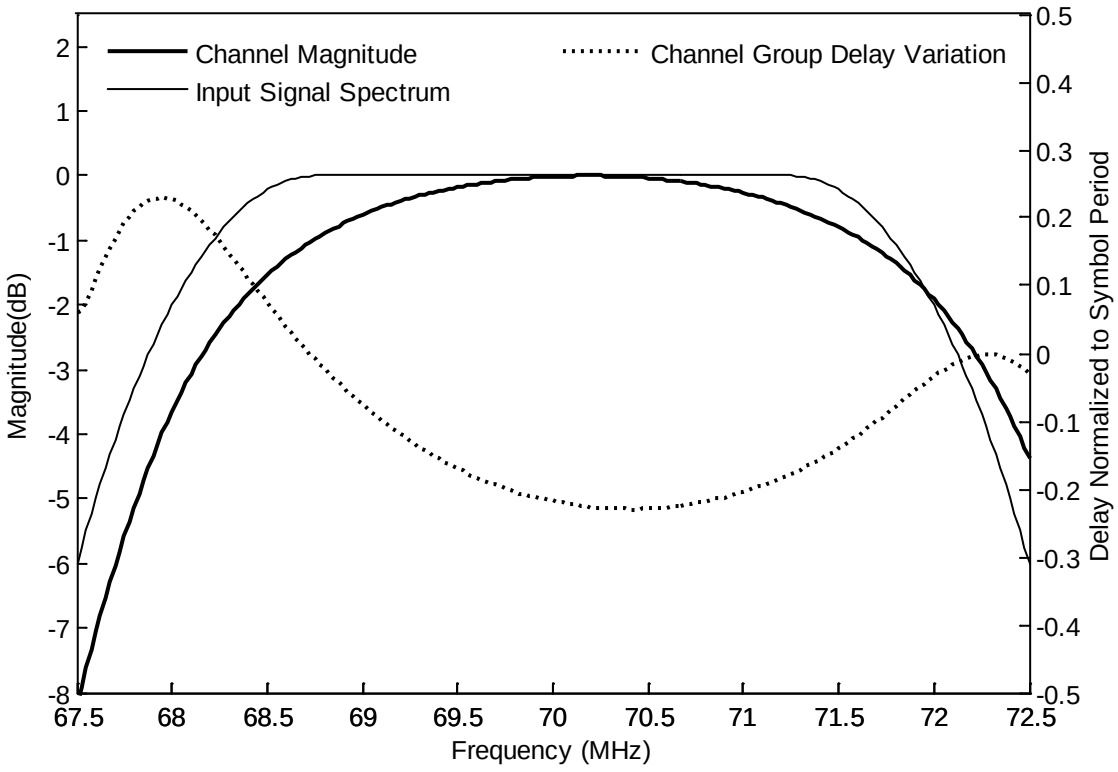

Figure 19 Input Signal Spectrum and Bandpass Filter Responses

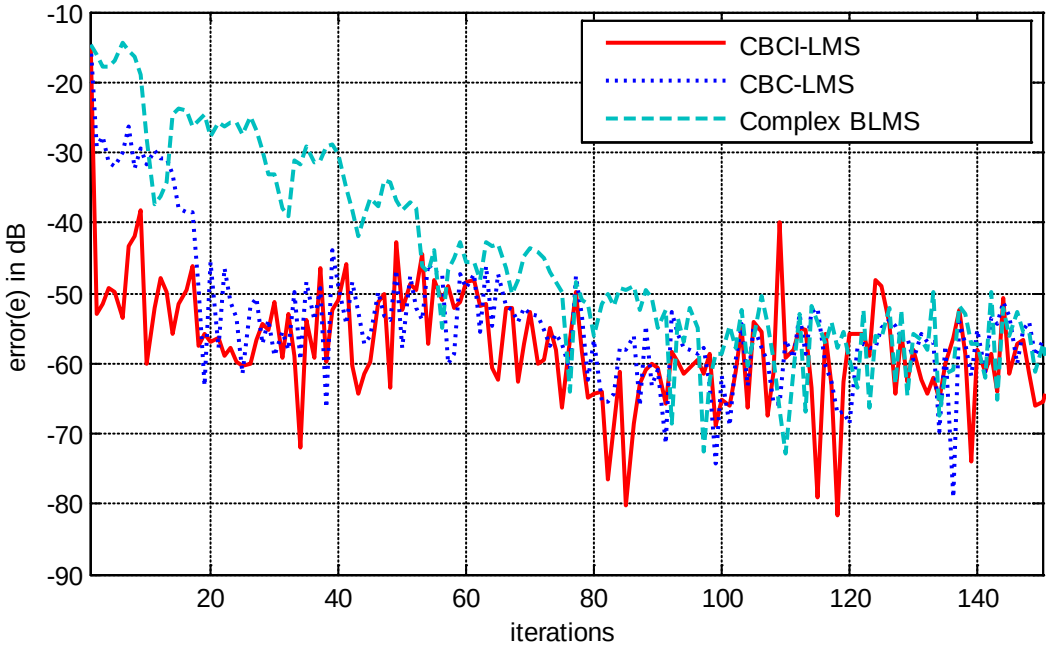

Figure 20 Error in dB vs. Iterations for Laboratory Data Experiment

In Fig 20, the error is shown as a function of the iteration index. The three methods, CBCI-LMS(1), CBC-LMS, and Complex BLMS are applied, and they yield comparable residual error after convergence. It is clear that the proposed CBCI-LMS(1) method converges immediately after adaptation, and CBC-LMS converges within 20 iterations. Both of the proposed algorithms converge much faster than 100 iterations yielded by the Complex BLMS. This further confirms the superiority of the proposed techniques in terms of convergence speed while maintaining comparable accuracy.

3.3 Implementation Issues

Implementation aspects are discussed in this subsection, including block shifting, block size selection, searching dimension parameter, and optional scaling factor. Same as the

simulation in 3.1, the input signal is complex white Gaussian signal. The adaptive filter has N = 10 coefficients for all the simulated algorithms. The coefficients of $T(z)$ are initialized to zero before adaptation. Time-invariant channel is simulated with $F(z)$ defined as in Table 5.

3.3.1 Block Shifting

The processing block for the CBCI-LMS and CBC- LMS methods generated earlier is shifted by one sample at each iteration. In this subsection, different shifting techniques are discussed. The blocks of the processing signals, $\mathbf{x}_l(k)$ in (2.2) and $d_l(k)$ in (2.4), can be either overlapping or disjoint. The shifting technique is carried out by dropping the oldest N_f signals and incorporating N_f new ones with $(L- N_f)$ overlapping signals between the previous and current blocks. N_f is the shifting window size. In other words, there are $(L- N_f)$ signals in the previous block which are reused in the current block. This is similar to the data-reusing technique discussed in [75], in which the Bi-Normalized Data-Reusing LMS (BNDR-LMS) technique improves the speed of convergence without sacrificing stability. As an illustration, the signals $\mathbf{x}_l(k)$ in (2.2) and $d_l(k)$ in (2.4) for both the CBCI-LMS and the CBC-LMS algorithms are redefined as

$$\mathbf{x}_l(k) = [x(kN_f + l - 1), x(kN_f + l - 2), \ldots x(kN_f + l - N)]^T \tag{3.6}$$

$$d_l(k) = d(kN_f + l - 1) \tag{3.7}$$

The range of N_f is from 0 to L.

It can be shown that only using the overlapping block, the CBCI-LMS algorithm can result in a recursive relation in the matrix inversion lemma given in APPENDIX. In other words, matrix inversion is not feasible when the disjoint block is used to implement CBCI-LMS.

Therefore, throughout this dissertation, overlapping block is employed for the CBCI-LMS algorithm, and $N_f = 1$ is the case investigated for the overlapping block.

The performance of the proposed algorithms using an overlapping block with $N_f = 1$, and a disjoint block with $N_f = L$, are compared in a noise free condition. The scaling factor is chosen to be 0.8 for both the algorithms, and the search dimension parameter $D = 5$. The obtained NEE is plotted in Figs 21 and 22, by both block shifting techniques with $L = 2N = 20$. Fig. 21 plots NEE vs. sample index, and Fig. 22 shows NEE vs. iteration index, for both algorithms with both block shifting techniques.

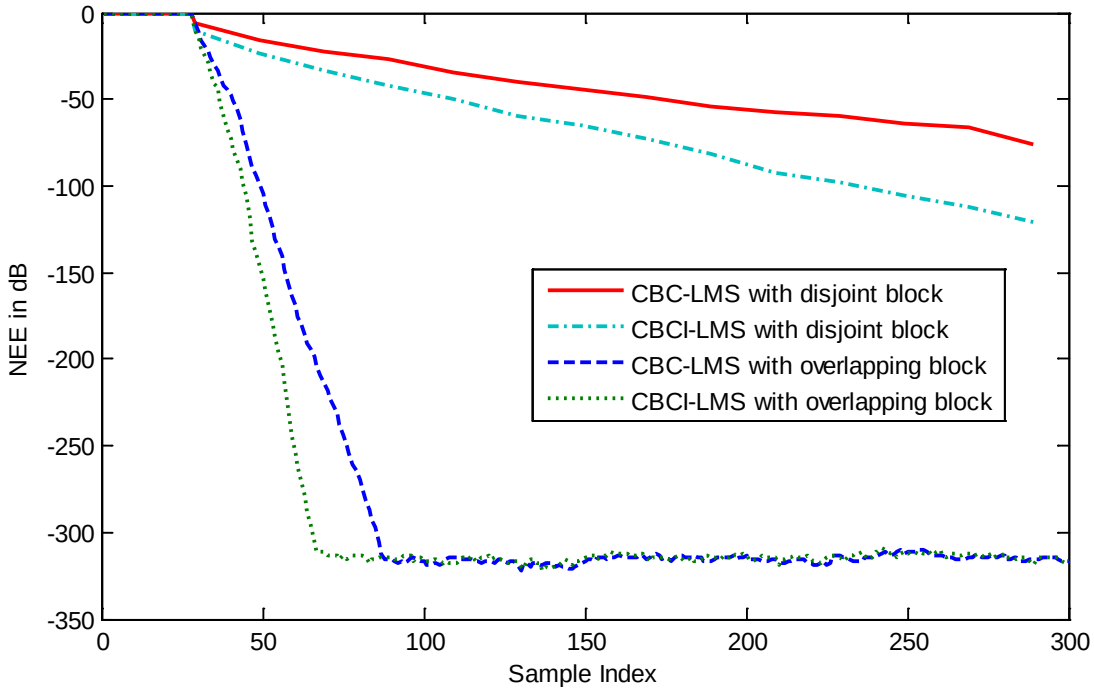

Figure 21 NEE vs. Sample Index with Disjoint and Overlapping Blocks for CBC-LMS and CBCI-LMS without Additive Noise

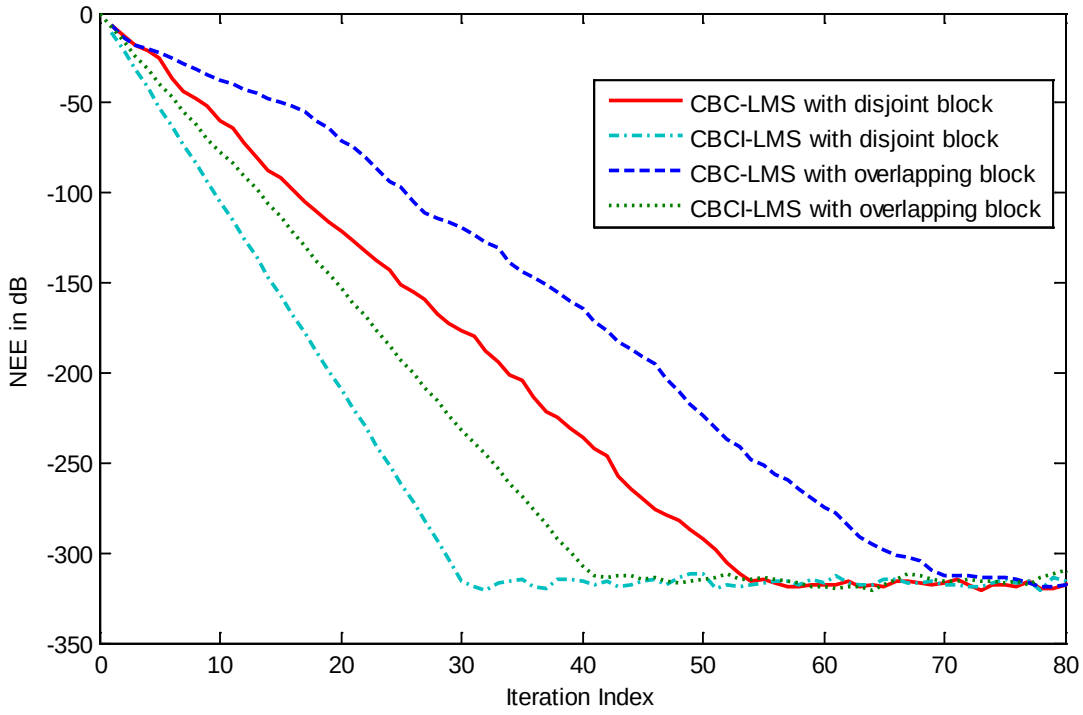

Figure 22 NEE vs. Iteration Index with Disjoint and Overlapping Blocks for CBC-LMS and CBCI-LMS without Additive Noise

An important observation is obtained from Figs 21 and 22 as follows. When the disjoint block is applied, both the algorithms require fewer iterations to achieve convergence, and thus resulting in lower computational complexity in total. The requirement of more iterations for the overlapping block is due to data redundancy. On the other hand, with an overlapping block, the algorithms require fewer samples to converge, so the actual required time is less in real-time applications. Therefore, the appropriate choice of N_f is made based on the specific performance requirements. In a system with high sample rate and slow hardware, the disjoint block is more appropriate. In contrast, if the hardware is fast enough and the fast convergence is required, e.g., to estimate a time-variant channel in a real-time system, the overlapping block is preferred.

3.3.2 Block Size

The CBCI-LMS and CBC-LMS algorithms are both block processing algorithms which use a block of data to estimate the "expectation" operator in (2.11) and (2.38). The block size is determined based on the tradeoff between the computational complexity and the performance accuracy.

If the block size L is small, the algorithm is more effective in tracking the time variation of the unknown channel. It is very important that the unknown channel parameters stay approximately constant within one processing block, which is quasi-stationary. Thus, the problem with convergence arises when the unknown channel is fast fading, in which case a large L violates the assumption of quasi-stationarity. Besides, a large block size requires large amount of computations, which increases the total computational complexity.

On the other hand, a small block size may lead to inaccurate estimation of the expected values, or even divergence, especially for the CBCI-LMS. If the block size L is equal to 1, the algorithm becomes an online sequential technique, which updates the coefficients of the adaptive filter based on the current input sample only. The sequential method eliminates the "expectation" operator, resulting in worse performance than a block processing approach.

The performance of the proposed algorithms using different block sizes with SNR=35dB is compared in terms of NEE's defined in (3.1) in Figs 23–25. The search dimension parameter $D = 5$ for the CBCI-LMS and CBC-LMS methods.

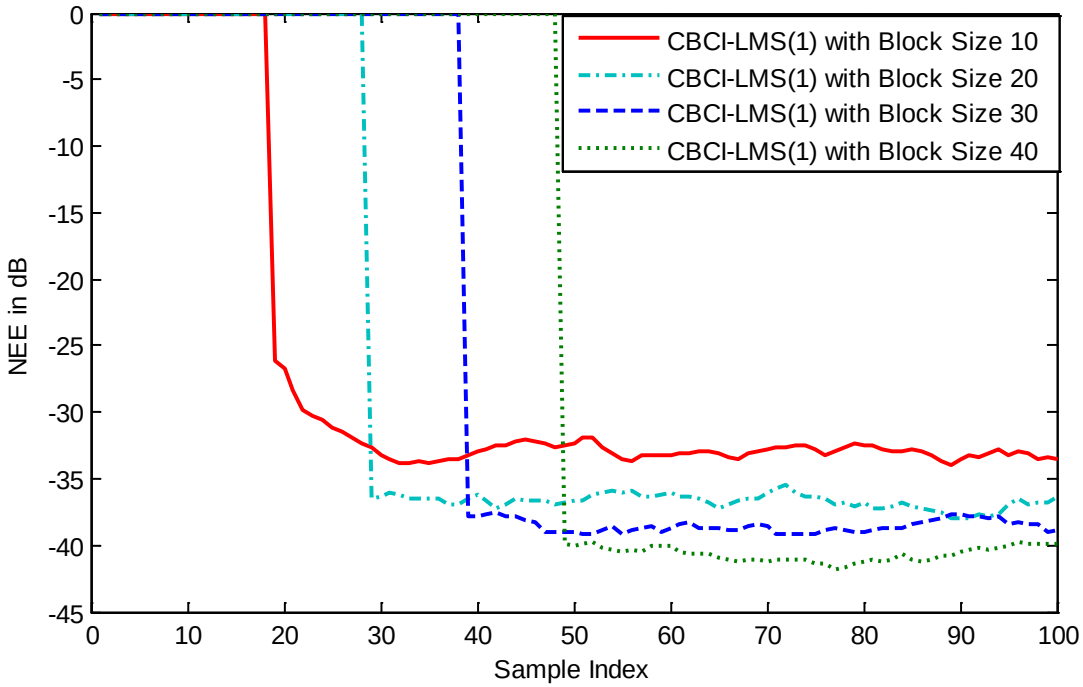

Figure 23 NEE vs. Sample Index for CBCI-LMS(1) with Different *L*

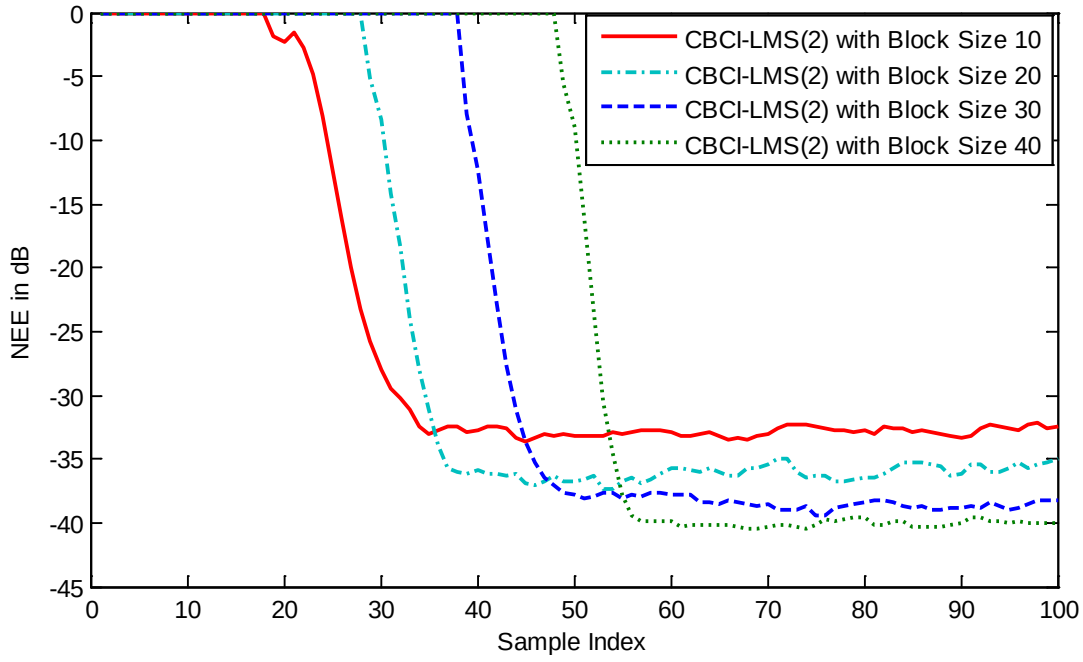

Figure 24 NEE vs. Sample Index for CBCI-LMS(2) with Different *L*

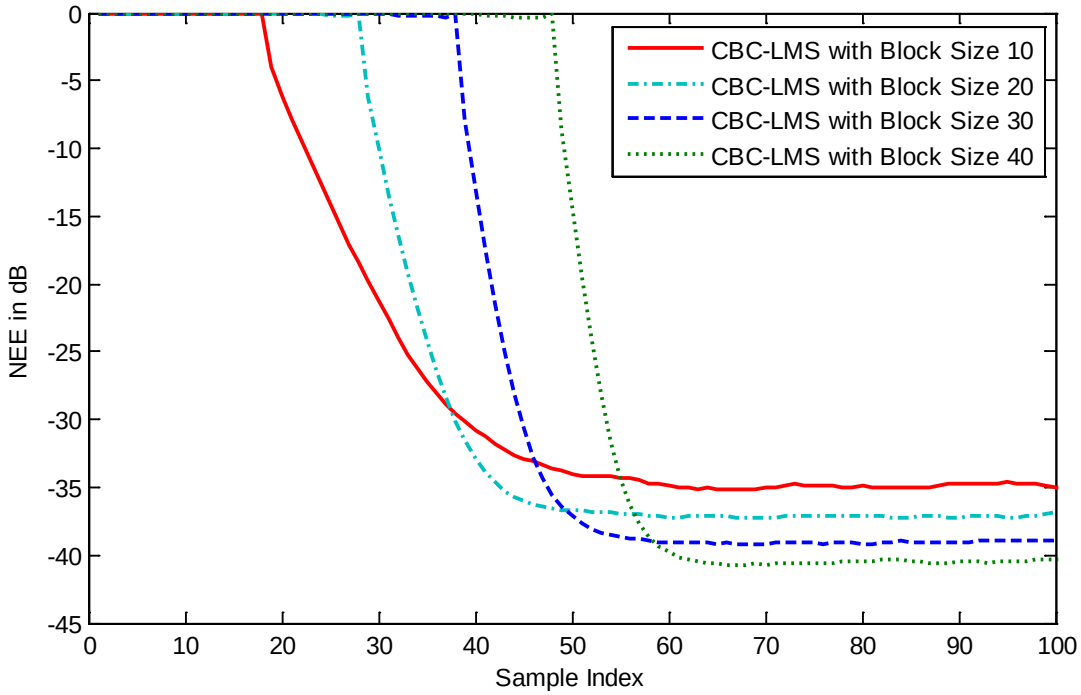

Figure 25 NEE vs. Sample Index for CBC-LMS with Different *L*

Figs 23–25 plot the NEE vs. sample index with different block sizes for CBCI-LMS(1), CBCI-LMS(2) and CBC-LMS, respectively. The input SNR is 35dB, and no scaling factor is used. It shows that the residual NEE decrease as the block size increases for all the algorithms. The reason is that both CBCI-LMS and CBC-LMS are optimal adaptive techniques involving the estimation of expectation values. Within a larger block of data, the expectation values can be estimated more accurately. This trend is more obvious for CBCI-LMS technique. Figs 24 shows that when the block size is small, the stability of the CBCI-LMS(2) decreases. That is because the correlation matrix $\mathbf{C}$ in the first iteration is estimated as a diagonal matrix $\mathbf{C}_d$, causing the estimation error. Because CBCI-LMS utilizes more degrees of freedom of the optimization space, it is more sensitive to the estimation error. All these three figures illustrate that a larger block

size requires more samples to fill in the signal processing block, which slows down the adaptation process. In this regard, a balance should be decided between the adaptation time and the accuracy required for convergence when selecting a block size. $L > N$ is found, expectedly, to have desirable convergence properties. Particularly, $L = 2N$ is always adopted.

3.3.3 Search Dimension Parameter

As mentioned in 2.1.2, D is the search dimension parameter. The valid range of D is $1 < D \leq N$. When $D = 1$, the proposed algorithms degrade to gradient based methods. When $D > N$, the adaptation uses more orthogonal directions than the actual dimensions of the system, resulting in the redundancy and high level of residual error. In this subsection, the search dimension parameter D is investigated.

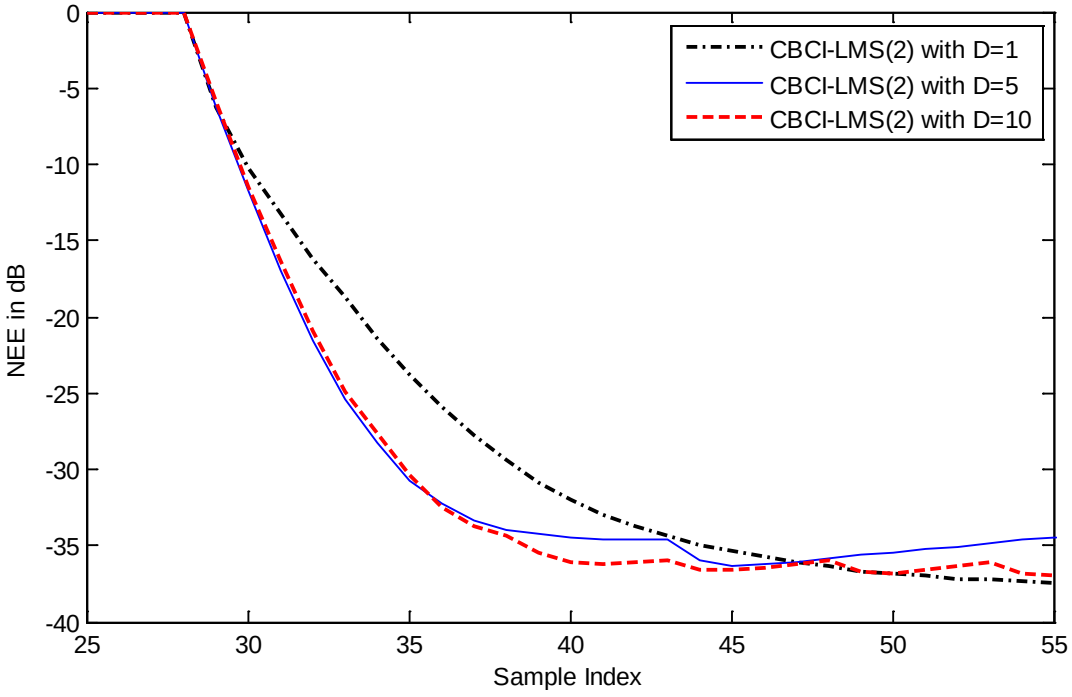

Figure 26 NEE vs. Sample Index for CBCI-LMS(2) with Different *D*

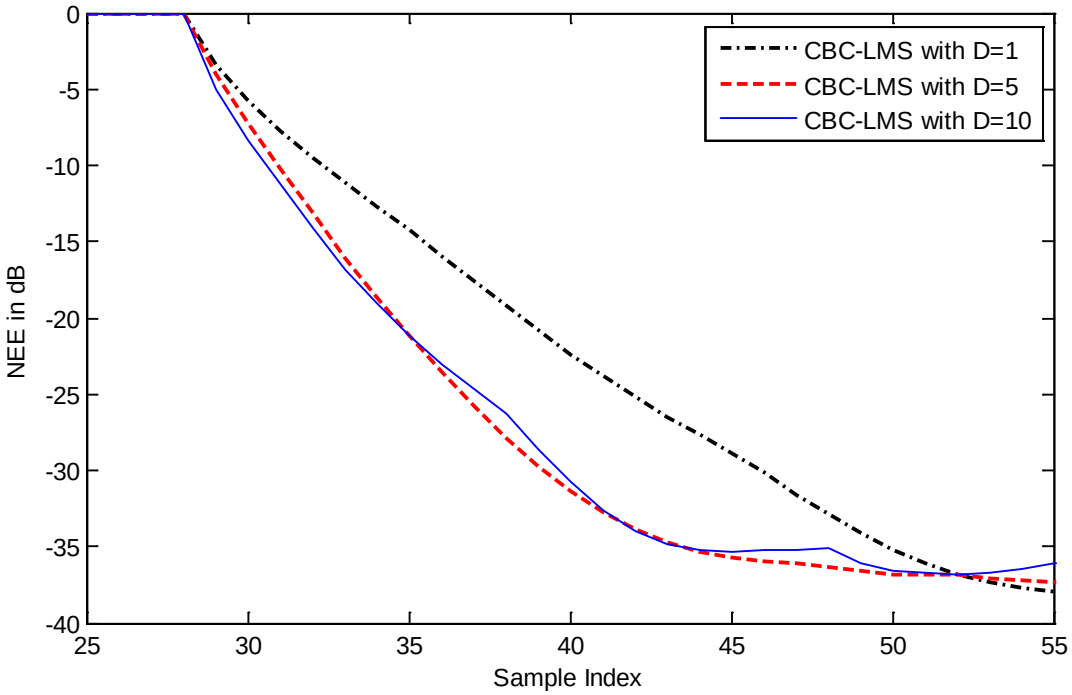

Figure 27 NEE vs. Sample Index for CBC-LMS with Different *D*

In the experiments, the complex white Gaussian noise with SNR=35dB is simulated. The block size L = 20, and the adaptive filter has N = 10 taps. Figs 26 and 27 plot the NEE vs. sample index with different D for CBCI-LMS(2), and CBC-LMS respectively. Since in this simulation setting, CBCI-LMS(1) can always converge within 1–2 iterations with different D, and thus the performance of CBCI-LMS(1) has not been investigated here.

A balance should be made between the adaptation speed and the accuracy required for convergence when selecting a search dimension parameter D. Figs 26 and 27 clearly show that when D is 5 or 10, the performance is comparable. The larger the value of D is, the higher the level of the residual error is. In this regard, $D = N/2$ is recommended to achieve fast convergence and satisfy accuracy requirement at the same time.

3.3.4 Optional Scaling Factor

In practice, it is desirable to introduce an additional adaptation parameter γ for the final weight update formula as in (2.51) and (2.60). Adding this optional scaling faction is based on two considerations. First, since both the CBCI-LMS and CBC-LMS techniques try to achieve the minimum MSE in one step, a scaling factor γ is introduced to ensure the convergence stability and enhance the adaptation performance. Second, according to the speed of the time variation, a mechanism should be available to adjust $\Delta\mathbf{w}(k)$, so that the algorithms can track the time variation regardless of the channel changing speed. The choice of γ should be made according to the convergence property and the speed of the unknown channel's time variation.

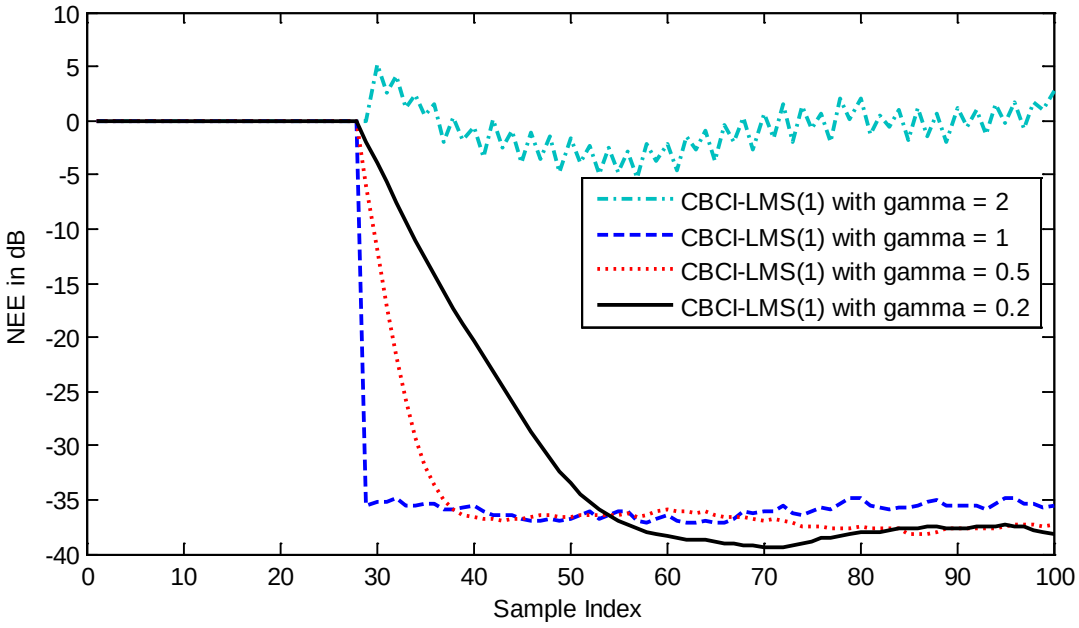

Figure 28 NEE vs. Sample Index for CBCI-LMS(1) with Different gamma

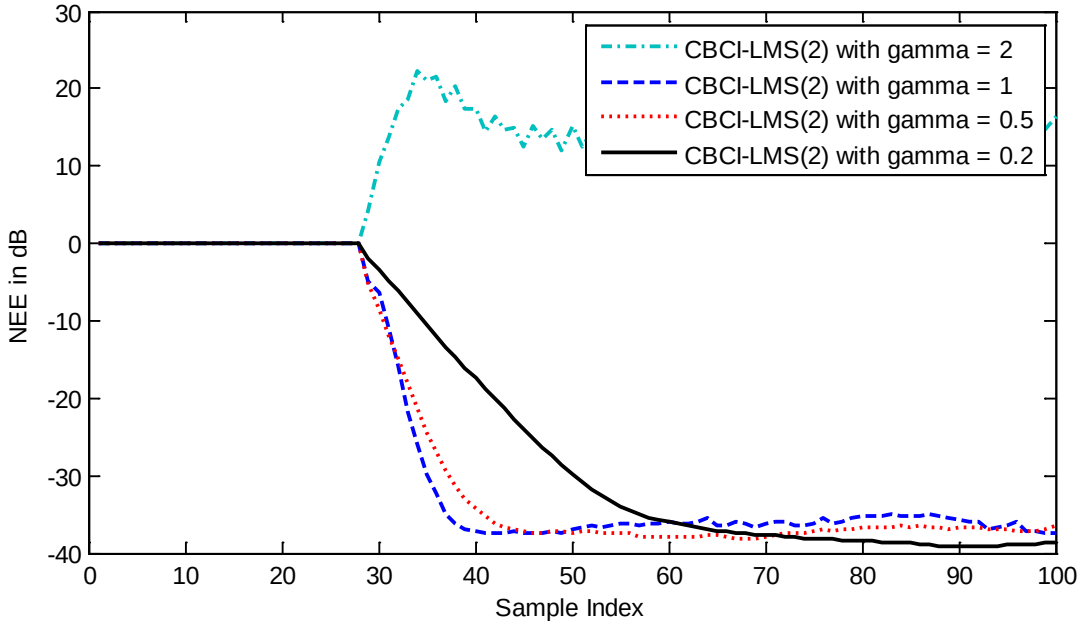

Figure 29 NEE vs. Sample Index for CBCI-LMS(2) with Different gamma

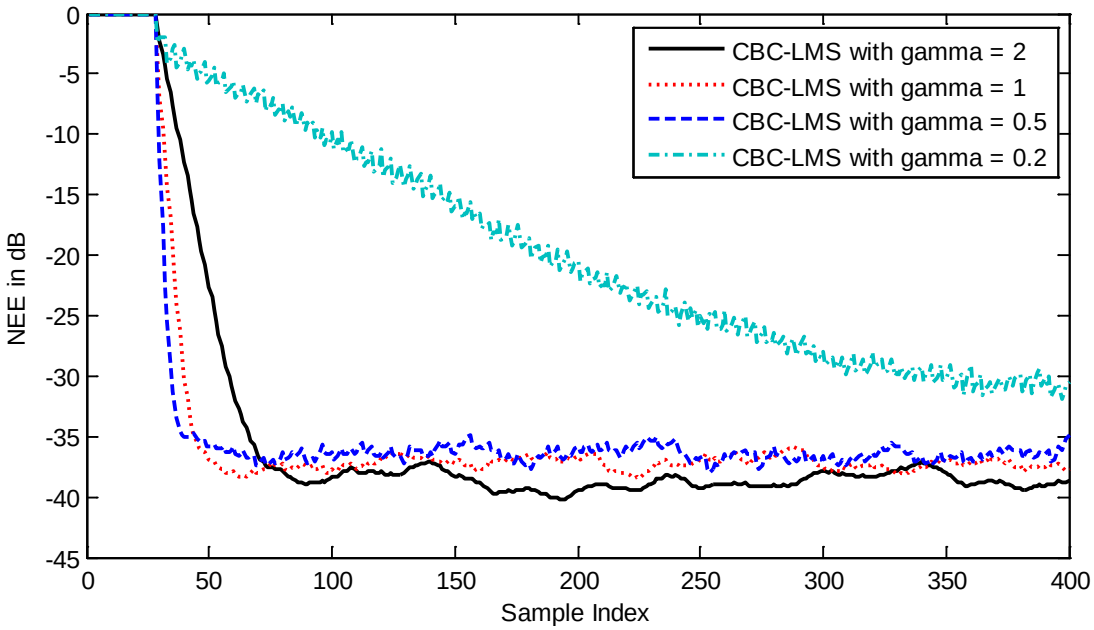

Figure 30 NEE vs. Sample Index for CBC-LMS with Different gamma

Figs 28–30 plot the NEE vs. sample index with different γ for CBCI-LMS(1), CBCI-LMS(2), and CBC-LMS, respectively. The search dimension parameter D = 5 for the CBCI-LMS and CBC-LMS methods. The block size L = 20 and the filter has N = 10 taps. When $\gamma = 2$, the CBCI-LMS(1) and CBCI-LMS(2) diverge and the CBC-LMS cannot converge to the comparable SNR value, –35dB. When γ = 0.2, 0.5, and 1, it is found out that a smaller γ results in smaller residual error but slower convergence, while a greater value of γ yields faster convergence but a higher level of error after adaptation. The optimal choice of γ varies according to the tradeoff between the performance requirement and the convergence speed. In fact, the CBCI-LMS and CBC-LMS algorithms have the capability to achieve convergence over a certain range of γ (approximately $0 < \gamma < 1.5$). From our intensive experiments, the range of 0.5–1 is recommended.

3.4 Comparison to Complex OBAI-LMS and Complex OBA-LMS

In this section, the proposed CBCI-LMS is compared to the Complex OBAI-LMS, and the proposed CBC-LMS is compared to the Complex OBA-LMS. Same as the simulation setup in 3.1.1, the input signal is complex white Gaussian signal. The search dimension parameter D = 5 for the CBCI-LMS and CBC-LMS methods. The number of adaptive filter coefficients is N = 10, and the block size is L = 20 for all the simulated algorithms. The coefficients of $T(z)$ are initialized to zero before adaptation. Time-invariant channel is simulated with $F(z)$ defined as in Table 5. All the simulation results are averaged over 100 Monte Carlo runs.

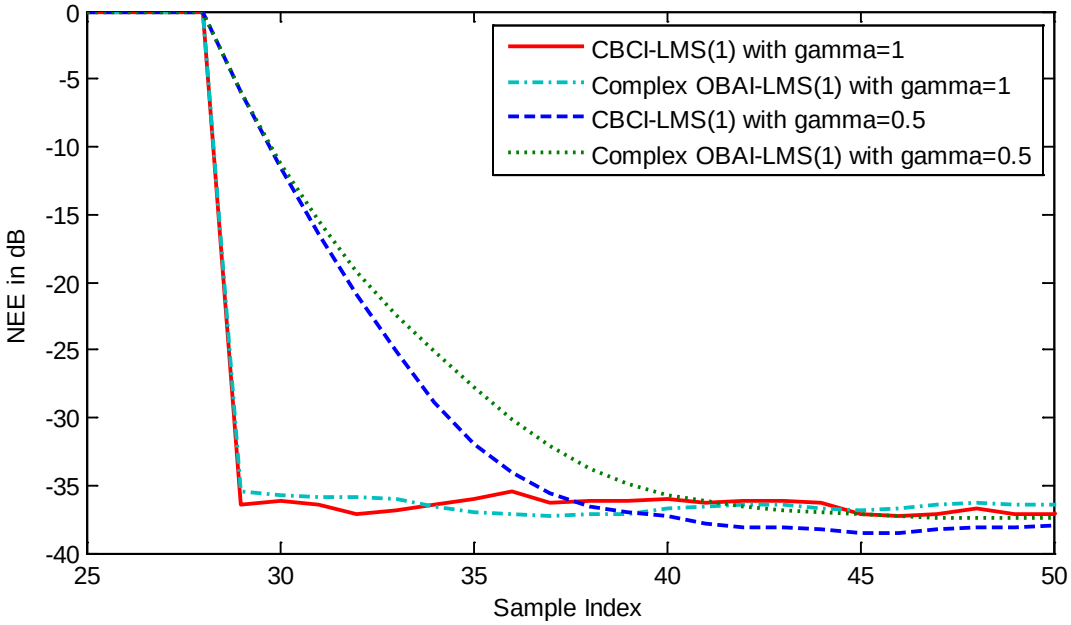

Figure 31 NEE vs. Sample Index for Comparisons of CBCI-LMS(1) and Complex OBAI-LMS(1) with Different Gamma

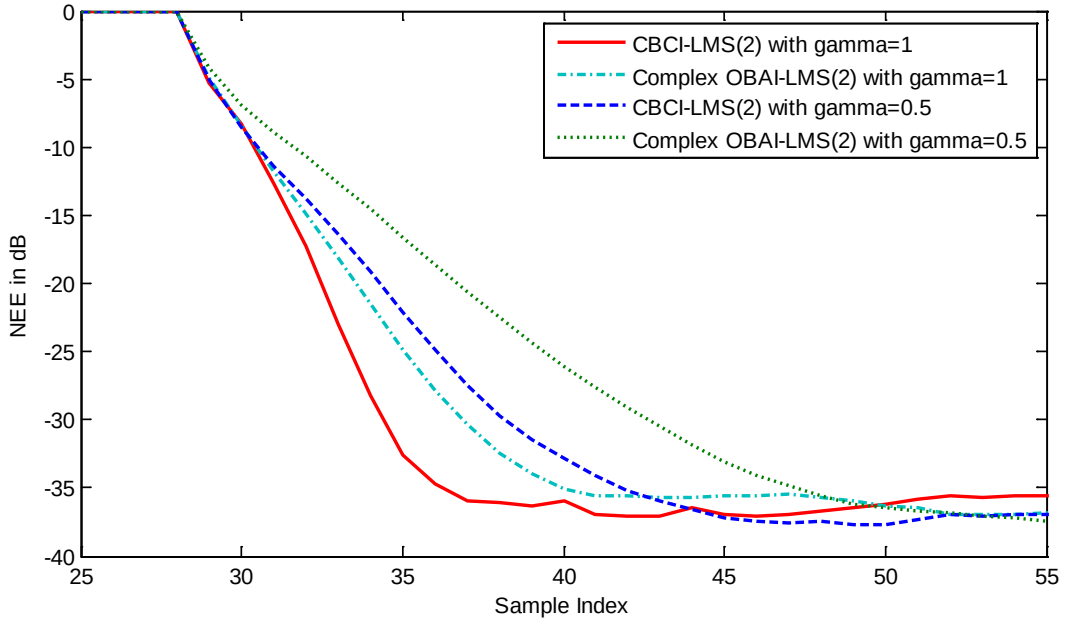

Figure 32 NEE vs. Sample Index for Comparisons of the CBCI-LMS(2) and Complex OBAI-LMS(2) with Different gamma

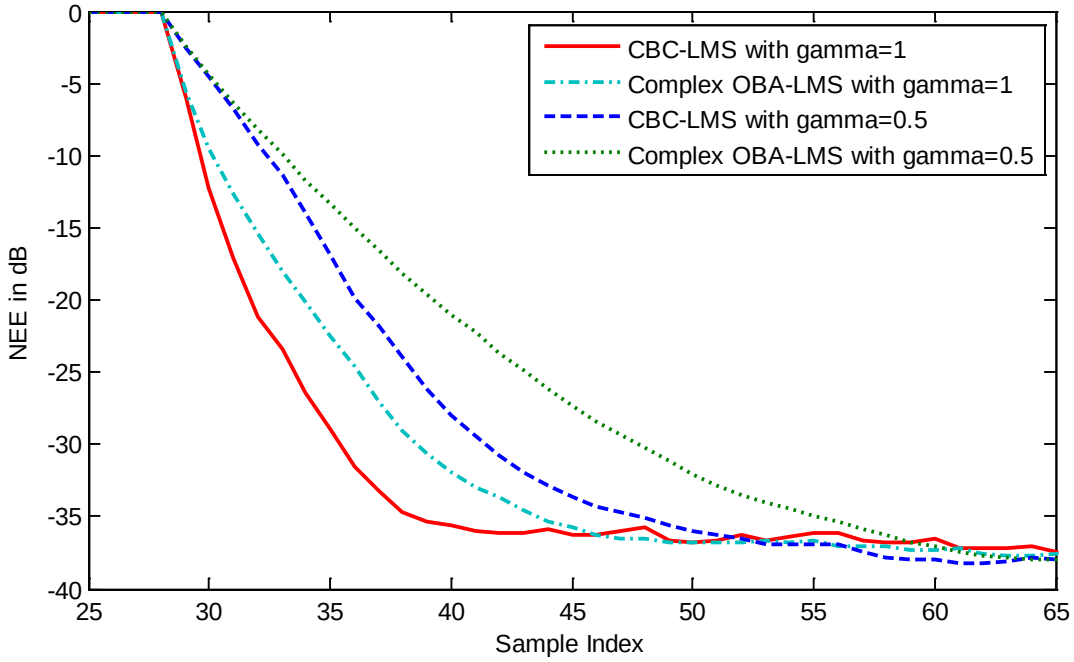

Figure 33 NEE vs. Sample Index for Comparisons of CBC-LMS and Complex OBA-LMS with Different gamma

All results from Figs 31–32 confirm that CBCI-LMS(1) and CBCI-LMS(2) demonstrate better performance than the Complex OBAI-LMS(1) and the Complex OBAI-LMS(2), respectively. From Fig. 33, the proposed CBC-LMS is compared to the Complex OBA-LMS method. In summary, the proposed algorithms improve the convergence speed and in turn require less time in adaptation than the existing algorithms, which is desirable in real-time implementations.

3.5 Conclusion

In this chapter, the performance of the CBCI-LMS and CBC-LMS has been tested in applications of channel estimation and equalization. Regarding the channel estimation, time-invariant, linear time-variant and abrupt time-variant channels are simulated. Regarding the

channel equalization, both computer simulation and real-world experiment are carried out. Several implementation issues are discussed, including the block shifting, the block size, the search dimension parameter, and the optional scaling factor. Also, the proposed techniques are compared to the Complex BLMS, the Complex OBAI-LMS and the OBA-LMS methods. The results confirm that the CBCI-LMS and CBC-LMS overcomes the drawback of the techniques with fixed step sizes and demonstrates remarkable improvement in convergence speed.

CHAPTER 4 ADAPTIVE ARRAY BEAMFORMING BASED ON PROPOSED CBCI-LMS AND CBC-LMS

In the recent decade, antenna arrays [29] frequently employ adaptive beamforming [76]–[81] for directional signal reception. Similar to other adaptive filtering problems, the LMS based algorithms [80], [81] are widely used in adaptive array beamforming. As mentioned before, the LMS algorithms are gradient descent methods and their performance depends on the appropriate choice of the step size.

In this chapter, the previously proposed complex block conjugate-gradient LMS algorithm with optimal step sizes, CBCI-LMS and CBC-LMS are applied to adaptive array beamforming.

4.1 Adaptive Array Beamforming System

An adaptive array beamforming receiver consists of a set of spatially disposed sensors or antenna elements connected to a single or multiple channel processor. Fig. 34 shows an adaptive beamformer employing N antenna elements. In this system, M user signals are transmitted from spatially separated sources at the same frequency. For the user signal m, its Angle Of Arrival (AOA) is denoted by θ_m, and its time delay at the antenna element n is denoted by $t_n(\theta_m)$. Assume $s_m(k)$ to be the signal transmitted from the user m at the time index k, and A_m to be the flat fading channel parameter for s_m.

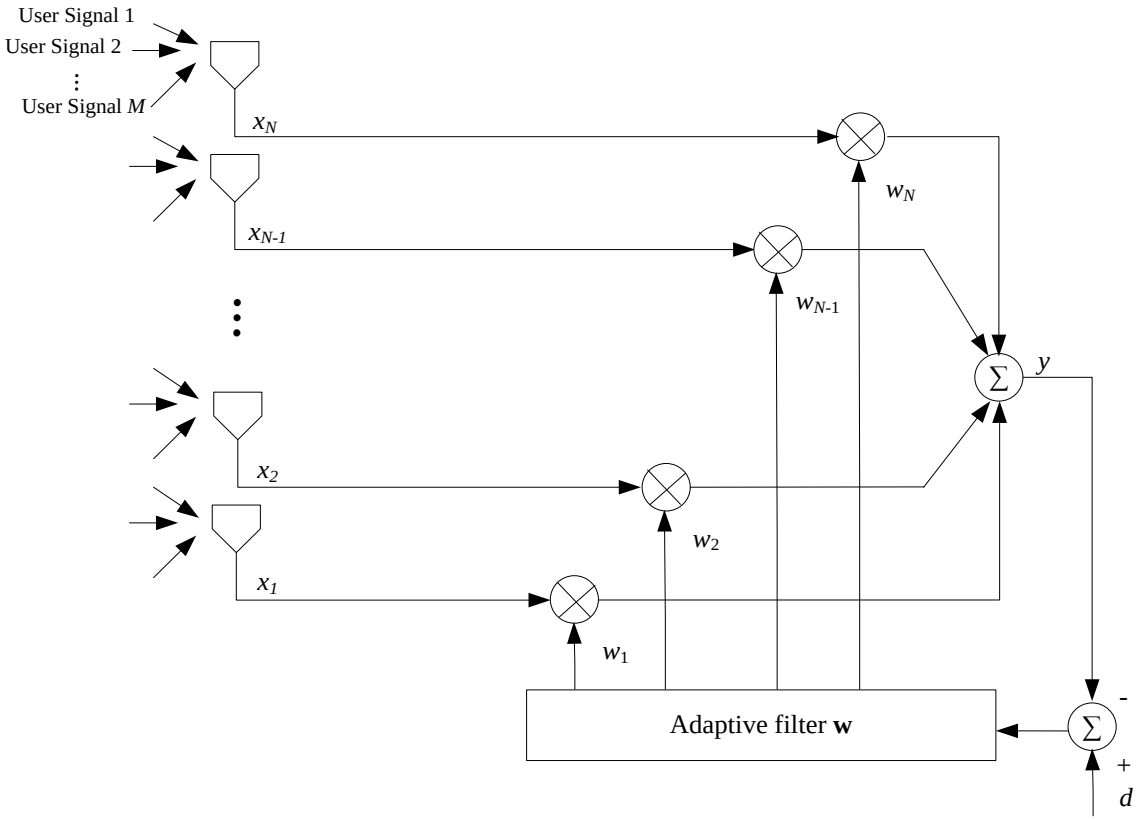

Figure 34 Adaptive Array Beamformer

All the antenna elements receive the desired and interference signals simultaneously. However, since the antenna elements are spatially separated, their outputs are different at any instant of time. The adaptive filter adjusts its weights to produce an output which is desired to resemble the wanted signal. The beamformer tries to cancel the interference signals in the system output so that the desired signal can be successfully recovered.

The received signal of the array element n, $x_n(k)$, is given by,

$$x_n(k) = \sum_{m=1}^{M} A_m s_m(k) e^{j\omega t_n(\theta_m)}, 1 \le n \le N. \tag{4.1}$$

The beamformer output is:

$$y(k) = \mathbf{w}^T(k) \cdot \mathbf{x}(k) \tag{4.2}$$

where $\mathbf{x}(k)$ and $\mathbf{w}(k)$ are the received signals and the filter weights at the time instant k, respectively, which are given by

$$\mathbf{x}(k) = [x_1(k), x_2(k), ...x_N(k)]^T \tag{4.3}$$

$$\mathbf{w}(k) = [w_1(k), w_2(k), ...w_N(k)]^T \tag{4.4}$$

Assuming user 1 is considered to be the desired user and the remaining sources are the interferers, then the Signal to Interference Ratio (SIR), for interferer m is given as

$$\text{SIR}_m = |A_1|^2 / |A_m|^2, 2 \le m \le M. \tag{4.5}$$

The error signal is formulated as the difference between the designed signal $d(k)$ and the actual signal $y(k)$, given by,

$$e(k) = d(k) - y(k) \tag{4.6}$$

The objective of the adaptive beamformer is to adjust the coefficients of the adaptive filter, so that the MSE obtained from (4.6) is minimized. Therefore, these antennas are successfully used as spatial filters to receive the desired signals coming from a specific direction by minimizing the reception of unwanted signals from other directions.

4.2 Computer Simulation

The performance of the proposed methods is compared to that of the well-known fixed step size Complex BLMS. In the simulation, M = 6 users are transmitting independent QPSK signals, and the corresponding AOA's of the user signals are shown in Table 8. The complex channel parameter A_m in (4.1) is generated randomly to ensure a thorough performance

evaluation under diverse channel conditions. The SNR is 35dB, which is typical in practice. The performance of the proposed algorithms are measured in terms of Symbol Error Rate (SER). From practical considerations, the block size is 20 for all the three algorithms. The step size of the Complex BLMS algorithm is found to be 0.01 by trial and error that gives the best results. Two sets of experiments are carried out, as follows.

Table 8 AOA of User Signals in Degrees

User *m*	1	2	3	4	5	6
AOA (degrees)	0	–45	30	–20	–10	18

In the first scenario, the randomly generated A_m yields $\mathrm{SIR}_m = 0$ dB, for all *m*. The number of antenna elements *N*, is varied between 10 and 15 elements. The SER (dB) vs. *N* achieved by the proposed CBCI-LMS(1), CBCI-LMS(2), CBC-LMS, and Complex BLMS algorithms is illustrated for QAM signal in Fig. 35 and QPSK signals in Fig. 36, respectively. The corresponding SER (dB) vs. iteration index for *N* = 15 is shown in Fig. 37 for QAM and Fig. 38 for QPSK, respectively.

In the second scenario, the $\mathrm{SIR}_m = 0$ dB for *m* =2 to 5, and $\mathrm{SIR}_6 = -6\mathrm{dB}$. The corresponding SER (dB) vs. *N* for QAM signal is illustrated in Fig. 39 and for QPSK signal in Fig. 40, respectively. Their corresponding SER (dB) vs. iteration index for *N* = 15 is shown in Figs 41 and 42**.**

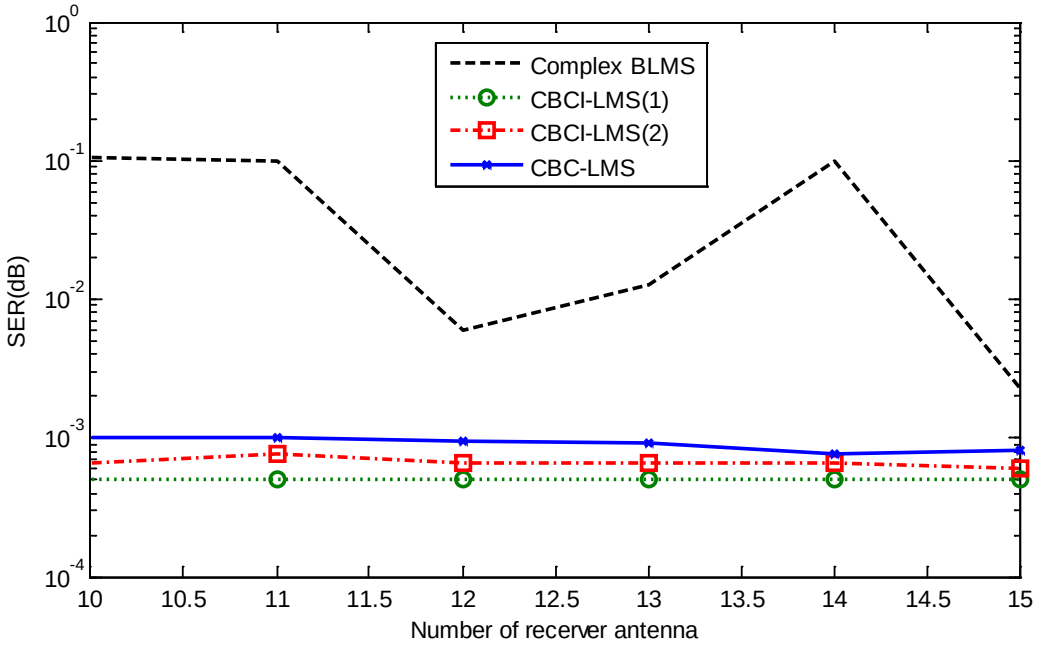

Figure 35 SER (dB) vs. Number of Receiver Antennas for QAM Signal with SIR_m = 0dB for *m* = 2 to 6

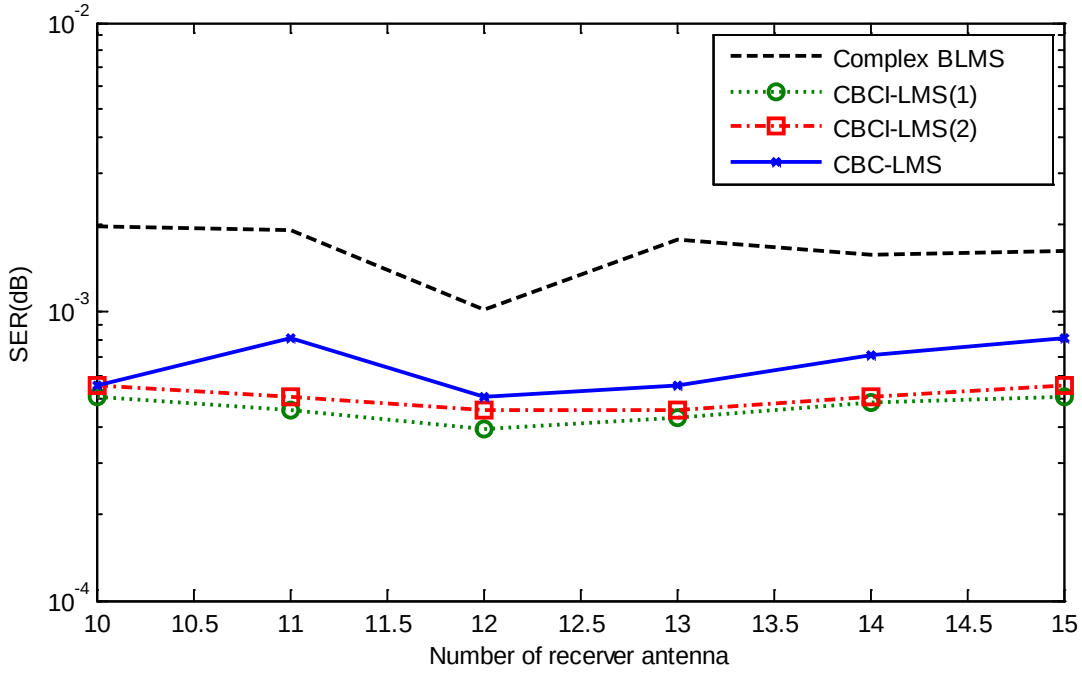

Figure 36 SER (dB) vs. Number of Receiver Antennas for QPSK Signal with SIR_m = 0dB for *m* = 2 to 6

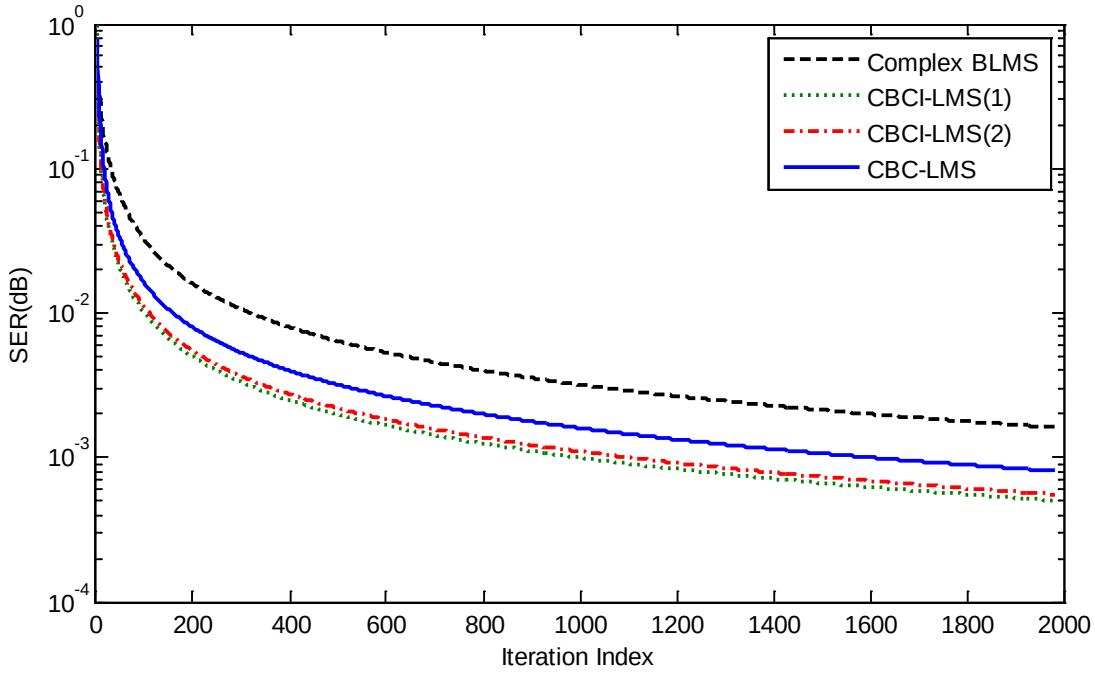

Figure 37 SER (dB) vs. Iteration Index for QAM Signal with SIR_m = 0dB for *m* = 2 to 6

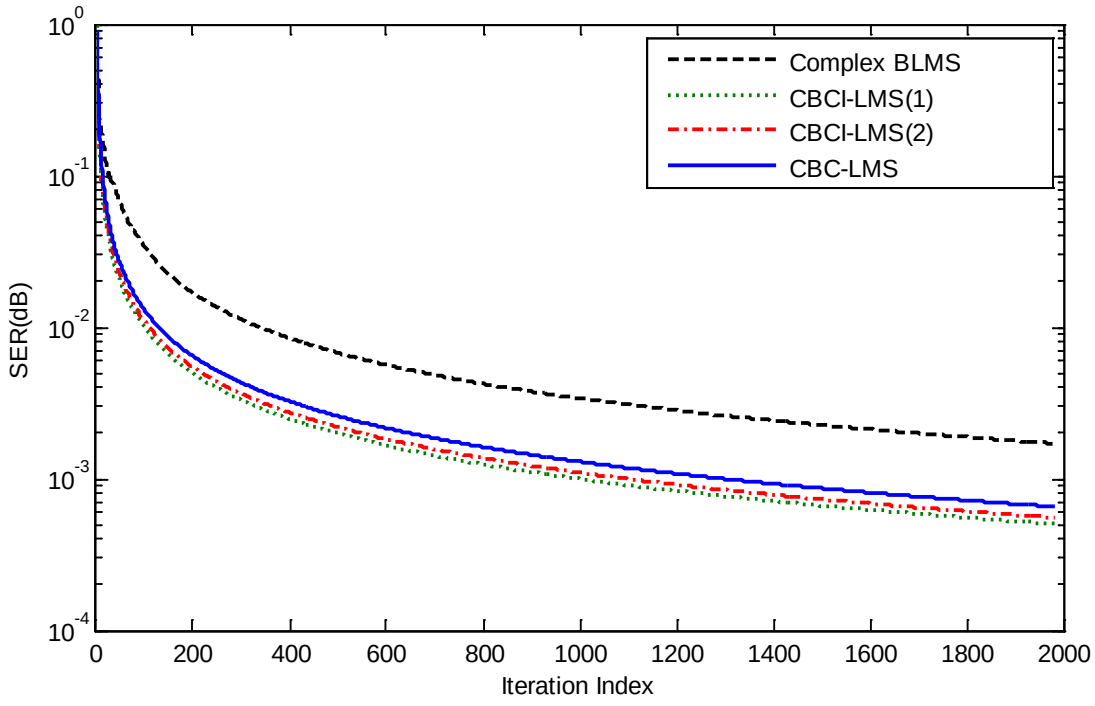

Figure 38 SER (dB) vs. Iteration Index for QPSK Signal with SIR_m = 0dB for *m* = 2 to 6

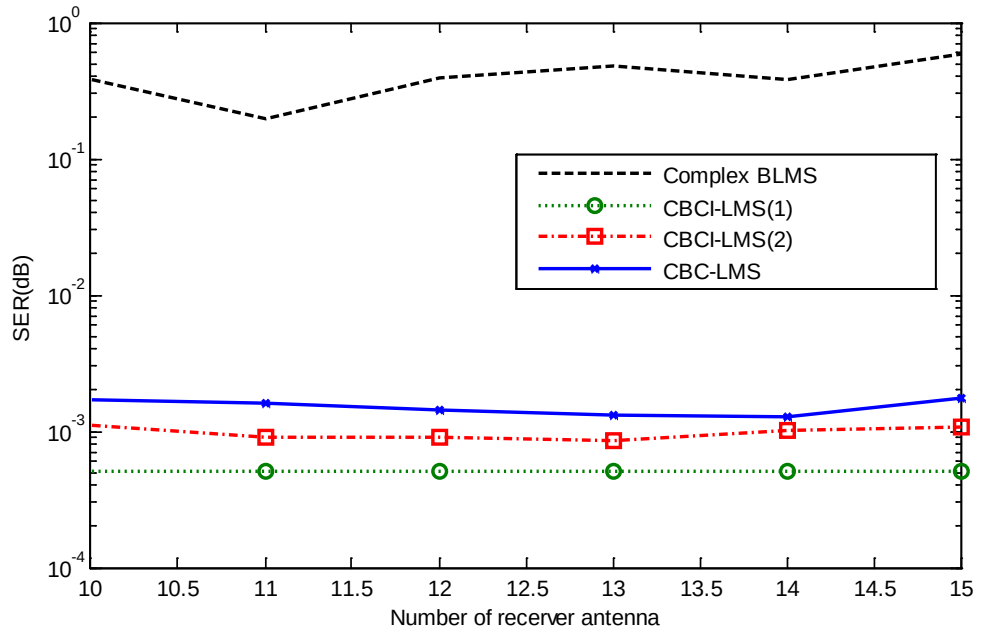

Figure 39 SER (dB) vs. Number of Receiver Antennas for QAM Signal with SIR_m = 0dB for m = 2 to 5, and SIR_6 = –6dB

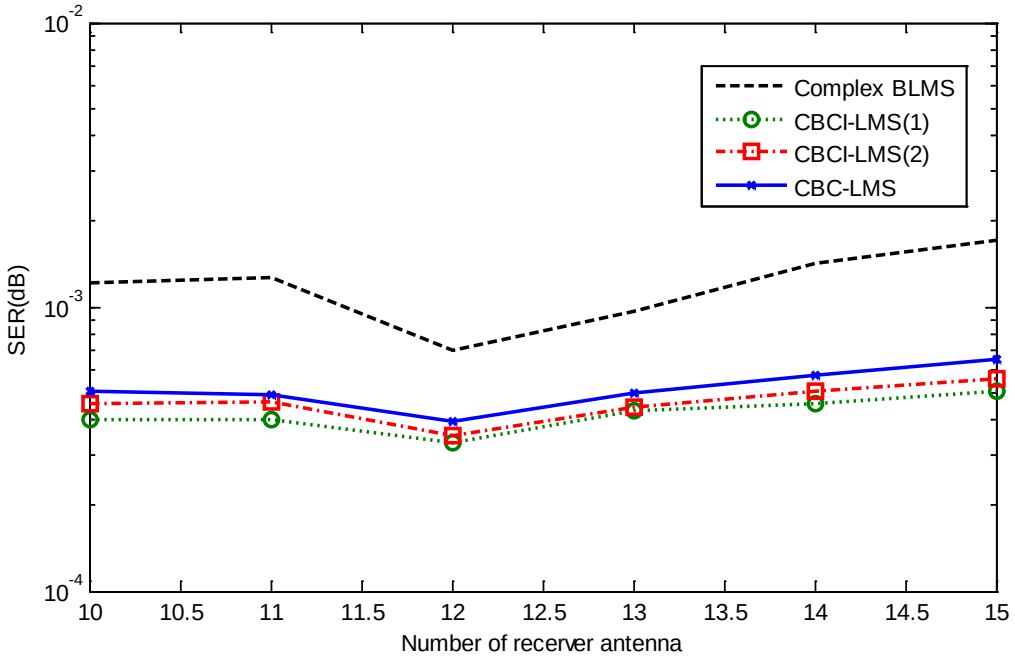

Figure 40 Number of Number of Receiver Antennas for QPSK Signal with SIR_m = 0dB for m = 2 to 5, and SIR_6 = –6dB

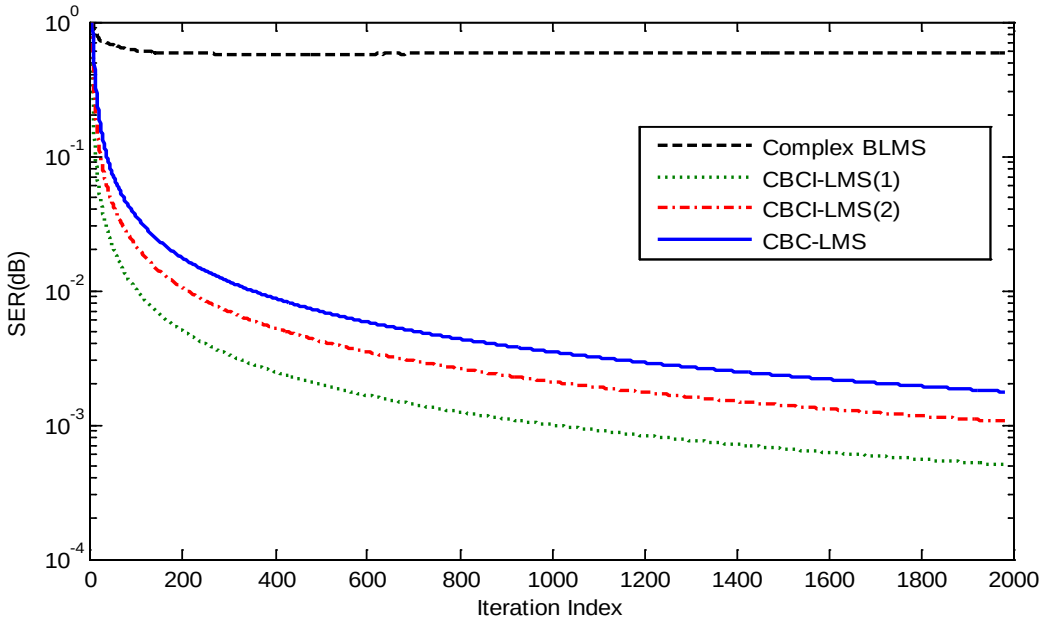

Figure 41 SER (dB) vs. Iteration Index for QAM Signal with SIR_m = 0dB for *m* = 2 to 5, and SIR_6 = –6dB

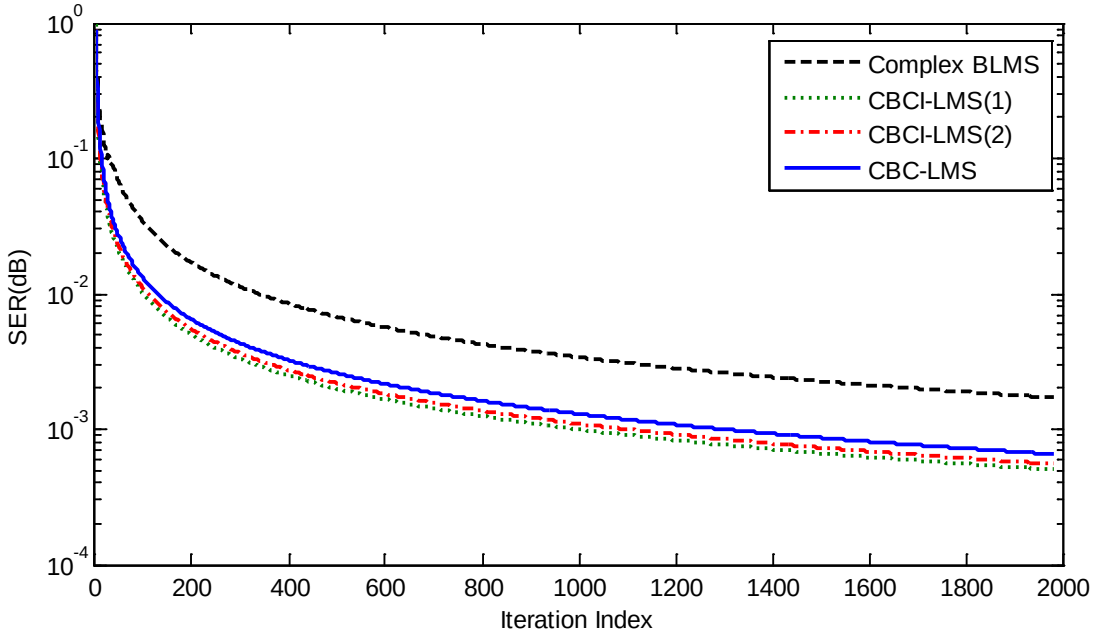

Figure 42 SER (dB) vs. Iteration Index for QPSK Signal with SIR_m = 0dB for *m* = 2 to 5, and SIR_6 = –6dB

4.3 Conclusion

Adaptive array beamforming is widely used in antenna arrays for directional signal reception. In this chapter, the two proposed adaptive FIR filtering algorithms, CBCI-LMS and CBC-LMS, are applied in adaptive array beamforming. The performance of the novel techniques is tested for varied number of receiver antenna elements, SIRs, and user signal modulations. The extensive simulation results confirm the excellent convergence speed and accuracy obtained from the proposed methods in all conditions, irrespective of SIRs, the number of antenna elements, and the type of the modulation employed by the users.

CHAPTER 5 OPTIMAL BLOCK ADAPTIVE FILTERING ALGORITHM BASED ON CIRCULARITY

Circularity and properness are important second-order statistics of a complex random variable, especially for the applications in wireless communication systems [82]–[86]. The circularity assumption of a complex communication signal is well grounded and intuitively justified, particularly in the linear I/Q modulation context. Commonly, the additive noise in a wireless system is also considered as a proper and circular signal (e.g., complex Gaussian signal), and thus it will not change the circular nature of the observed signal. However, other transceiver imperfections or interference from other signal sources may lead to noncircular observed signals. The circularity/noncircularity property of the signals can be exploited in designing wireless transceivers or array processors, such as direction of arrival algorithms, Blind Source Separation (BSS) methods [87], [88], etc. In [89], [90], techniques have been proposed to mitigate the image interference and compensate for the imperfection of a complex signal by restoring the circularity of the distorted signal.

In this chapter, an adaptive blind filtering algorithm is proposed [91]–[93] to restore the circularity of a distorted complex signal. The proposed technique is Optimal Block Adaptive filtering algorithm based on Circularity, OBA-C. Similar to [89], [90], the proposed algorithm employs the concept that under the influence of impairment in wireless communications, the received complex signal may lose its circularity. Then the proposed adaptive filtering technique compensates for the distortion. Different from [89], [90], to avoid manually selecting an appropriate step size, the presented algorithm employs the Taylor series expansion to optimally update the adaptive filter coefficients at each iteration. The proposed method fully exploits the

degrees of freedom of the optimization space, and an individual complex update is generated for each filter coefficient at each iteration.

This chapter is organized as follows. The second-order statistics of a complex signal is described in 5.1. In 5.2, the formulation of the proposed algorithm, OBA-C, is developed. The conclusion is given in 5.3.

5.1 Second-order Statistics: Properness and Circularity

In this subsection, the second-order statistics of a complex random variable, properness and circularity, are studies. In 5.1.1, the mathematical concepts of autocorrelation and complementary autocorrelation are briefly reviewed. The definitions of properness and circularity are given in 5.1.2. In 5.1.3, the proper and circular nature of a complex communication signal is studied.

5.1.1 Autocorrelation and Complementary Autocorrelation

Autocorrelation is the cross-correlation of a signal with itself. It is a mathematical tool for finding repeating patterns, such as the presence of a periodic signal which has been buried under noise, or identifying the missing fundamental frequency in a signal implied by its harmonic frequencies. It is widely used in various applications for analyzing time domain signals [94].

In statistics, the autocorrelation function of a complex signal $s(t)$, is defined as

$$R_{s(t)}(t,\tau) = E\{s(t)s^*(t-\tau)\} \tag{5.1}$$

If the signal is termed wide-sense stationary, then its mean and variance values are time-independent. In this case, the autocorrelation function only depends on the time distance between

the pair of values but not on their coordinates in timeline. This further implies that the autocorrelation can be expressed as a function of the time lag τ only, given by

$$R_{s(t)}(\tau) = E\{s(t)s^*(t-\tau)\} \tag{5.2}$$

From this point on, all signals are assumed essentially wide-sense stationary, which is reasonable expectation in practice.

To fully describe the second-order statistics, the autocorrelation is not sufficient in all cases. Therefore, the complementary autocorrelation function [95] is defined as follows,

$$C_{s(t)}(\tau) = E\{s(t)s(t-\tau)\} \tag{5.3}$$

Same as autocorrelation function $R_s(\tau)$, if a signal is wide-sense stationary, its complementary autocorrelation function $C_s(\tau)$ depends only on the time difference, τ .

5.1.2 Definitions of Properness and Circularity

In this subsection, the essential second-order statistics, properness and circularity, of a complex random signal are defined. A second-order stationary signal $s(t)$ is defined to be proper [82] if its complementary autocorrelation function equals to zero regardless of τ, i.e.,

$$C_{s(t)}(\tau) = E\{s(t)s(t-\tau)\} = 0, \forall \tau. \tag{5.4}$$

A complex random signal $s(t)$ is defined to be circular [84] if the complementary autocorrelation of the signal is equal to 0, when $\tau = 0$.

$$C_{s(t)}(0) = E\{s^2(t)\} = 0 \tag{5.5}$$

It is obvious that properness is a more general and stronger version of circularity. Proper signals are always circular, but a circular signal can be improper.

It is obvious that (5.5) cannot be established for any real-valued quantity. Generally, a complex signal $s(k)$ can be formulated as follows,

$$s(k) = s_{\mathrm{I}}(k) + j \cdot s_{\mathrm{Q}}(k) \tag{5.6}$$

where $s_{\mathrm{I}}(t)$ and $s_{\mathrm{Q}}(t)$ are the I and Q components of $s(k)$, respectively.

$s^2(t)$ can be expressed in terms of $s_{\mathrm{I}}(t)$ and $s_{\mathrm{Q}}(t)$, as follows,

$$s^2(t) = [s_{\mathrm{I}}(t) + j s_{\mathrm{Q}}(t)]^2 = s_{\mathrm{I}}{}^2(t) - s_{\mathrm{Q}}{}^2(t) + j 2 s_{\mathrm{I}}(t) s_{\mathrm{Q}}(t) \tag{5.7}$$

Substituting (5.7) into (5.5), the real and imaginary parts of $E\{s^2(t)\}$ are both equal to 0,

$$E\{s_{\mathrm{I}}{}^2(t) - s_{\mathrm{Q}}{}^2(t)\} = 0 \tag{5.8}$$

$$E\{2 s_{\mathrm{I}}(t) s_{\mathrm{Q}}(t)\} = 0 \tag{5.9}$$

From (5.8)–(5.9), the circular nature indicates that the real and imaginary components of the signal have the equal power, and they are mutually uncorrelated instantaneously. As a stronger version of circularity, properness implies that the real and imaginary parts of $s(t)$ are mutually uncorrelated for all the possible relative time shifts.

In the following, the theory of second-order statistics is developed for a discrete complex signal, $s(k)$, with the sampling interval T. Similar interpretations can be established. The autocorrelation and complementary autocorrelation of $s(k)$ are then defined respectively, as follows,

$$R_{s(k)}(\Delta) = E\{s(k) s(k-\Delta)\} = R_{s(t)}(\Delta T) \tag{5.10}$$

$$C_{s(k)}(\Delta) = E\{s(k) s(k-\Delta)\} = C_{s(t)}(\Delta T) \tag{5.11}$$

where Δ is the difference of the sample indexes.

Similar interpretations can be established as above. A discrete complex signal is defined proper if

$$C_{s(k)}(\Delta) = E\{s(k)s(k-\Delta)\} = 0, \forall \Delta . \tag{5.12}$$

A discrete complex signal is defined circular if

$$C_{s(k)}(0) = E\{s^2(k)\} = 0 \tag{5.13}$$

5.1.3 Circularity and Properness of a Communication Signal

The proper and circular nature of a discrete communication signal is investigated in this subsection. In a linear I/Q modulation scheme, the complimentary autocorrelation function of $s(k)$ is computed as,

$$C_{s(k)}(\Delta) = E\{s(k)s(k-\Delta)\} = E\{s_I(k)s_I(k-\Delta)\} - E\{s_Q(k)s_Q(k-\Delta)\}$$
$$+ jE\{s_Q(k)s_I(k-\Delta)\} + jE\{s_Q(k-\Delta)s_I(k)\} \tag{5.14}$$

If $s(k)$ is one of the most practical complex-alphabet-based communication signals, such as QAM and *M*-PSK, $s_{\mathrm{I}}(k)$ and $s_{\mathrm{Q}}(k)$ are always uncorrelated with each other [96], which yields the following two equations,

$$E\{s_{\mathrm{Q}}(k)s_{\mathrm{I}}(k-\Delta)\} = 0, \forall \Delta. \tag{5.15}$$

$$E\{s_{\mathrm{Q}}(k-\Delta)s_{\mathrm{I}}(k)\} = 0, \forall \Delta. \tag{5.16}$$

Since $s(k)$ is a wide-sense stationary signal, $s_{\mathrm{I}}(k)$ and $s_{\mathrm{Q}}(k)$ are both wide-sense stationary. The following two equations are satisfied,

$$E\{s_{\mathrm{I}}(k)s_{\mathrm{I}}(k-\Delta)\} = 0, \forall \Delta \neq 0. \tag{5.17}$$

$$E\{s_{\mathrm{Q}}(k)s_{\mathrm{Q}}(k-\Delta)\}=0,\forall\Delta\neq 0\,. \tag{5.18}$$

When $\Delta=0$, (5.8) is satisfied. Thus, it is easy to prove that

$$C_{s(k)}(\Delta)=0,\forall\Delta. \tag{5.19}$$

Therefore, the signal $s(k)$ is proper, and then it is circular for sure.

As mentioned before, the exception is real-valued modulation signals, such as Binary PSK (BPSK), and *M*-Pulse-Amplitude-Modulation (PAM), for which the complementary autocorrelation function is identical to the autocorrelation function.

5.2 Formulation of the OBA-C Algorithm

This subsection presents the OBA-C algorithm, which restores the circularity of the received signal, using an adaptive FIR filtering structure.

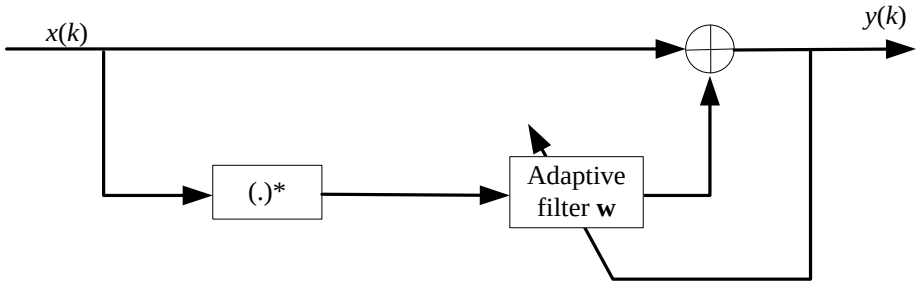

Figure 43 Proposed OBA-C Compensation Structure

A block diagram of the OBA-C compensation structure is illustrated in Fig. 43. The proposed structure employs an adaptive FIR filter, which is easy to implement in practice. After adaptation, the filter output, $y(k)$, is desired to resemble the non-mismatched signal.

Assuming the FIR filter has *N* taps, the weight vector $\mathbf{w}(k)$ and the input vector $\mathbf{x}(k)$ are given by,

$$\mathbf{w}(k) = [w_1(k), w_2(k)...w_N(k)]^T \tag{5.20}$$

$$\mathbf{x}(k) = [x(k), x(k-1)...x(k-N+1)]^T \tag{5.21}$$

The filter output, $y(k)$, can be expressed by vector manipulation as follows,

$$y(k) = x(k) + \mathbf{w}^T(k)\mathbf{x}^*(k) \tag{5.22}$$

The Discrete-Time Fourier Transform (DTFT) of $y(k)$, is given by,

$$Y(f) = X(f) + W(f) \cdot X^*(-f) \tag{5.23}$$

where $X(f)$ and $X^*(-f)$ are the DTFT of $x(k)$ and $x^*(k)$, respectively, and $W(f)$ is the frequency response of the adaptive filter.

The compensation scheme is now reduced to finding a blind update rule for the adaptive filter coefficients, $\mathbf{w}(k)$. The idea is to force the output of the compensator to regain the circular nature at next iteration. In other words, the complementary autocorrelation function defined in (5.13) should be satisfied for $s(k+1)$, as follows,

$$C_{y(k+1)}(0) = E\{y^2(k+1)\} = 0 \tag{5.24}$$

Employing the Taylor series expansion, $y^2(k+1)$ can be expressed in terms of $y^2(k)$ and $w_n(k)$, as follows,

$$y^2(k+1) = y^2(k) + \sum_{n=1}^{N} \frac{\partial y^2(k)}{\partial w_n(k)} \Delta w_n(k) + \sum_{m=1}^{N}\sum_{l=1}^{N} \frac{\partial^2 y^2(k)}{\partial w_m(n)\partial w_l(n)} \Delta w_m(n)\Delta w_l(n) + ...$$

$$\approx y^2(k) + \sum_{n=1}^{N} \frac{\partial y^2(k)}{\partial w_n(k)} \Delta w_n(k) \tag{5.25}$$

where $\Delta w_n(k) = w_n(k+1) - w_n(k), n = 1,2,...,N.$ (5.26)

The second and higher order derivative terms can be omitted if $\Delta\mathbf{w}(k)$ is controlled to be sufficiently small. By substituting (5.25) into (5.24), $C_{y(k+1)}(0)$ can be expressed as,

$$\begin{aligned} C_{y(k+1)}(0) &\approx E\{y^2(k)\} + \sum_{n=1}^{N} \frac{\partial E\{y^2(k)\}}{\partial w_n(k)} \Delta w_n(k) \\ &= E\{y^2(k)\} + \Delta\mathbf{w}^T(k) \cdot E\{2y(k) \cdot \mathbf{x}^*(k)\} \end{aligned} \tag{5.27}$$

Therefore, $\Delta\mathbf{w}(k)$ is obtained as follows,

$$\Delta\mathbf{w}^T(k) = -E[y^2(k)] \cdot \{E[2y(k) \cdot \mathbf{x}^*(k)]\}^+ \tag{5.28}$$

where $\{.\}^+$ denotes the pseudo-inverse.

From linear algebra, the pseudo-inverse A^+ can be implemented in two ways [97]: left inverse and right inverse. If the matrix A has dimensions $M \times N$, then the left inverse is implemented if $M > N$, and right inverse if $M < N$. Here, $E[2y(k) \cdot \mathbf{x}^*(k)]$ in (5.28) is a $N \times 1$ ($N > 1$) vector, and thus the left inverse is carried out, as follows,

$$A^+ = (A^H A)^{-1} A^H \tag{5.29}$$

In (5.28), $\{E[2y(k) \cdot \mathbf{x}^*(k)]\}^+$ is a $1 \times N$ vector and $E[y^2(k)]$ is a scalar, thus the resulting $\Delta\mathbf{w}^T(k)$ is a vector with size $1 \times N$.

The final update formula of the adaptive filter coefficients is

$$\begin{aligned} \mathbf{w}(k+1) &= \mathbf{w}(k) + \gamma \cdot \Delta\mathbf{w}(k) \\ &= \mathbf{w}(k) - \gamma \cdot E[y^2(k)] \cdot (\{E[2y(n) \cdot \mathbf{x}^*(n)]\}^+)^T \end{aligned} \tag{5.30}$$

where γ is an optional scaling factor to further optimize the algorithm performance and to compensate for dropping the higher order derivative terms in (5.25).

It can be inferred from (5.24), that the expectation operator cannot be ignored. Otherwise the recovered signal will approach 0 after convergence, which is obviously incorrect. To estimate the expectation values, a block processing technique is chosen instead of an iterative technique. In a block processing algorithm, the expectation values, $E\{y^2(k)\}$ and $E[2y(k)\cdot\mathbf{x}^*(k)]$ in (5.28) can be approximated by the average over a block of samples. The block size is determined based on the tradeoff between the computational complexity and the performance accuracy. A large block size requires large amount of computations while a small block size may lead to inaccurate estimation of the expected values. Further analysis of the scaling factor and the block size will be presented in Chapter 6.

In summary, the proposed OBA-C I/Q mismatch compensation algorithm with a block size L is described as follows.

1) *Initialize*

   Start with $k = 0$; $\mathbf{w}(k) = 0$.

2) *Calculate the recovered signal* $y(k)$,

   $$y(k) = x(k) + \mathbf{w}^T(k)\mathbf{x}^*(k).$$

3) *Estimate* $E[2y(k)\cdot\mathbf{x}^*(k)]$ *within the block*

   $$A(k) = E[2y(k)\cdot\mathbf{x}^*(k)] \approx \frac{1}{L}\cdot\sum_{l=0}^{L-1} y(k-l)\cdot\mathbf{x}^*(k-l).$$

4) *Compute the pseudo inverse of* $E[2y(k)\cdot\mathbf{x}^*(k)]$

   $$A^+ = (A^H A)^{-1} A^H.$$

5) *Estimate* $E[y^2(k)]$ *within the block*

$$E[y^2(k)] \approx \frac{1}{L} \cdot \sum_{l=0}^{L-1} y^2(k-l) .$$

6) Update $\mathbf{w}(k+1)$

$$\mathbf{w}(k+1) = \mathbf{w}(k) - \gamma \cdot E[y^2(k)] \cdot (\{E[2y(n) \cdot \mathbf{x}^*(n)]\}^+)^T$$

7) Check the convergence of the algorithm

Calculate the Euclidean distance of the performance measurement at iterations k and k+1. If this distance is less than a threshold value ε, terminate the adaptation; otherwise, $k = k$+1, and go back to Step *2*.

5.3 Conclusion

This chapter introduces the essential second-order statistics of a complex signal, and gives the formulation of the OBA-C algorithm. The proposed OBA-C is a novel FIR filtering algorithm, which utilizes the circular nature of the ideal baseband signal. To avoid manually selecting a step size, this technique exploits complex Taylor series expansion to guide the update of the adaptive filter coefficients at each iteration. The proposed technique fully exploits the degrees of freedom of the optimization space, in order to improve the convergence speed.

CHAPTER 6 IQ MISMATCH COMPENSATION EMPLOYING OBA-C IN PRACTICAL WIRELESS RECEIVERS

As mentioned in Chapter 1, wireless systems frequently employ the quadrature relationship between a pair of signals to effectively develop compact, yet flexible multimode radio systems. The quadrature receivers use two independent channels to form the in-phase and the quadrature-phase components of the received signal. Each channel, at a minimum, consists of a mixer, a Low Pass Filter (LPF), an amplifier and an ADC.

However, there are still big challenges ahead before I/Q downconversion principle can be applied to receive signals with high dynamic range. These challenges mainly stem from the imperfections of the analog components in the I and Q branches of the receiver FE, which is called I/Q imbalance problem [23], [28], [40]. The problem is cause by the amplitude and phase imbalances between the characteristics of the I and Q branches. These mismatches are unavoidable and limit the image frequency attenuation in practical receivers.

The I/Q imbalance problem has received considerable attention in the past decade. Research on DSP-based, both blind and data-aided I/Q imbalance compensation techniques continues to receive significant attention [89]–[90], [98]–[103]. Most of the reported work focuses on *frequency-independent* I/Q imbalance compensation in specific receiver architectures [23], [28], [98], [99] and assumes certain modulation schemes possibly combined with training data. In narrowband wireless transmission, the I/Q imbalance parameters can indeed be modeled as a gain and a phase imbalance scalars. However, in modern wideband communications, the analog FE is often frequency dependent. Therefore, the I/Q imbalance has to be modeled as the difference between the impulse responses of the I and the Q branches.

The techniques proposed in [89], [90], [100]–[103] are able to compensate for *frequency-dependent* I/Q imbalances. In [100], the pilot data is assumed to be known in advance. The method in [101] is based on the ICA, but a reference signal is still required to resolve the ambiguity issue of the ICA output signal. Recently, blind approaches were proposed to solve the frequency-dependent I/Q imbalance problem based on circularity [89], [90], [102], [103]. These iterative algorithms depend on a critical parameter, namely, the step size, to adaptively adjust the filter coefficients. These methods have their limitations of slow convergence and dependence on the proper choice of the step size according to different signal types and mismatch levels. Furthermore, an inappropriate step size may lead to divergence. Regarding the convergence speed, the method in [89] requires at least 15,000 samples to converge to an acceptable compensation level. This technique was modified in [90] by adding an optional scaling factor to improve performance. However, the modified algorithm requires 40,000–50,000 samples to reach steady state. Another algorithm was proposed in [90] based on a moment estimator, which uses 50,000 received samples, as reported in the simulations of [90]. Compared to [89], the technique in [102] uses 30,000 samples, with much higher computational complexity at each iteration. The algorithm in [103] utilizes the Constant Modulus Algorithm (CMA) method to compensate for the signal in the frequency domain for OFDM receivers. The principal of this algorithm can be considered as the circularity-based method implemented in the frequency domain. This approach needs more time-domain samples, compared with the algorithms in [89], [90], and [102]. In the computer simulations reported in [103], 4,000 OFDM symbols processed with 64-point FFT require 256,000 samples, regardless of the guard interval.

In this chapter, the proposed non-data-aided algorithm, OBA-C, is applied to solve the frequency-dependent I/Q mismatch problem. Computer simulations are carried out to investigate the performance of the OBA-C for practical mismatch levels. The simulation results illustrate that the OBA-C converges in 4000 samples with a 3-tap compensator, and in only 100 samples with a 1-tap filter. In addition, OBA-C is shown to be robust against different I/Q mismatch levels in analog components.

This chaptrer is organized as follows. Section 6.1 presents the basic I/Q signal model under frequency-dependent I/Q imbalance. In 6.2, the performance of the OBA-C is evaluated under practical mismatch levels. Section 6.3 discusses the implementation issues and 6.4 analyzes the effects of practical impairments. Finally, conclusion is drawn in 6.5.

6.1 Frequency-dependent I/Q Imbalance

In this subsection, the frequency-dependent I/Q imbalance is studies. In 6.1.1, a mathematical I/Q mismatch model is developed. The ideal solution for I/Q compensation scheme is derived in 6.1.2. In 6.1.3, the circularity of the ideal, the mismatched, and the recovered signals is investigated.

6.1.1 Mathematical Representations of the I/Q Mismatch Model

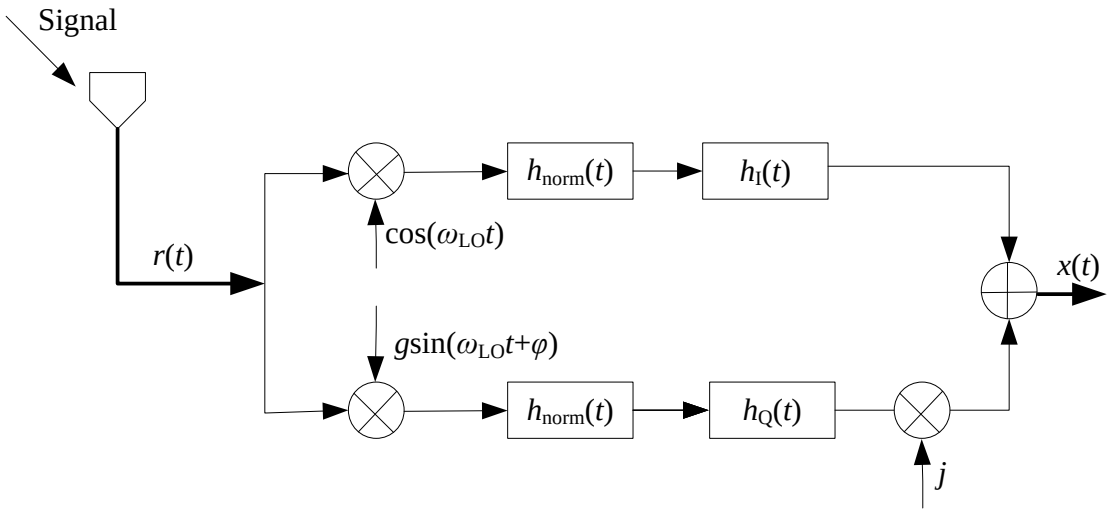

Figure 44 Generalized I/Q Imbalance Model for the Analog FE

Fig. 44 is the mathematical model of a quadrature receiver with I/Q imbalance. $r(t)$ is the received RF signal, and $x(t)$ is the complex mismatched signal. A major source of I/Q imbalance is the Local Oscillator (LO). The non-ideal LO's generate the signals $\cos(\omega_{\mathrm{LO}}t)$ and $g \cdot \sin(\omega_{\mathrm{LO}}t + \varphi)$, where ω_{LO}, g, and φ are the radian frequency, the amplitude imbalance, and the phase imbalance, respectively. Another I/Q imbalance source is the non-ideal channel characteristics of the I and the Q branches. In Fig. 44, $h_{\mathrm{norm}}(t)$ denotes the ideal nominal impulse response of all the other analog components, (e.g., LPF, amplifier, etc.) while $h_{\mathrm{I}}(t)$ and $h_{\mathrm{Q}}(t)$ model the non-ideal channel characteristics of the I and Q branches, respectively.

From Fig. 44, the observed I/Q signal can be expressed as

$$x(t) = h_{\mathrm{norm}}(t) * [h_{\mathrm{I}}(t) * r(t)\cos(\omega_{\mathrm{LO}}\mathrm{t}) + j \cdot h_{\mathrm{Q}}(t) * r(t) \cdot g\sin(\omega_{\mathrm{LO}}\mathrm{t} + \varphi)] \tag{6.1}$$

Assume $z(t)$ to be the non-mismatched desired signal, formulated as a complex variable,

$$z(t) = z_{\mathrm{I}}(t) + j \cdot z_{\mathrm{Q}}(t) \tag{6.2}$$

The in-phase and quadrature-phase components of $z(t)$, $z_{\mathrm{I}}(t)$ and $z_{\mathrm{Q}}(t)$, are given by the following two equations, respectively,

$$z_{\mathrm{I}}(t) = h_{\mathrm{norm}}(t) * r(t)\cos(\omega_{\mathrm{LO}}\mathrm{t} + \theta) \tag{6.3}$$

$$z_{\mathrm{Q}}(t) = h_{\mathrm{norm}}(t) * r(t)\sin(\omega_{\mathrm{LO}}\mathrm{t} + \theta) \tag{6.4}$$

From (6.1) to (6.4), the observed signal $x(t)$ can be formulated using the ideal signal $z(t)$ and the image interference $z^*(t)$,

$$x(t) = g_1(t) * z(t) + g_2(t) * z^*(t) \tag{6.5}$$

where $g_1(t)$ and $g_2(t)$ are given by:

$$g_1(t) = [h_{\mathrm{I}}(t) + g \cdot \exp(j\varphi) \cdot h_{\mathrm{Q}}(t)]/2 \tag{6.6}$$

$$g_2(t) = [h_{\mathrm{I}}(t) - g \cdot \exp(-j\varphi) \cdot h_{\mathrm{Q}}(t)]/2 \tag{6.7}$$

In general, complex conjugation in the time domain corresponds to complex conjugation and mirroring in the frequency domain. Thus, if the Fourier Transform (FT) of $z(t)$ is $Z(f)$, then the FT of $z^*(t)$ is $Z^*(-f)$. Therefore, applying the FT of $x(t)$ formulated in (6.5), $X(f)$, is then obtained,

$$X(f) = G_1(f) \cdot Z(f) + G_2(f) \cdot Z^*(-f) \tag{6.8}$$

where $G_1(f)$, $G_2(f)$ are the FT of $g_1(t)$, $g_2(t)$, respectively. From (6.8), the Image Rejection Ratio (IRR) of the analog FE is defined as

$$\mathrm{IRR}_{\mathrm{FE}}(f) = \frac{|G_1(f)|^2}{|G_2(f)|^2} \tag{6.9}$$

Under perfect I/Q balance, $g = 1$, $\varphi = 0$, $h_{\mathrm{I}}(t) = h_{\mathrm{Q}}(t) = 1$, and thus $g_1(t) = 1$, and $g_2(t) = 0$. In this case, the value of $\mathrm{IRR}_{\mathrm{FE}}(f)$ is infinity, $x(t) = z(t)$, and the observed signal $x(t)$ does not contain any image interference, $z^*(t)$.

The obtainable image frequency attenuation is limited by analog component matching to the 20–40 dB range. From the discussion above, it is clear that the conjugate term $Z^*(-f)$ in the frequency domain, or $z^*(t)$ in the time domain, is the source of image interference. Hence, in order to improve the image rejection ratio, this conjugate signal term should be removed or mitigated.

In narrowband transmission, the frequency dependent factors $h_{\mathrm{I}}(t)$ and $h_{\mathrm{Q}}(t)$ can be neglected. In this case, the I/Q imbalance model is simplified to the frequency independent scenario, as reported in [98], [99].

6.1.2 Ideal Solution for I/Q Compensator

Substituting (6.8) into (5.23), $Y(f)$ can be expressed in terms of $Z(f)$ and $Z^*(-f)$, as follows,

$$\begin{aligned} Y(f) &= [G_1(f) + W(f) \cdot G_2^*(-f)] \cdot Z(f) \\ &\quad + [G_2(f) + W(f) \cdot G_1^*(-f)] \cdot Z^*(-f) \end{aligned} \tag{6.10}$$

The performance measurement is the overall IRR, which is the sum of the image attenuation from the FE and the DSP. From (6.10), the IRR is obtained as a function of frequency, given by

$$\mathrm{IRR}(f) = \frac{\left|G_1(f) + W(f)G_2^*(-f)\right|^2}{\left|G_2(f) + W(f)G_1^*(-f)\right|^2} \tag{6.11}$$

Ideally, to remove the image interference, $Z^*(-f)$, the compensation filter $W(f)$ should be selected such that $G_2(f) + W(f) \cdot G_1^*(-f) = 0$. Therefore, the ideal solution of $W(f)$ is given by,

$$W_{\text{ideal}}(f) = -\frac{G_2(f)}{G_1^*(-f)} \tag{6.12}$$

6.1.3 Circularity of the Ideal, the Mismatched and the Recovered Signals

Before the update of the filter coefficients is formulated, the circularity of the ideal signal, $z(t)$, mismatched signal, $x(t)$, and the compensated signal, $y(t)$, are discussed in this subsection.

First, since the I/Q compensation technique happens after the downconvertion of the RF signals, the properness of the ideal IF signal is being explored. In general, it is unrealistic to assume that the exact phase of the incoming signal is known at the receiver. Therefore, to reflect this phase uncertainty, a random phase term θ is included in the complex modulating exponential, which is assumed to be uniformly distributed over the unit circle and statistically independent of the baseband waveform $s(t)$. In mathematical formulation, the IF signal $z(t)$ is given as follows,

$$z(t) = s(t)e^{j(\omega_{\text{IF}}t+\theta)} \tag{6.13}$$

where $s(t)$ is the baseband equivalent and ω_{IF} is the IF frequency. Then, it is straightforward to prove that a single IF signal $z(t)$ is circular if its corresponding baseband equivalent, $s(t)$, is circular,

$$\begin{aligned} C_{z(t)}(0) &= E\{z^2(t)\} = E\{s^2(t)\}e^{j\cdot 2(\omega_{\text{IF}}t+\theta)} \\ &= C_{s(t)}(0)e^{j\cdot 2(\omega_{\text{IF}}t+\theta)} \end{aligned} \tag{6.14}$$

The "moment" $C_{s(t)}(0)$ pulls $C_{z(t)}(0)$ towards zero. Then the conclusion is made that randomly phased IF signals with circular baseband waveforms are inherently circular.

Second, the complementary autocorrelation function of the mismatched signal, $x(t)$, at $\tau = 0$, is derived as,

$$\begin{aligned} C_{x(t)}(0) &= E\{x^2(t)\} \\ &= E\{[g_1(t) * z(t) + g_2(t) * z^*(t)]^2\} \\ &= \int_{-\infty}^{\infty}\int_{-\infty}^{\infty} g_1(\lambda_1)g_2(\lambda_2)R_{z(t)}(\lambda_1-\lambda_2)d\lambda_1 d\lambda_1 \end{aligned} \tag{6.15}$$

where, $R_{z(t)}(\lambda_1-\lambda_2)$ is the autocorrelation function of $z(t)$, which is obviously nonzero. It is clear that $c_{x(t)}(0) \neq 0$ if $g_1(t) * g_2(t) \neq 0$. Therefore, under the mismatch scenario, the signal loses its circularity.

Third, the circularity nature of the compensated signal $Y(f)$ given by (6.10) is investigated. Without any image interference $Z^*(-f)$, the perfectly compensated signal is written as

$$Y_{\text{ideal}}(f) = K(f)\cdot Z(f) \tag{6.16}$$

where $K(f) = G_1(f) + W(f) \cdot G_2^*(-f)$.

It is easy to prove that if $Z(f)$ is circular, the perfectly compensated signal, $Y_{\text{ideal}}(f)$, is also circular.

6.2 Computer Simulation for Frequency-dependent I/Q Mismatch Compensation

In this section, the performance of the proposed OBA-C technique is tested and compared to another circularity based algorithm [89], using the compensation block diagram in Fig. 43. The observed signal from the analog FE, $x(t)$, is digitized to obtain $x(kT)$, where k is the sample index and T is the sampling period. For simplicity of notation, T is dropped. The performance measurement is the overall IRR, which is defined in (6.11). Two mismatch levels are simulated, a low mismatch level and a high mismatch level. A 3-tap adaptive filter is applied and an overlapping block with size L=18 samples is used. The optional scaling factor γ = 0.5, and the input SNR = 30dB.

6.2.1 Low Mismatch Level Simulation

In the low mismatch level scenario, which is the same level reported in [91]. The desired source signal is a QPSK waveform with a carrier at 3 MHz intermediate frequency. The symbol rate is 3.84 MHz and the pulse shaping is 25% roll-off raised-cosine, yielding roughly a 3.84×(1+25%) ≈ 5 MHz channel bandwidth. The FE sampling rate is 4×3.84=15.36 MHz. The LO mismatch levels are 3% in amplitude and 3º in phase, and the non-ideal channels are modeled as $H_I(z) = 0.98 + 0.02z^{-1}$ and $H_Q(z) = 1.0 - 0.005z^{-1}$. The analog FE has frequency-

dependent I/Q imbalances, with the resulting image attenuation smoothly varying between 25 and 35 dB, as shown in Fig. 45.

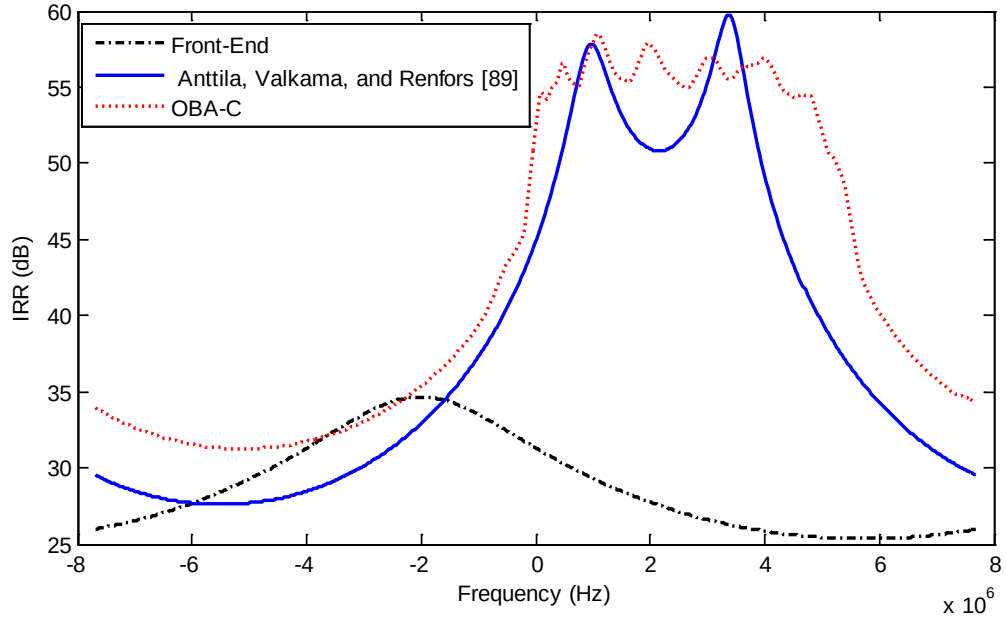

Figure 45 IRR before/after Compensation under Low Mismatch Level

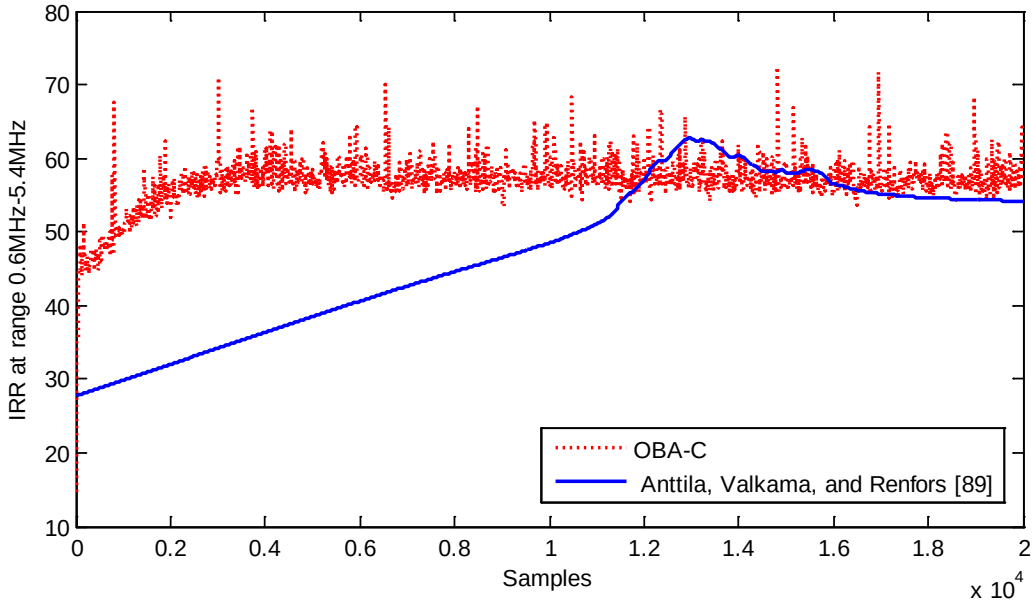

Figure 46 Convergence under Low Mismatch Level

Fig. 45 shows the achieved IRR before and after compensation with a 3-tap adaptive filter. In Fig. 46, the averaged IRR over the image frequency band (0.6–5.4 MHz) vs. sample index is plotted.

6.2.2 High Mismatch Level Simulation

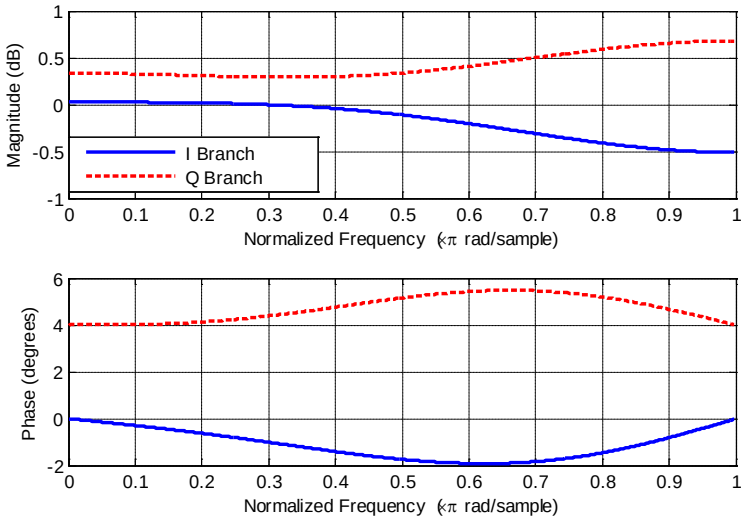

Figure 47 Frequency Responses of I and Q Branches

In the high mismatch level scenario, the desired source signal is a QPSK signal modulated at 6 MHz, with 25% roll-off raised-cosine pulse-shaping. The symbol rate is 7.68 MHz, yielding roughly a 10 MHz channel bandwidth, which in many applications is wide enough to result in frequency dependent I/Q imbalance. The FE sampling rate is 4×7.68=30.72 MHz. The input SNR is 30dB. The LO mismatch levels are 5% in amplitude and 4º in phase. The nonideal branch filters are $H_I(z) = 0.98 + 0.02z^{-1} – 0.007z^{-1}$ and $H_Q(z) = 1.0 – 0.02z^{-1} + 0.01z^{-1}$. The above non-ideality gives a frequency dependent mismatch scenario with the maximum gain imbalance of 1.19 dB and the maximum phase imbalance of 7.39 degrees, as shown in Fig. 47,

which are reasonable expectation in practice. The analog front-end limits the image attenuation to the range of 22–30dB, as shown in Fig. 48.

Fig. 48 shows the achieved IRR before and after compensation. The IRR over the image frequency band (1.2–10.8 MHz) vs. sample index is given in Fig. 49. Fig. 50 plots the signal spectrum before and after compensation using the OBA-C I/Q imbalance compensator. Fig. 51 plots the magnitude and phase of the achieved filter coefficients $W(f)$ vs. frequency (1.2–10.8MHz) using a 3-tap compensator.

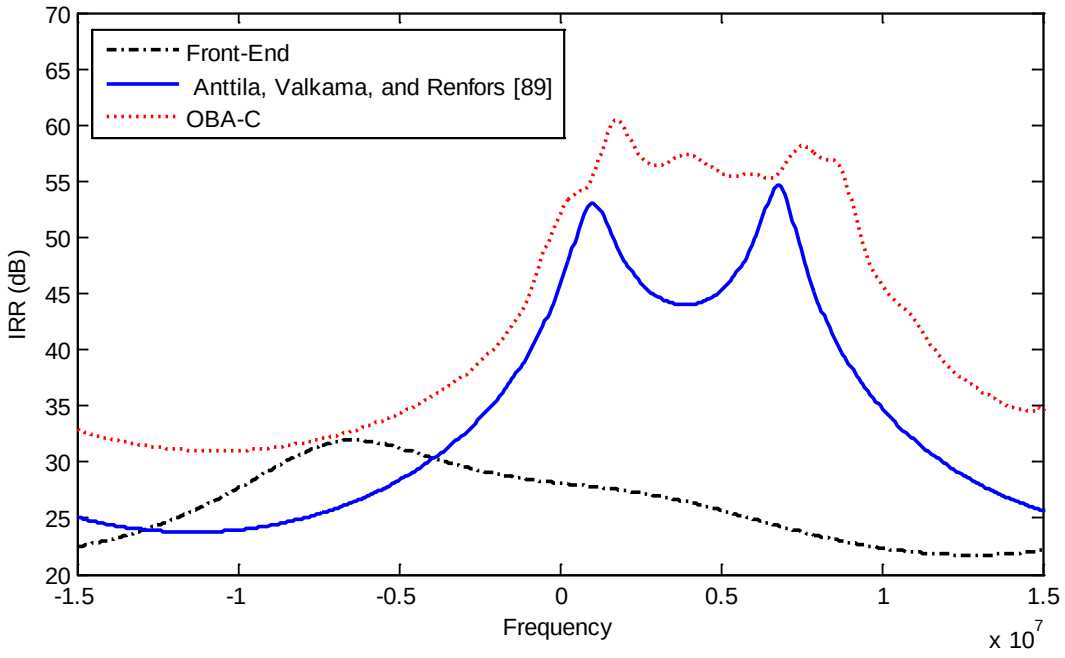

Figure 48 IRR before/after Compensation under High Mismatch Level

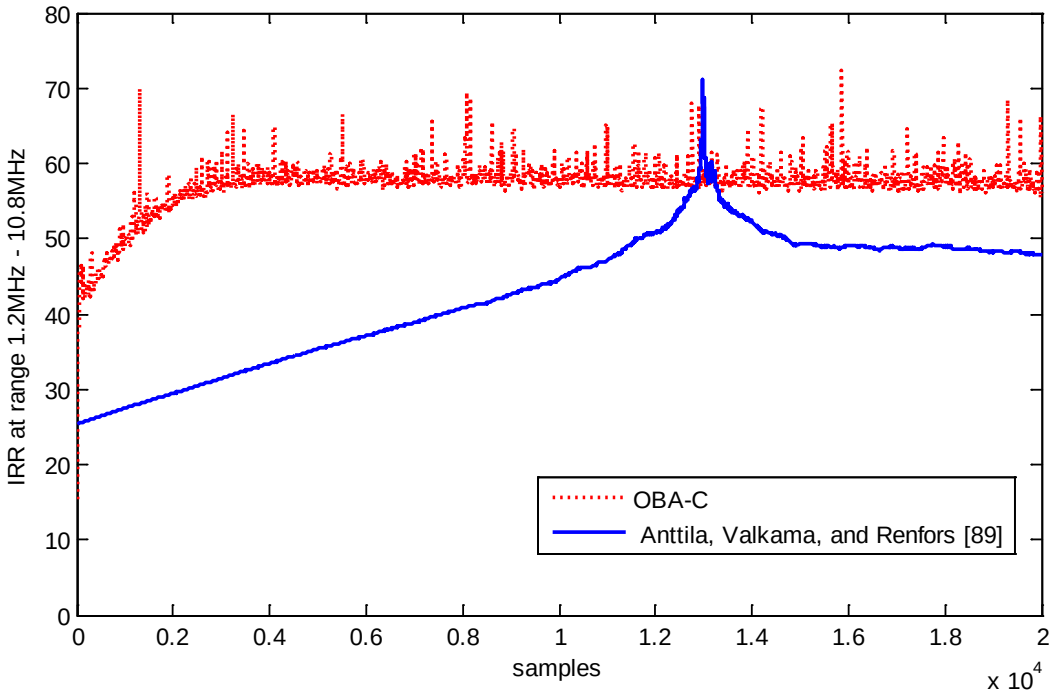

Figure 49 Convergence under High Mismatch Level

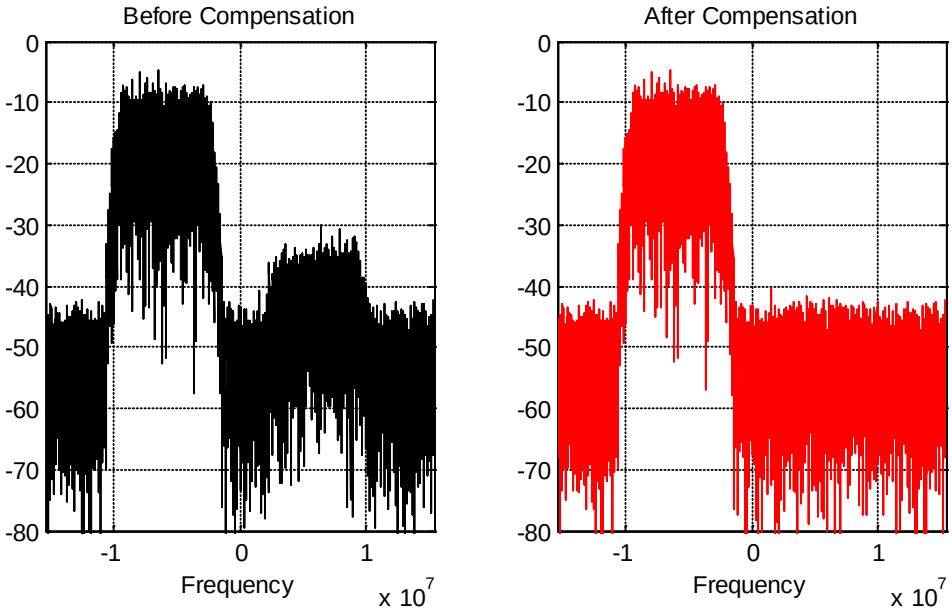

Figure 50 Frequency Spectrum before/after Compensation

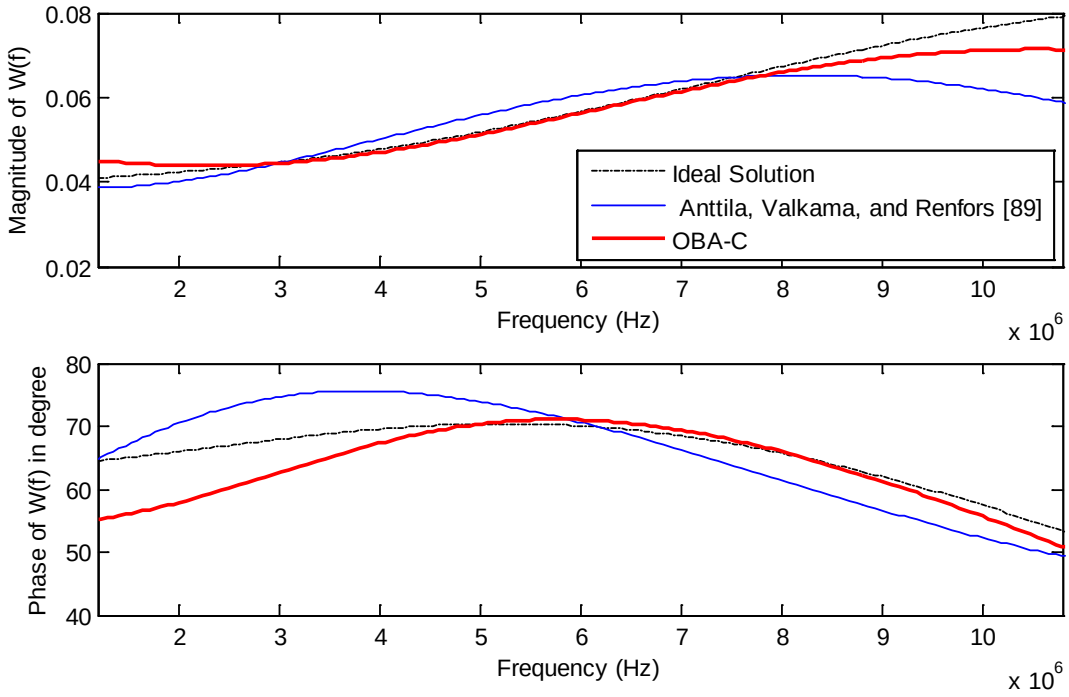

Figure 51 *W*(*f*) vs. Frequency at Image Band (1.2–10.8MHz) with a 3-tap Compensator

6.2.3 Discussion

Compared to the algorithm in [89], Figs 45, 46, 48–51 clearly show OBA-C has significant improvement in the convergence speed and the achieved IRR. From Figs 45 and 48, it can be clearly seen that the OBA-C I/Q imbalance compensation algorithm demonstrates excellent IRR while maintaining wider image rejection bandwidth than the algorithm in [89]. It is clear that the proposed OBA-C technique achieves the peak value of IRR around +3MHz in Fig. 45 and +6MHz in Fig. 48, which are the central frequencies of the image signals. Figs 46 and 49 indicate that the presented method yields a significant improvement in convergence speed. Fig. 50 illustrates that after OBA-C I/Q compensation, the image interference signal is significantly attenuated. Fig. 51 clearly shows that at the high mismatch level, OBA-C converges

to a solution which is closer to the ideal solutiont obtained from (6.12), compared to the algorithm in [89].

It is worthwhile to mention that the convergence curves for OBA-C in Figs 46 and 49 are noisier than the algorithm in [89]. However, the noise is always pointing to a higher IRR value. The potential reason is illustrated as follows. The technique in [89] uses a fixed step size, ending with a smooth convergence curve. The OBA-C employs the optimal adaptation, which theoretically restores the circularity of the mismatched signal in one iteration. The result is that the convergence curve oscillates to reach a higher IRR value, theoretically, infinity. However, the limitation of the performance has been decided by practical conditions and cannot be exceeded. That is why the oscillation always directs up to an extremely high IRR value and then drops back to the limitation value. It is shown that while the IRR of the algorithm in [89] degrades as the I/Q mismatch level increases, the IRR value of the OBA-C stays almost the same regardless of the mismatch levels. Therefore, an additional advantage of OBA-C is its robustness against I/Q imbalance levels.

6.3 Implementation Issues

Implementation issues are discussed in this section, including the optional scaling factor, the block shifting and block size, and the number of filter taps. The simulations are set up the same as in Section 6.2. All the simulation results are averaged over 1000 Monte Carlo runs.

6.3.1 Optional Scaling Factor

In practice, it is desirable to introduce one additional adaptation parameter γ for the final weight update based on two considerations. First, since the higher order derivative term in (5.25) is dropped in our formulation, an additional adaptation parameter can help to ensure reliable convergence. Second, the iterative update of the filter coefficient is formulated in a noise free scenario. A mechanism should be available to adjust $\Delta\mathbf{w}$, so that the algorithm can compensate for the effect of the additive noise in practical receivers.

To study the scaling factor γ, simulations are carried out with a 3-tap OBA-C compensator. A block with size L = 18 is used, and the input SNR is assumed to be 30dB. Fig. 52 plots the convergence curve of the averaged IRR over the image band (1.2–10.8 MHz) using different values of γ. It illustrates that when γ = 5, OBA-C diverges; when γ = 0.5, 1, and 2, the algorithm converges within 4000 samples; when γ = 0.2, more samples are required for the OBA-C to achieve steady convergence. Fig. 53 plots the achieved IRR averaged over image band by OBA-C with different scaling factors for both mismatch levels. Fig. 54 illustrates the required iterations for OBA-C to achieve convergence with different scaling factors. From our experiments, the OBA-C diverges when $\gamma \geq 5$. Within the convergence range, a smaller γ yields slower convergence but better image rejection performance, while a larger γ yields faster convergence but a lower image rejection ratio. It is found in our simulation that the optimal value of γ varies according to different signals and systems. In general, OBA-C has the capability to achieve convergence over a certain range of γ (approximately $0 < \gamma \leq 4$). From our intensive experiments, the range of 0.5–1 is recommended.

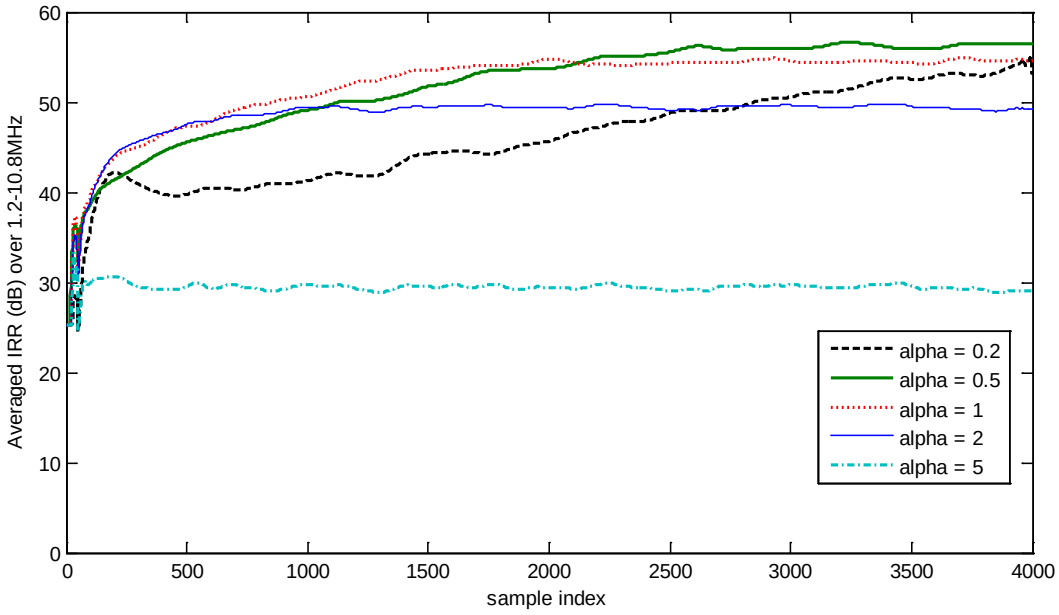

Figure 52 Convergence Curve of IRR over Image Band Using Different Scaling Factors

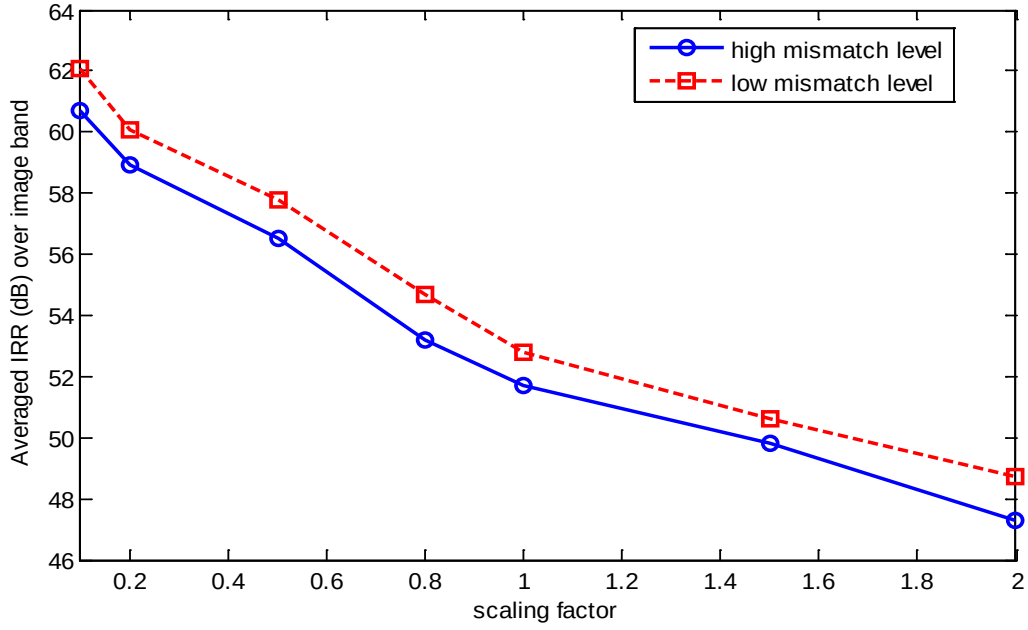

Figure 53 Achieved IRR Averaged over Image Band by OBA-C with Different Scaling Factors

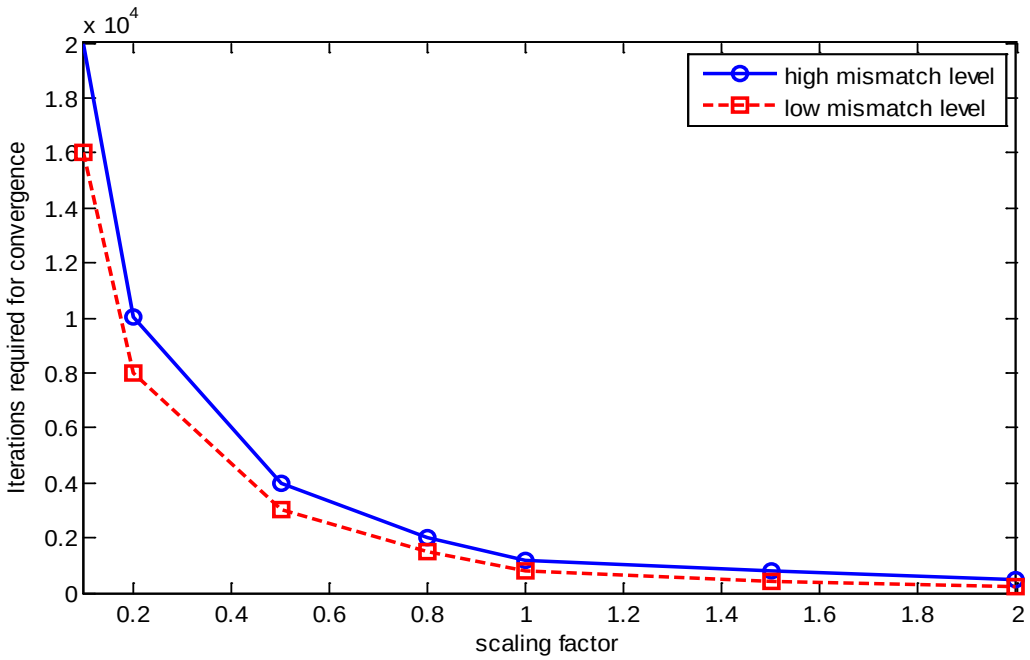

Figure 54 Required Iterations for OBA-C to Achieve Convergence with Different Scaling Factors

6.3.2 Block Shifting and Block Size

In the OBA-C algorithm presented in 5.2, an overlapping block with the shifting window size $N_f = 1$ is applied, i.e., the processing block is shifted by one sample at each iteration, with the oldest sample dropped and a new sample incorporated. The formulation of the algorithm can be modified with a user-defined shifting window size N_f within the range $0 \le N_f \le L$. When $N_f = 0$, the same block of input signal is used repeatedly until the convergence is achieved. When $N_f = L$, a disjoint block scheme is adopted, which discards all the previous samples in memory, and waits for L new inputs at each iteration to calculate $\Delta\mathbf{w}(k)$.

Since OBA-C is a block algorithm which utilizes a block of data to estimate the "expectation" operator in (5.30), the selection of block size L is discussed and analyzed here. A larger block size yields more accurate approximation of the expected values while a small block

size degrades the performance. From our simulations, the OBA-C diverges when $L < 3$. The average IRR over image band vs. different block sizes is plotted in Fig. 55. It confirms that a larger block size improves the image rejection performance. Fig. 56 plots the required iterations of the OBA-C algorithm vs. different block sizes. With a larger block size, the OBA-C requires fewer iterations to converge and yields smoother convergence curve.

On the other hand, it is very important that the proposed technique keeps computational efficient while satisfying certain performance requirements. In this regard, a smaller block size is preferred since it yields lower computational complexity than a bigger block size.

Figs 55 and 56 also indicate that when OBA-C converges, there are limitations for the achieved IRR and the number of required iterations. In other words, even if *L* is further increased beyond 50, the achieved IRR will not go out of boundary and the required iterations hardly further decreases. Considering both the computational complexity and the adaptation performance, a block size within the rage of 10–20 is recommended.

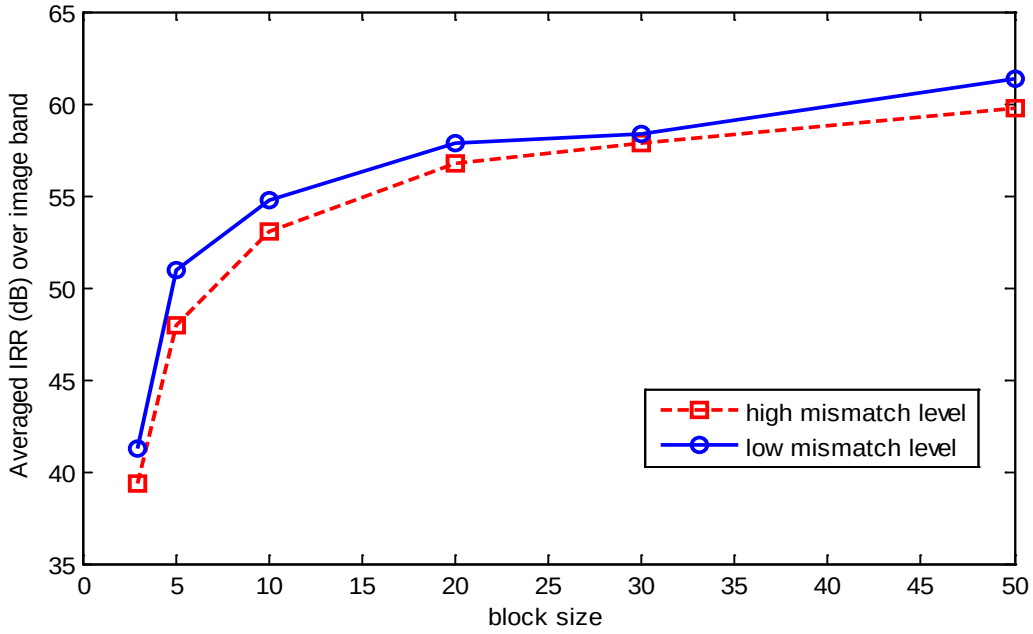

Figure 55 Achieved IRR Averaged over Image Band by OBA-C with Different Block Sizes

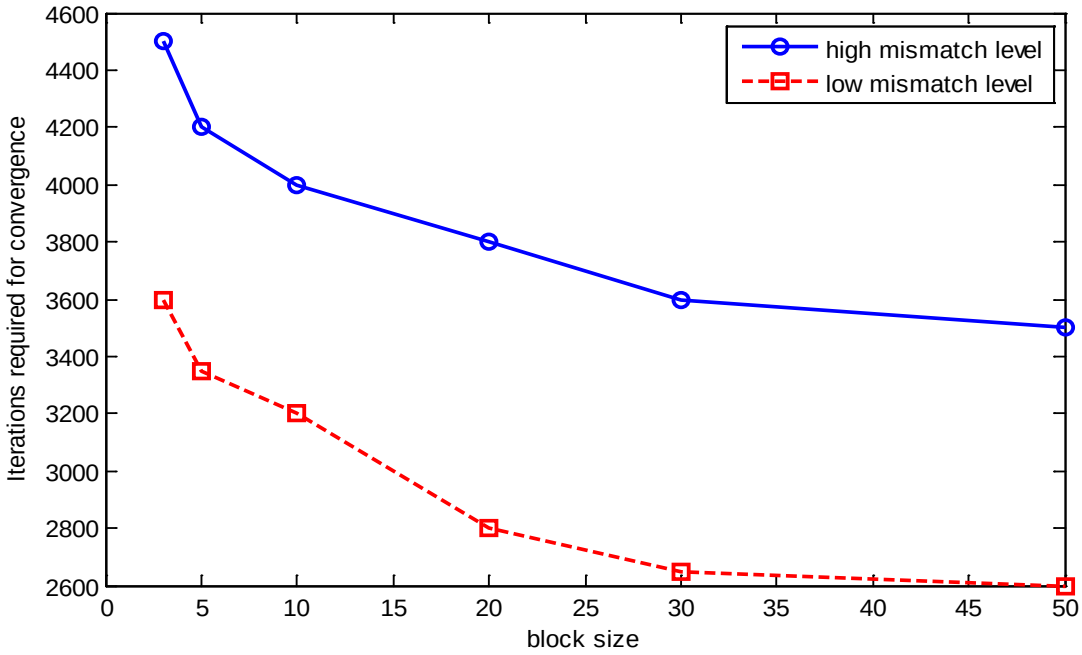

Figure 56 Required Iterations for OBA-C to Achieve Convergence with Different Block Sizes

6.3.3 Number of Adaptive Filter Taps

In this subsection, the selection of the OBA-C filter taps is investigated. The OBA-C is tested using a compensation filter with different taps and the results are compared to those obtained using the algorithm in [89].

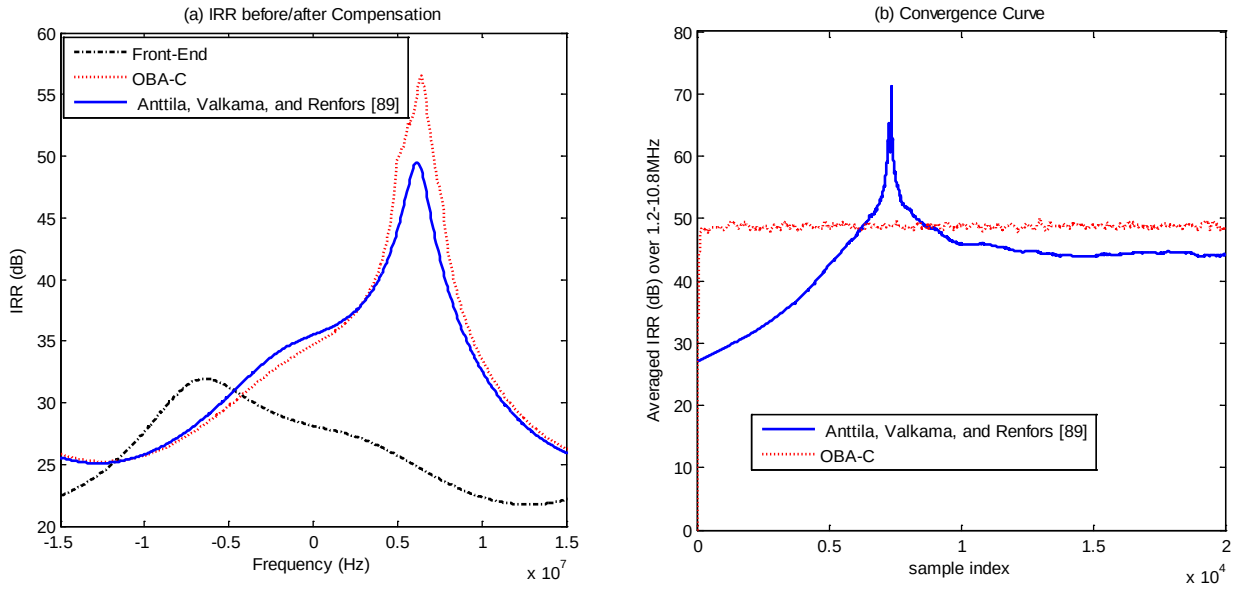

Figure 57 Simulation Results with a 1-tap Compensator

Fig. 57 plots the simulation results for a compensator with 1 tap at the high mismatch level. Fig. 57(a) is the achieved IRR vs. frequency before and after compensation. The corresponding IRR curve of the analog FE alone is also shown as a comparison. An important observation is that comparing with the results obtained by the 3-tap compensator from 6.2.2, the 1-tap filter yields worse image attenuation performance for both the algorithms. This is, indeed, due to the frequency-selective nature of the I/Q imbalance. Fig. 57(b) plots the averaged IRR over the image frequency band vs. the processing sample index at the high mismatch level. It

demonstrates the improvement in the convergence speed of the OBA-C method is surprisingly significant, especially for the 1-tap compensator. The 1-tap compensator reduces the required iterations for convergence from 8,000 to 100, while the 3-tap filter reduces the iteration number from 14,000 to 4,000 as shown in 6.2.2. Along with the faster convergence, the 1-tap compensator improves the IRR value from 44.5dB to 49.2dB.

Figs 58 and 59 plot the achieved IRR and required iterations vs. filter tap numbers, respectively. From Fig. 58, it is shown that the peak IRR appears with a 3-tap compensator. The reason is that the ideal solution of this compensation system can be best represented by a 2nd-order (3-tap) model. Therefore, with more taps, the system is overdetermined, which degrades the achieved image rejection performance. Fig. 59 indicates that the OBA-C method converge slowest with a 2-tap filter. In general, the trend is that the OBA-C needs more iterations with a tap number which yields better image rejection performance.

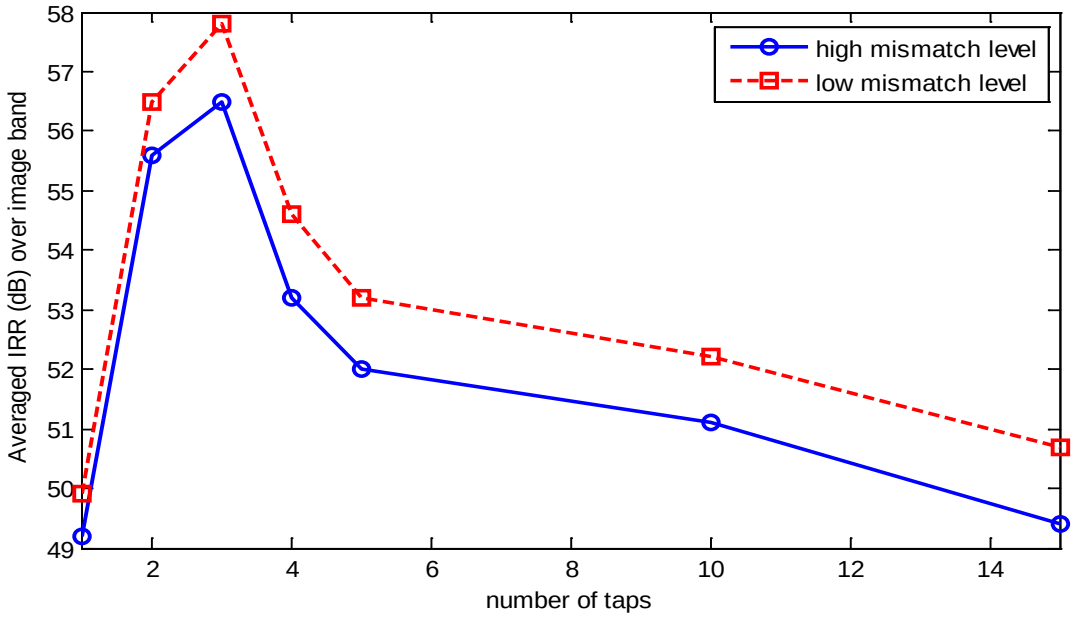

Figure 58 Achieved IRR Averaged over Image Band by OBA-C with Different Numbers of Taps

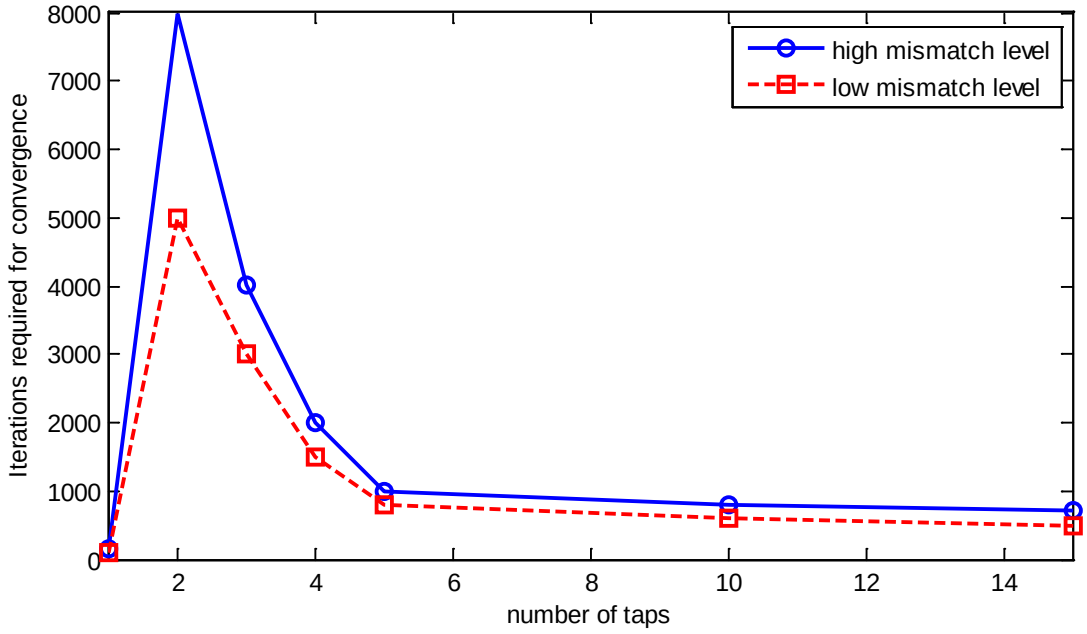

Figure 59 Required Iterations for OBA-C to Achieve Convergence with Different Numbers of Taps

6.4 Practical Impairments

The effects of practical impairments on the OBA-C compensator are analyzed in this section, including channel fading, frequency and phase offsets, and additive noise.

6.4.1 Channel Fading

As mentioned before, the fading channel can be modeled as a FIR filter. For a discrete-time FIR filter, the output is a weighted sum of the current and a finite number of previous values of the input. The operation is described by the following equation, which defines the baseband equivalent of the channel output $u(k)$ in terms of its input sequence $z(k)$, as follows

$$u(k) = \sum_{i=0}^{I} a_i z(k-l) \tag{6.17}$$

where a_i is the filter coefficient.

Then the complimentary autocorrelation function of $u(k)$ is computed as follows,

$$C_{u(k)}(\Delta) = E\{u(k)u(k-\Delta)\} = E\{\sum_{m=0}^{I}\sum_{n=0}^{I} a_m a_n z(k-m)z(k-n-\Delta)\}$$

$$= \sum_{m=0}^{I}\sum_{n=0}^{I} a_m a_n E\{z(k-m)z(k-n-\Delta)\} \tag{6.18}$$

Since $z(k)$ is the baseband equivalent of channel input, which is proper and circular, the following is satisfied,

$$E\{z(k-m)z(k-n-\Delta)\} = 0, \forall m, n, \Delta. \tag{6.19}$$

Therefore, (6.18) is equal to 0 for any Δ. The conclusion is that the baseband equivalent of the channel output $u(k)$ is proper and circular as well.

6.4.2 Frequency and Phase Offset

The baseband equivalent of an observed signal, $v(k)$, distorted by frequency and phase offsets is formulated as follows

$$v(k) = e^{j\cdot(\Delta\omega\cdot kT+\Delta\theta)} z(k) \tag{6.20}$$

where $\Delta\omega$ and $\Delta\theta$ are the frequency and phase offset parameters, respectively.

Then the complimentary autocorrelation function of $v(k)$ is computed as follows,

$$C_{v(k)}(\Delta) = E\{v(k)v(k-\Delta)\} = E\{e^{j\cdot[\Delta\omega\cdot(2k-\Delta)T+2\Delta\theta]} z(k)z(k-\Delta)\}$$

$$= e^{j\cdot[\Delta\omega\cdot(2k-\Delta)T+2\Delta\theta]}E\{z(k)z(k-\Delta)\} = 0, \forall\Delta\,. \tag{6.21}$$

Here goes the conclusion that the baseband equivalent of the channel output $v(k)$ is proper and circular under frequency and phase offsets.

6.4.3 Additive Noise

When the OBA-C method is formulated in 5.2, the effect of the additive noise is ignored. If an accurate I/Q downconversion model including complex white Gaussian noise is considered, adjustment should be made for the OBA-C formulation in 5.2. The noise discussed here can arise everywhere during the analog processing procedure at the receiver side, which starts from the antenna where the signal is received and ends right before the ADC. It is clear that the I/Q mismatch problems are caused by the same analog process. However, any different individual noise effect on the I or Q branch is discussed in Section 6.1. Only the common effect to both I and Q branches is considered in this subsection.

With additive noise, the input signal to the imbalance compensation model, $x(k)$, is modified to $x'(k)$, as

$$x'(k) = x(k) + n(k) \tag{6.22}$$

where $n(k)$ is the noise signal.

The formulated recovered signal $y(k)$ in (5.22) is modified as

$$\begin{aligned} y'(k) &= x'(k) + \mathbf{w}^T(k)\mathbf{x}'^*(k) = x(k) + n(k) + \mathbf{w}^T(k)[\mathbf{x}^*(k) + \mathbf{n}^*(k)] \\ &= [x(k) + \mathbf{w}^T(k)\mathbf{x}^*(k)] + [n(k) + \mathbf{w}^T(k)\mathbf{n}^*(k)] \end{aligned} \tag{6.23}$$

where

$$\mathbf{n}(k) = [n(k), n(k-1), ..., n(k-N+1)]^T \tag{6.24}$$

Substituting (5.22) into (6.23), $y'(k)$ is expressed as

$$y'(k) = y(k) + [n(k) + \mathbf{w}^T(k)\mathbf{n}^*(k)] \tag{6.25}$$

Thus, the complementary autocorrelation function of $y'(k+1)$ at $\Delta = 0$, is derived as,

$$\begin{aligned} C_{y'(k+1)}(0) = E\{y'^2(k+1)\} &= E\{(y(k+1) + n(k+1) + [\mathbf{w}^T(k+1)\mathbf{n}^*(k+1)])^2\} \\ &= E\{(y^2(k+1)\} \\ &+ E\{y(k+1)[n(k+1) + \mathbf{w}^T(k+1)\mathbf{n}^*(k+1)]\} \\ &+ E\{[n(k+1) + \mathbf{w}^T(k+1)\mathbf{n}^*(k+1)]^2\} \end{aligned} \tag{6.26}$$

The basic objective in the noise scenario should be the same as the noise free scenario, i.e., to restore the circularity of the noise-free output of the compensator at next iteration,

$$E\{(y^2(k+1)\} = 0 \tag{6.27}$$

Generally, the noise $n(k)$ is uncorrelated with $y(k)$, so that

$$E\{y(k+1)[n(k+1) + \mathbf{w}^T(k+1)\mathbf{n}^*(k+1)]\} = 0 \tag{6.28}$$

The third term in (6.26), $E\{[n(k+1) + \mathbf{w}^T(k+1)\mathbf{n}^*(k+1)]^2\}$ is more complicated than the first two terms. Thus, it is being further expanded as follows,

$$\begin{aligned} &E\{[n(k+1) + \mathbf{w}^T(k+1)\mathbf{n}^*(k+1)]^2\} \\ &= E\{n^2(k+1)\} \\ &+ E\{2n(k+1)\mathbf{w}^T(k+1)\mathbf{n}^*(k+1)]\} \\ &+ E\{[\mathbf{w}^T(k+1)\mathbf{n}^*(k+1)]^2\} \end{aligned} \tag{6.29}$$

$n(k)$ is complex white Gaussian noise, and it is assumed to be proper, and thus circular as well. Therefore, the first and third terms in (6.29) are both equal to 0, as follows,

$$E\{n^2(k+1)\} = 0 \tag{6.30}$$

$$E\{[\mathbf{w}^T(k+1)\mathbf{n}^*(k+1)]^2\} = 0 \tag{6.31}$$

The second term in (6.29) becomes,

$$\begin{aligned} E\{2n(k+1)\mathbf{w}^T(k+1)\mathbf{n}^*(k+1)]\} &= E\{2w_1(k+1)n(k+1)n^*(k+1)]\} \\ &= 2\cdot w_1(k+1)\cdot E\{n(k+1)n^*(k+1)]\} \end{aligned} \tag{6.32}$$

where $E\{n(k+1)n^*(k+1)]\}$ is the noise power.

Therefore, combining (6.26)–(6.32), the following is obtained,

$$C_{y'(k+1)}(0) = 2\cdot w_1(k+1)\cdot E\{n(k+1)n^*(k+1)]\} \tag{6.33}$$

However, practically, it is unrealistic to measure the noise power at either transmitter or receiver side. When the SNR is within a certain range, the derivation in 5.2 still works as an approximation of the solution.

Table 9 and Fig. 60 compare the averaged IRR's over the image frequency band using the OBA-C and the algorithm in [89], under different SNR levels. Both the high and low mismatch levels are simulated. It is worthwhile to mention that the I/Q imbalance becomes a problem only if the image interference is above the noise floor. In other words, a reasonable SNR value for simulation should be larger than the IRR value of the FE. Since the image attenuation of the FE in practical receivers is within the range of 20–40 dB, the SNR range of 25–50dB is simulated.

Table 9 Averaged IRR (dB) over Image Band vs. SNR

SNR (dB)	OBA-C		Anttila, Valkama, and Renfors [89]	
	High Mismatch Level	Low Mismatch Level	High Mismatch Level	Low Mismatch Level
25	53.4	54.9	47.8	54.5
30	56.5	57.8	48.2	55.2
35	59.7	60.8	48.2	55.3
40	63.4	64.5	48.2	55.3
45	65.0	66.4	48.2	55.3
50	65.5	67.2	48.2	55.5
Infinity	65.9	67.9	48.2	55.8

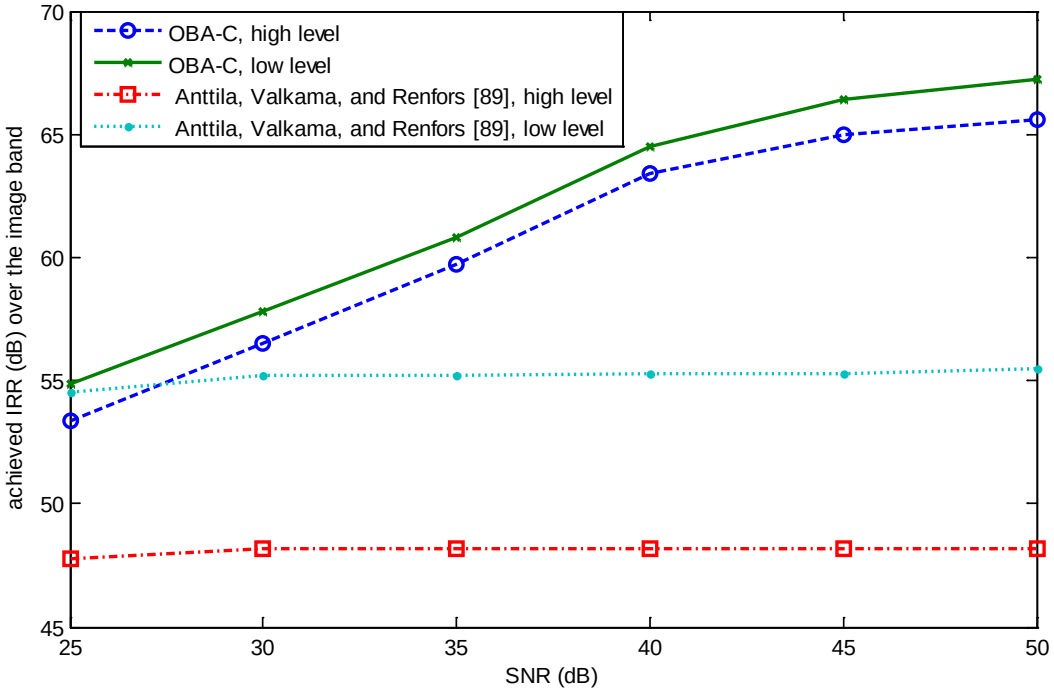

Figure 60 IRR vs. SNR for both High and Low Mismatch Levels

Table 9 and Fig. 60 further confirm the superior performance of the OBA-C. The result indicates that for both mismatch levels, OBA-C demonstrates significant improvement in image rejection performance compared to the approach in [89].

Table 9 and Fig. 60 show that the additive noise affects the image rejection performance of the OBA-C. However, the performance limit of the OBA-C algorithm, measured by the IRR value in the noise free (SNR = infinity) scenario, is higher than that of the method in [89]. Also, within the reasonable SNR range for practical receivers (25–50dB), OBA-C always achieves a higher IRR value compared to the algorithm in [89].

6.5 Conclusion

In this chapter, the performance of the OBA-C I/Q imbalance compensation technique is tested using computer simulation, and compared to a recently proposed algorithm. Implementation issues and practical impairments are also discussed and analyzed. Computer simulation shows that the proposed OBA-C technique demonstrates fast convergence, while maintaining excellent IRR over a wide signal bandwidth. In addition, it is concluded that OBA-C is resistant to different mismatch levels, and robust to RF impairments. Therefore, OBA-C is a promising frequency-dependent I/Q mismatch compensation solution for practical radio receiver design.

CHAPTER 7 EFFECT OF SIGNALS' PROBABILISTIC DISTRIBUTIONS ON PERFORMANCE OF ADAPTIVE INTERFERENCE CANCELING ALGORITHMS

Achieving particular performance requirements in noise rejection is a major design criterion for wireless receivers. Therefore, an appropriate choice of noise suppression algorithms which can satisfy the ever-increasing demand for better performance on one side and fit different types of waveforms on the other side is crucial to wireless receiver design. In recent years, research on adaptive filter based, both LMS and ICA noise cancellation techniques continue to receive significant attention [104]–[109]. Traditionally, the LMS algorithm based on second-order decorrelation has been widely applied in adaptive noise cancellation problems [104]. In recent years, ICA-based algorithm utilizing higher order statistics are frequently adopted to improve the interference rejection performance [105]–[109]. However, most of the reported works on ICA-based noise canceling approaches are limited to real-world acoustic echo cancelling applications [106]–[109].

In this chapter, the performance of the LMS- and ICA-based approaches with different signals' probabilistic distributions is studied [110]. It is observed that ICA based approach works better than LMS for super-Gaussian signals, which is the reason that most reported ICA-based noise reduction works focus on super-Gaussian analog signals, including the speech, music vocal and audio signals. In contract, for sub-Gaussian and Gaussian signals, LMS is superior to ICA due to its stable high interference rejection ratio and its computational efficiency. The performance of these two algorithms is evaluated using computer simulations for signals with different distributions. The obtained results lead to the conclusion that if prior information of the

signal's probabilistic distribution is available, a smart choice between the LMS- and ICA-based approaches can be made to achieve better noise rejection performance.

This chapter is organized as follows. Section 7.1 gives the typical interference cancelling system model. The conventional LMS learning rule is given in 7.2. An overview of different ICA-based interference cancelling methods and their essential relations are presented in 7.3. Section 7.4 discusses the effect of signals' probabilistic distributions on the performance of adaptive interference canceling algorithms. Simulation results are given in 7.5, followed by conclusion in 7.6.

7.1 Interference Cancellation Model

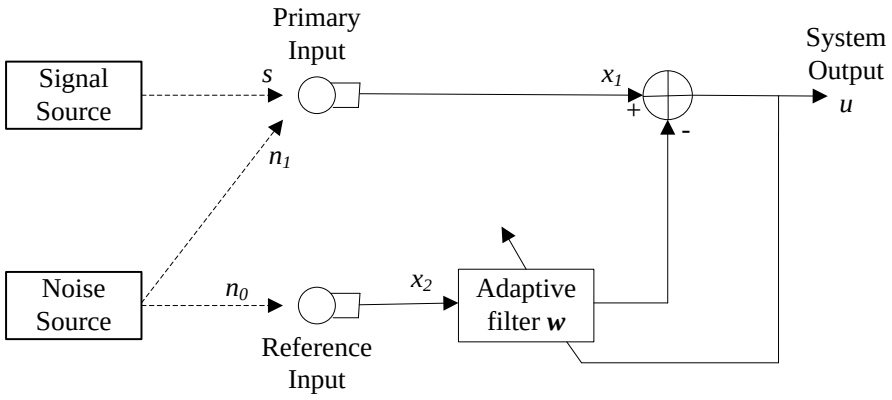

Figure 61 Adaptive Interference Cancellation Model

The typical adaptive interference cancelling system is given in Fig. 61. The primary sensor receives a message signal s corrupted by an additive noise n_1. The obtained primary input signal x_1 is $s + n_1$. Another sensor receives a noise signal n_0, which provides the reference input signal x_2. The assumption is made that s is uncorrelated with n_0 and n_1, and n_1 is

correlated with n_0 as $n_1 = h * n_0$. The objective is to get a system output u which is the best estimate of s.

7.2 LMS Learning Rule

The most popular algorithm for noise cancellation is the LMS algorithm [104]. It removes noise components from the primary input signal based on the second-order statistics. Assume $\mathbf{w}(k)$ to be the weight vector of the adaptive filter at time index k, given by

$$\mathbf{w}(k) = [w_1(k), w_2(k), ... w_N(k)]^T \tag{7.1}$$

where N is the number of the adaptive filter coefficients.

The system output $u(k)$ can be expressed as

$$u(k) = x_1(k) - \mathbf{w}(k) \cdot \mathbf{x}_2(k) \tag{7.2}$$

where

$$\mathbf{x}_2(k) = [x_2(k), x_2(k-1), ... x_2(k-N+1)]^T \tag{7.3}$$

Adjusting or adapting the filter to minimize the total output power forces the output $u(k)$ to be a best estimate of the signal $s(k)$ at a LMS sense. The update formula for $\Delta\mathbf{w}(k)$ can be derived using the MSE function $f_{\text{MSE}}(k)$,

$$\Delta\mathbf{w}(k) = -\mu \cdot \frac{\partial f_{\text{MSE}}(k)}{\partial \mathbf{w}(k)} \tag{7.4}$$

$$f_{\text{MSE}}(k) \approx \frac{1}{N} \cdot \mathbf{u}^H(k)\mathbf{u}(k) \tag{7.5}$$

where μ is the fixed convergence factor and $\mathbf{u}(k)$ is the vector containing $u(k)$ and the previous $N-1$ system outputs, given by

$$\mathbf{u}(k) = [u(k), u(k-1), ...u(k-N+1)]^T \tag{7.6}$$

7.3 ICA Learning Rule

ICA-based noise cancelling algorithms, in general, have received lots of research attention in the past decade [105]–[109]. The estimation criteria of the ICA model can be different, including cumulants [105], entropy [106], likelihood [107], mutual information [108], and nonlinear decorrelation [109]. In fact, all of these estimation criteria can be considered as different versions of the same general concept.

Noise cancellation can be considered as a typical BSS problem. The objective is to retrieve the desired signal from the received signals. The received signal vector can be obtained as follows,

$$\begin{bmatrix} x_1 \\ x_2 \end{bmatrix} = \begin{bmatrix} 1 & \mathbf{h}^T \\ 0 & 1 \end{bmatrix} * \begin{bmatrix} s \\ n_0 \end{bmatrix} \tag{7.7}$$

For simplicity, assume that the channels from the signal source to the primary sensor and from the noise source to the reference sensor are both equal to 1, as shown in (7.7). The ICA learning rule separate the independent components using a demixing matrix **B**, formulated as follows,

$$\mathbf{y} = \mathbf{B} \cdot \mathbf{x} \tag{7.8}$$

where $\mathbf{y} = [y_1, y_2]^T$ are the recovered independent components, and $\mathbf{x} = [x_1, x_2]^T$ are the two received mixed signals as shown in Fig. 61.

The mutual information of this system is defined as

$$I(y_1, y_2) = H(y_1) + H(y_2) - H(\mathbf{y}) \tag{7.9}$$

The constraint is made that y_1 and y_2 are uncorrelated and of unit variance. Thus, the last term on the right-hand side, $H(\mathbf{y})$ is constant and its value does not rely on **B**. In this way, (7.9) indicates that minimizing mutual information is equivalent to minimizing the individual entropies $H(y_1)$ and $H(y_2)$. Entropy is maximized by a Gaussian distribution, thus minimization of mutual information means maximizing the sum of the nongaussianities of the estimated components. That is the connection between the mutual information and entropy.

Alternatively, approximating mutual information can be done by estimating the densities of the components using the log-density approximations. Thus, (7.9) can be reformulated as

$$I(y_1, y_2) = H(y_1) + H(y_2) - H(\mathbf{y}) = -\sum_{i=1}^{2} E\{\log p_i(y_i)\} - H(\mathbf{y}) \tag{7.10}$$

where $p_i(\cdot)$ denotes *probability density function* (pdf). Therefore, a formula of mutual information essentially equivalent to the Maximum Likelihood (ML) estimator is obtained.

The relationship between the above mentioned criteria and the cumulant-based criterion is revealed by approximating negentropy using cumulants [111], as follows,

$$J(y) \approx \frac{1}{12} E\{y^3\}^2 + \frac{1}{48} kurt(y)^2 \tag{7.11}$$

To see the connection to nonlinear decorreltation, [112] indicates that the natural gradient methods for ML estimation has the same form as the nonlinear decorrelation algorithm. Thus, the ML estimator gives a thought for connecting ICA and LMS techniques. In fact, introducing nonlinearity to the LMS algorithm has been studied by many researchers [106], [109], [112].

7.4 Effects of pdf on the Choice of Cost Functions

Interference cancellation is a special case of the general BSS problem. Since one independent component is already known as the received reference signal n_0, only the other independent component *s* is of interest. The recovered signal y_1 can be formulated as

$$y_1 = \begin{bmatrix} \mathbf{b}_{11} & \mathbf{b}_{12} \end{bmatrix} * \begin{bmatrix} x_1 \\ x_2 \end{bmatrix} \tag{7.12}$$

Upon adaptation, both LMS and ICA should yield the estimates of the message signal *s,* so y_1 is actually proportional to the LMS output *u*,

$$y_1 = k \cdot u = k \cdot (x_1 - \mathbf{w} \cdot \mathbf{x}_2) \tag{7.13}$$

From (7.12) and (7.13), the convergence of the ICA method can be achieved by forcing $\mathbf{b}_{11}$ to be the scaling coefficient *k* and $\mathbf{b}_{12}$ to become $-k\mathbf{w}$. It is obvious that *k* does not affect the final SNR, so only the coefficient vector $\mathbf{w}$ or the ratio $\mathbf{b}_{12} / \mathbf{b}_{11}$ is interested.

The update equation for ICA can be expressed by maximazing the negentropy of y_1 [106], as follows,

$$\Delta \mathbf{w}(k) \propto \frac{\partial J(y_1(k))}{\partial \mathbf{w}(k)} = -\gamma \cdot E\{\mathbf{x}_2(k) \cdot g(y_1(k))\} \tag{7.14}$$

$$J(y_1) = [E\{G(y_1)\} - E\{G(v)\}]^2 \tag{7.15}$$

where *G*(.) is some nonlinear function, and the score function *g*(.) is the derivative of *G*(.). γ is a constant, and *v* is a Gaussian variable of the same mean and variance as y_1.

From a statistical point of view, the choice from different ICA estimation criteria is now reduced to the choice of the nonquadratic function *G*(.) or *g*(.), which provide information on the higher order statistics. As can been seen from (7.10), the introduced nonlinearity *G*(.) can be

chosen as some form of the pdf. Theoretically, the nonlinear $g(.)$ or $G(.)$ can be trained for any signal with any distribution. Published works [111], [112] have presented the approaches to construct one universal estimator $G(.)$ for all signals.

Many reported works have indicated ICA is nonrobust for sub-Gaussian signals. [113] conjectures that unwanted higher entropy solutions may be achieved only when the inputs are sub-Gaussian signals. [114] explains it through convergence of the nonlinear subspace rule. It presents that the nonlinearity can be chosen as the simple odd polynomial. While $g(y) = y$ never gives asymptotic stability, and $g(y) = y^{\alpha}(\alpha = 5,7,...)$ are computationally complicated and vulnerable to outliers, the best choice, cubic function $g(y) = y^3$, leads to asymptotic stability if and only if the density is super-Gaussian.

The research work in [111] discusses the robustness of the ICA method through the nonquadratic function $G(.)$. Section 14.3.2 in [111] indicates that if $G(.)$ grows fast with $|y|$, the estimator becomes highly nonrobust against outliers. From the ML view of point, the optimal $G(.)$ is different according to signal's pdf. Roughly for sub-Gaussian densities, the optimal function $G(.)$ is a function that grows faster than quadratically; for super-Gaussian densities, $G(.)$ grows slower than quadratically. Thus, the optimal choice of $G(.)$ for sub-Gaussian signals will be highly nonrobust estimator, which can be completely ruined by a couple of bad outliers. In this scenario, LMS can be applied as an alternative algorithm for sub-Gaussian signals.

The analysis above is useful in cases where priori information on the distributions of the independent components is available. If prior gaussianity of the desired signal is available, a better choice between LMS and ICA based approaches can be made. For sub-Gaussian signals, it is not guaranteed to get robust optimization value when the typical ICA-based algorithm is

applied, thus the LMS approach works better. Gaussian signals can be described by only the first and second-order statistics without higher order statistics, and thus LMS is adequate. Furthermore, ICA requires more computations than LMS, so LMS is preferred. Only for super-Gaussian signals, ICA-based approach is superior to LMS due to its higher order statistics.

7.5 Simulations

In this section, the performance of the LMS and ICA algorithms are compared using signals with different distributions. The performance measurement is the SNR of the output u or y_1, which is defined as follows,

$$\text{SNR} = \frac{< (s(k))^2 >}{< (u(k) - s(k))^2 >} \tag{7.16}$$

The transfer function h from the noise source to the primary input is 9^{th} order and generated randomly by Matlab function *rand*(1,10). The noise n_0 is a zero-mean white Gaussian noise. Laplacian and uniform distributed signals are artificially generated as super-Gaussian and sub-Gaussian message signals, respectively. The number of the adaptive filter taps is set to be 10 and *tanh*(.) is chosen as $g(.)$. Step sizes are adjusted so that LMS and ICA have the same convergence speeds. All results shown are averaged over 1000 Monte Carlo simulation runs.

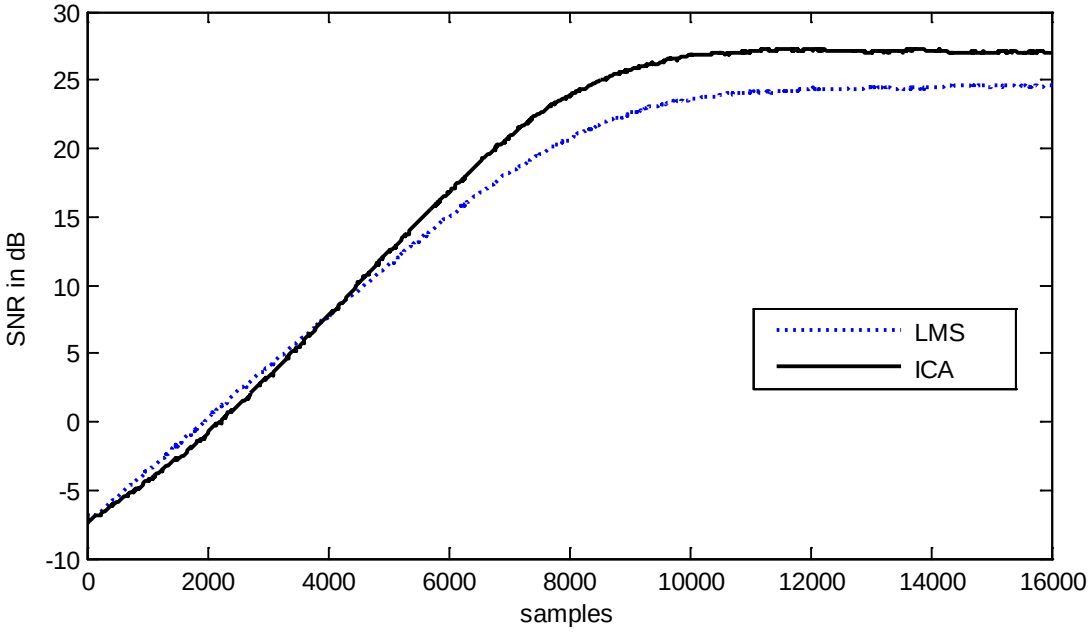

Figure 62 Convergence Curve for Super-Gaussian Signal

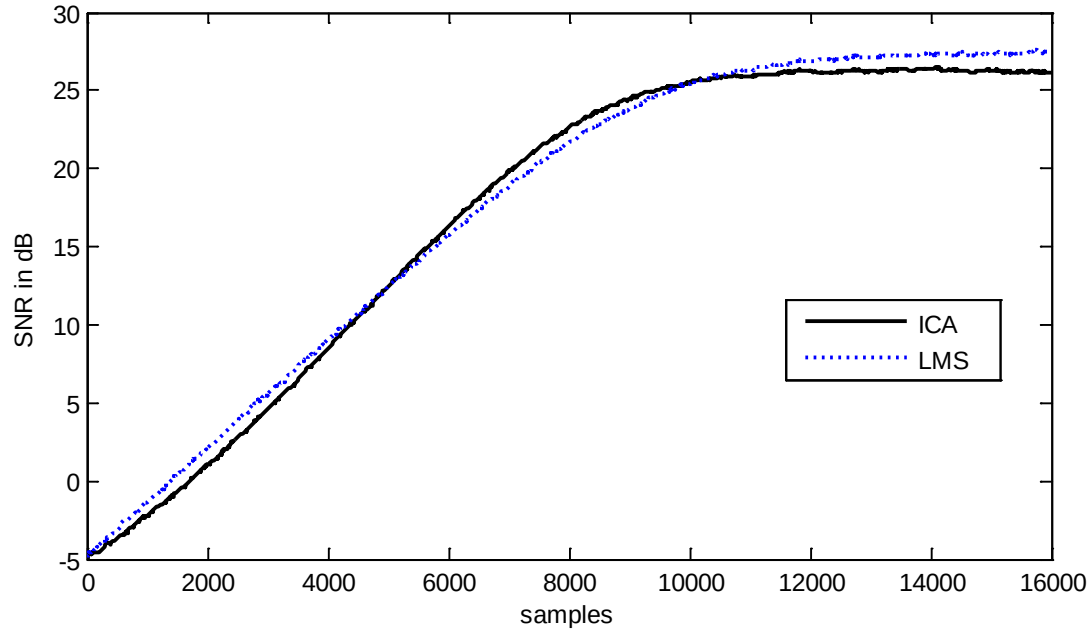

Figure 63 Convergence Curve for Gaussian Signal

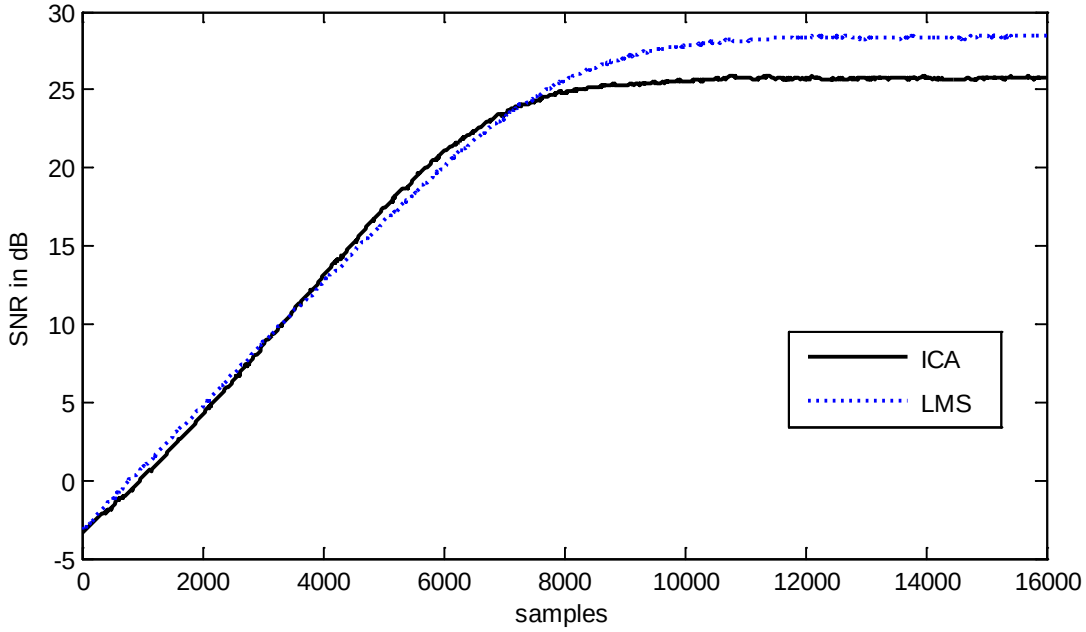

Figure 64 Convergence Curve for Sub-Gaussian Signal

Figs 62–64 plot the convergence curves of ICA and LMS based algorithms for super-Gaussian, Gaussian and sub-Gaussian signals, respectively. Fig. 62 shows that the performance of the ICA-based approach is better than LMS for super-Gaussian signals. The potential reason is that there exist components in the primary input which involve higher order statistics of the reference signal. These noise components can be cancelled by the ICA-based learning rule. Fig. 63 illustrates that for Gaussian signals, the ICA-based approach provides comparable or slightly worse SNR value than LMS. That is because Gaussian signals can be described by only the first and second-order statistics, so the ICA-based approach which utilizes higher order statistics does not have any advantage over the LMS algorithm. For sub-Gaussian signal simulation shown in Fig. 64, while LMS achieves higher SNR, the performance of the ICA-based approach degrades because the robust nonlinearity function $G(.)$ is not the optimal choice according to the pdf of the signal.

7.6 Conclusion

In this chapter, the effect of signals' probabilistic distributions on the performance of adaptive noise canceling algorithms is studied. Both theoretical analysis and computer simulation lead to the conclusion that the ICA-based approach yields higher SNR than the conventional LMS algorithm for super-Gaussian signals and LMS performs better for other signals with higher computational efficiency. Therefore, signal distribution can be a universal criterion to choose the better adaptive noise cancellation algorithm between LMS and ICA.

CHAPTER 8 CONTRIBUTIONS AND FUTURE WORKS

8.1 Major Contributions

An outline of the contributions is given below.

Chapter 2 derives a unified block based approach for generating optimal complex adaptive FIR filtering algorithms. The general formulation leads to two classes of adaptive algorithms, CBCI-LMS and CBC-LMS, both based on the block adaptation, complex conjugate gradients, and complex Taylor series expansion. Also, the computational complexity and the matrix inversion lemma are addressed.

In Chapter 3, the proposed CBCI-LMS and CBC-LMS are applied to channel identification and equalization in wireless communications. The implementation issues, including the block shifting technique, block size selection, search dimension parameter and an optional scaling factor, are discussed. Simulation results confirm the significant improvement in the convergence speed of the proposed algorithms, while maintaining excellent accuracy.

In Chapter 4, the CBCI-LMS and CBC-LMS are applied to adaptive array beamforming. The simulation results show that the proposed methods exhibit improved convergence speed and accuracy, irrespective of SIR, number of antenna elements, and user modulation schemes.

Chapter 5 proposes a novel FIR filtering algorithm, OBA-C, to restore the circularity of a distorted complex signal. The proposed technique exploits the concept of circularity to guide the update direction for the filter weights. In addition, it uses Taylor series expansion to dynamically adjust the coefficients of the adaptive filter at each iteration. The OBA-C is a totally blind processing algorithm and it fully exploits the degrees of freedom of the optimization space to improve performance.

Chapter 6 applies the OBA-C method to compensate for frequency-dependent I/Q imbalance. Computer simulations show that the OBA-C has attractive properties in terms of the image rejection performance and the convergence speed, as compared to the existing method. Other desirable features of the OBA-C technique include the simplicity of implementation, the ability to support multimode, multiband radio systems, and the robustness against different mismatch levels and RF impairments.

Chapter 7 studies the performance of LMS- and ICA-based approaches with different signals' probabilistic distributions. It is observed that ICA based approach works better for super-Gaussian signals while LMS is preferable for sub-Gaussian signals. The obtained results lead to the conclusion that if prior information of the signal's probabilistic distribution is available, an appropriate choice between LMS- and ICA-based approaches can be made to achieve better noise rejection performance.

The methodology adopted in this research work is consistent with current trend in the area of wireless receiver design. The proposed schemes are helpful towards the realization of SDR, in which the hardware complexity can be significantly reduced without performance degradation.

8.2 Future Research Directions

The research work presented in this dissertation can be extended in several directions.

8.2.1 Complex Block Conjugate LMS Algorithm for Underdetermined Systems

The conjugate gradient method continues to be a versatile tool in various adaptive filtering applications, due to its unique tradeoff between convergence speed and computational complexity. In Chapter Two, the CBCI-LMS and the CBC-LMS algorithms have been developed.

One interesting yet challenging future research area is the feasibility of the proposed algorithms for underdetermined optimization systems. The problem of underdetermined system arises when the number of antenna elements is less than the actual number of users. For example, consider applying the adaptive beamforming technology presented in Chapter 4 to mobile communications. In the downlink of a cellular system, it is impossible to know in advance the exact number of interferers, especially when the number is not fixed in practice. Also, installing a large set of antenna elements in mobile units is not practical due to the limited size and high cost. Therefore, it is highly desirable to use fewer antennas than the number of user signals.

8.2.2 Complex Block Adaptive I/Q Compensation Scheme for Wireless Transmitters

The I/Q imbalance happens in the upconversion at the transmitter [115] and the down-conversion at the receiver. These mismatches are unavoidable in practical implementation, and limit attenuation of the mirror frequencies. In Chapter 5, the OBA-C algorithm has been developed to correct the I/Q imbalance at the receiver by utilizing the circularity nature of most communication signals. Similarly, a circularity based adaptive filtering algorithm can be developed to compensate for the I/Q imbalance at the wireless transmitter.

8.2.3 Effect of Complex Signals' pdf on Performance of Adaptive Interference Canceling Algorithms

Chapter 7 studies the performance of two adaptive noise cancellation approaches with different signals' probabilistic distributions for real-valued system. In modern wireless communications, the complex LMS algorithm [57]–[59] and complex ICA algorithm [17], [32] have been widely used. The effect of complex signals' pdf on the performance of adaptive interference cancelling algorithms is a useful yet challenging future research topic. Similarities are expected between the real-valued and complex-valued systems.

8.2.4 Adaptive Interference Canceling Algorithms for Correlated Interference

The work in Chapter 7 can be extended to examine the performance of different algorithms when the desired signal is correlated with the interference. Serious study on this topic is recommended for different orders (second-order, forth-order, etc.) of correlation between the desired signal and the interference.

8.2.5 Hybrid ICA-LMS Algorithm

The performance of the LMS and ICA approaches with different signals' probabilistic distributions is studied in Chapter 7, which indicates that the ICA based approach works better for super-Gaussian signals, while LMS based method is preferable for sub-Gaussian signals.

Considering the same problem from a different perspective, the performance of the LMS-based algorithm starts deteriorating if the desired signal leaks to the reference sensor. In order to

remove this limitation, the ICA-based approach is a promising alternative solution to help achieve convergence.

On the other hand, ICA is a widely used BSS method to separate a set of multivariate signals into independent components. Instead of the second-order estimator applied in LMS, ICA employs higher order statistics to provide more accurate solutions in most applications. However, it has the drawback of high computational complexity and the issue of order, sign and energy ambiguities. Traditionally, the ambiguity problems can be solved using sophisticate algorithms, which further increases the overall computational complexity. If a sequence of training data is available at the beginning phase of the adaptation process, the ambiguity problems can be solved by some computational efficient supervised algorithms (e.g., LMS).

Intuitively, the idea of a hybrid LMS-ICA technique is generated, which has the potential advantages of both LMS and ICA, providing an accurate and efficient solution for many wireless applications. There is a great possibility that the hybrid ICA-LMS algorithm has desirable features in convergence speed as well as accuracy, especially in a high interference scenario. Applying this method would significantly improve system capacity and reduce network cost. The preliminary formulation of the LMS-ICA algorithm is developed as follows,

$\mathbf{w}(k)$ is defined as the weight vector of the adaptive filter at time index *k*, given by

$$\mathbf{w}(k) = [w_1(k), w_2(k), ...w_N(k)]^T \tag{8.1}$$

The update function of $\mathbf{w}(k)$ based on LMS and ICA methods are given as follows, respectively,

$$\mathbf{w}(k+1) = \mathbf{w}(k) - \mu_{\text{LMS}}(k) \cdot \frac{\partial f_{\text{MSE}}(k)}{\partial \mathbf{w}(k)} \tag{8.2}$$

$$\mathbf{w}(k+1) = \mathbf{w}(k) + \mu_{\mathrm{ICA}}(k) \cdot \frac{\partial f_{\mathrm{ICA}}(k)}{\partial w(k)} \tag{8.3}$$

where $f_{\mathrm{MSE}}(k)$ and $f_{\mathrm{ICA}}(k)$ are the MSE function and the ICA cost function. $f_{\mathrm{ICA}}(k)$ can be the equation of kurtosis [101], negentropy [102], or some other criteria. $\mu_{\mathrm{LMS}}(k)$ and $\mu_{\mathrm{ICA}}(k)$ are the step sizes for the LMS and ICA methods, respectively, both of which can be time invariant or time variant.

The suggested formula to update the adaptive filter coefficients is given as,

$$\mathbf{w}(k+1) = \mathbf{w}(k) - \mu_{\mathrm{LMS}}(k) \cdot \frac{\partial f_{\mathrm{MSE}}(k)}{\partial \mathbf{w}(k)} + \mu_{\mathrm{ICA}}(k) \cdot \frac{\partial f_{\mathrm{ICA}}(k)}{\partial \mathbf{w}(k)} \tag{8.4}$$

More research efforts are needed to find the best choice for the hybrid LMS-ICA cost function. Also, the selection of $\mu_{\mathrm{LMS}}(k)$ and $\mu_{\mathrm{ICA}}(k)$ needs to be seriously studied.

APPENDIX: MATRIX INVERSION LEMMA

For any invertible $N \times N$ matrices **A** and **B**, $(\mathbf{AB})^{-1} = \mathbf{B}^{-1}\mathbf{A}^{-1}$. More generally, if $\mathbf{A}_1$, $\mathbf{A}_2$, ..., $\mathbf{A}_k$ are invertible $N \times N$ matrices, then $(\mathbf{A}_1\mathbf{A}_2\cdots\mathbf{A}_{k-1}\mathbf{A}_k)^{-1} = \mathbf{A}_k^{-1}\mathbf{A}_{k-1}^{-1}\cdots\mathbf{A}_2^{-1}\mathbf{A}_1^{-1}$.

The autocorrelation matrix $\mathbf{R}(k)$ is defined as,

$$\mathbf{R}(k) = \mathbf{X}^H(k)\mathbf{X}(k) \tag{A.1}$$

Since $\mathbf{Q}(k)$ and $\mathbf{R}(k)$ are both $N \times N$ matrices, the following term in (2.49) is obtained,

$$\begin{aligned}[\mathbf{Q}^H(k)\cdot\mathbf{X}^H(k)\mathbf{X}(k)\cdot\mathbf{Q}(k)]^{-1} &= [\mathbf{Q}^H(k)\cdot\mathbf{R}(k)\cdot\mathbf{Q}(k)]^{-1} \\ &= \mathbf{Q}^{-1}(k)\cdot\mathbf{R}^{-1}(k)\cdot(\mathbf{Q}^H(k))^{-1}\end{aligned} \tag{A.2}$$

It is worthwhile to mention that $\mathbf{Q}(k)$ is a diagonal matrix, so the matrix inversion of $\mathbf{Q}(k)$ is affordable.

The matrix inversion lemma [54] can be applied to invert an $N \times N$ matrix $\mathbf{R}(k)$ at the k^{th} iteration, provided it contains the $(N-1)\times(N-1)$ section of the matrix at the $(k-1)^{\text{th}}$ iteration, i.e., $\mathbf{R}(k-1)$. The description of the lemma proceeds as follows.

The N x N matrix $\mathbf{R}(k)$ is partitioned into sub-matrices as follows,

$$\mathbf{R}(k) = \left[\begin{array}{c|c} \overline{R}_{11}(k) & \overline{R}_{12}(k) \\ \hline \overline{R}_{12}^H(k) & \overline{\overline{R}} \end{array}\right] \tag{A.3}$$

where $\overline{R}_{11}(k)$ is a scalar, $\overline{R}_{12}(k)$ is a $1\times(N-1)$ row vector, and $\overline{\overline{R}}$ is a $(N-1)\times(N-1)$ square matrix. Since $\mathbf{R}(k-1)$ is also known, it is partitioned in the following manner,

$$\mathbf{R}(k-1)=\left[\begin{array}{c|c} \overline{R} & \hat{R}_{12}(k-1) \\ \hline \hat{R}_{12}^{H}(k-1) & \hat{R}_{22}(k-1) \end{array}\right] \tag{A.4}$$

where $\hat{R}_{12}(k-1)$ is a $(N-1)\times 1$ column vector, $\hat{R}_{22}(k-1)$ is a scalar, and $\overline{R}$ is a matrix defined in (A.3).

The lemma recursively computes the matrix inverse, which means it computes $\mathbf{R}^{-1}(k)$ based on $\mathbf{R}^{-1}(k-1)$ given by

$$\mathbf{R}^{-1}(k-1)=\left[\begin{array}{c|c} v_{11} & v_{12} \\ \hline v_{12}^{H} & v_{22} \end{array}\right] \tag{A.5}$$

where v_{22} is a scalar, v_{12} is a $(N-1)\times 1$ vector, and v_{11} is a $(N-1)\times(N-1)$ matrix.

Since $\mathbf{R}(k)$, $\mathbf{R}(k-1)$, and $\mathbf{R}^{-1}(k-1)$ in (A.3), (A.4), and (A.5), are already known, the matrix inversion lemma utilizes this information to compute $\mathbf{R}^{-1}(k)$, which can be expressed as

$$\mathbf{R}^{-1}(k)=\left[\begin{array}{c|c} u_{11} & u_{12} \\ \hline u_{12}^{H} & F \end{array}\right] \tag{A.6}$$

where

$$u_{11}=\frac{1}{\overline{R}_{11}(k)}+\frac{1}{\overline{R}_{11}^{2}(k)}\overline{R}_{12}(k)F\overline{R}_{12}^{H}(k) \tag{A.7}$$

$$u_{12}=-\frac{1}{\overline{R}_{11}(k)}\overline{R}_{12}(k)F \tag{A.8}$$

$$F=[\overline{R}-\frac{1}{\overline{R}_{11}(k)}\overline{R}_{12}^{H}(k)\overline{R}_{12}(k)]^{-1} \tag{A.9}$$

The $(N-1)\times(N-1)$ matrix F is computed using the following lemma,

$$F=\overline{R}^{-1}-\overline{R}^{-1}\overline{R}_{12}^{H}(k)C\overline{R}_{12}(k)\overline{R}^{-1} \tag{A.10}$$

where

$$C = [\overline{R}_{12}(k)\overline{R}^{-1}\overline{R}_{12}^{H}(k) - \overline{R}_{11}(k)]^{-1} \tag{A.11}$$

$$\overline{R}^{-1} = v_{11}[I - \hat{R}_{12}(k-1)v_{12}^{H}]^{-1} \tag{A.12}$$

Applying another matrix inversion lemma, the inverse in (A.12) can be calculated as follows,

$$\overline{R}^{-1} = v_{11}\{I + \hat{R}_{12}(k-1)v_{12}^{H}/[1 - v_{12}^{H}\hat{R}_{12}(k-1)]\} \tag{A.13}$$

In this manner, (A.6)–(A.13) can be used to compute the inverse of the matrix $\mathbf{R}(k)$, which significantly reduces the computational complexity.

LIST OF REFERENCES

[1] ITU, *The World in 2011: ICT Facts and Figures*, http://www.itu.int/ITU-D/ict/facts/2011/material/ICTFactsFigures2011.pdf.

[2] Portio Research Ltd, *Mobile Factbook 2012*, http://www.portioresearch.com/en/free-mobile-factbook.aspx.

[3] Mak, P.-I.; U, S-P; Martins, R.P., "Transceiver Architecture Selection: Review, State-of-the-Art Survey and Case Study", in *IEEE Circuits and Systems Magazine*, Vol. 7, Issue 2, pp. 6–25, 2007.

[4] Hueber, G.; Zou, Y.; Dufrene, K.; Stuhlberger, R.; Valkama, M., "Smart Front-End Signal Processing for Advanced Wireless Receivers", in *IEEE Journal of Selected Topics in Signal Processing*, Vol. 3, Issue 3, pp. 472–487, 2009.

[5] Namgoong, W.; Meng, T. H., "Direct-Conversion RF Receiver Design", in *IEEE Transactions on Communications*, Vol. 49, No.3, pp. 518–529, Mar. 2001.

[6] Martin, K.W., "Complex signal processing is not complex", in *IEEE Transactions on Circuits and Systems I: Regular Papers*, Vol.51, No.9, pp. 1823–1836, Sep. 2004.

[7] Schreier, R.; Temes, G., *Bandpass and Quadrature DeltaSigma Modulation*, ISBN: 9780470546772, pp. 139–178, Wiley-IEEE Press, 2005.

[8] Lyons, R., *Recursive Discrete Time Sinusoidal Oscillators*, ISBN: 9780470170090, pp. 203–222, Wiley-IEEE Press, 2007.

[9] Mirabbasi, S.; Martin, K., "Hierarchical QAM: A Spectrally Efficient DC-Free Modulation Scheme", in *IEEE Communications Magazine*, Vol. 38, Issue 11, pp. 140–146, Nov. 2000.

[10] Saberinia, E.; Tang, J.; Tewfik, A.H.; Parhi, K.K., "Pulsed-OFDM Modulation for Ultrawideband Communications", in *IEEE Transactions on Vehicular Technology*, Vol.58 , Issue 2, pp. 720–726, 2009.

[11] "IEEE Standard for Information technology– Local and metropolitan area networks– Specific requirements– Part 11: Wireless LAN Medium Access Control (MAC) and Physical Layer (PHY) specifications Amendment 8: IEEE 802.11 Wireless Network Management", in *IEEE Std 802.11v-2011 (Amendment to IEEE Std 802.11-2007 as amended by IEEE Std 802.11k-2008, IEEE Std 802.11r-2008, IEEE Std 802.11y-2008, IEEE Std 802.11w-2009, IEEE Std 802.11n-2009, IEEE Std 802.11p-2010, and IEEE Std 802.11z-2010)*, pp.1–433, Feb. 9, 2011.

[12] Tolli, A.; Codreanu, M.; Juntti, M., "Linear Multiuser MIMO Transceiver Design With Quality of Service and Per-Antenna Power Constraints", in *IEEE Transactions on Signal Processing*, Vol. 56 , Issue 7 , Part 1, pp. 3049–3055, 2008.

[13] Narasimha, A.; Analui, B.; Liang, Y.; Sleboda, T.J.; Abdalla, S.; Balmater, E.; Gloeckner, S.; Guckenberger, D.; Harrison, M.; Koumans, R.G.M.P.; Kucharski, D.; Mekis, A.; Mirsaidi, S.; Song, D.; Pinguet, T., "A Fully Intergrated 4× 10-Gb/s DWDM Optoelectronic Transceiver Implemented in a Standard 0.13 μm CMOS SOI Technology", in *IEEE Journal of Solid-state circuits*, Vol. 45, Issue 12, pp. 2736–2744, Dec. 2007.

[14] Adali, T.; Haykin, S., *Adaptive Signal Processing: Next Generation Solutions*, Digital Object Identifier: 10.1002/9780470575758.ch1, pp. 1–85, Wiley-IEEE Press, 2010.

[15] Emira, A.A.; Sanchez-Sinencio, E., "A pseudo differential complex filter for Bluetooth with frequency tuning", in *IEEE Transactions on Circuits and Systems II: Analog and Digital Signal Processing*, Vol. 50, Issue 10, pp. 742–754, Oct. 2003.

[16] Mikhael, W.B.; Ranganathan, R., "Complex Adaptive FIR Digital Filtering Algorithm with Time-Varying Independent Convergence Factors", in *Signal Processing*, Vol. 88, Issue 7, pp. 1889–1893, Jul. 2008.

[17] Ranganathan, R.; Mikhael, W.B., "A Comparative Study of Complex Gradient and Fixed-Point ICA algorithms for Interference Suppression in Static and Dynamic Channels", in *Signal Processing*, Vol. 88, Issue 2, pp.399–406, Feb. 2008.

[18] Cuypers, C.; Voo, N.Y.; Teplechuk, M.; Sewell, J.I., "General synthesis of complex analogue filters", in *IEE Proceedings – Circuits, Devices and Systems*, Vol. 152, Issue 1, pp. 7–15, 2005.

[19] Kobayashi, H.; Kang, J.; Kitahara, T.; Takigami, S.; Sadamura, H., "Explicit transfer function of RC polyphase filter for wireless transceiver analog front-end", in *IEEE Asia-Pacific Conference (ASIC)*, pp. 137–140, 2002.

[20] Sedra, A.; Snelgrove, W.; Allen, R., "Complex Analog Bandpass Filters Designed by Linearly Shifting Real Low-Pass Prototypes", in *of Int. Symp. on Circuits and Systems (ISCAS' 85)*, Vol. III, pp. 1223–1226, 1985.

[21] Teo, T.H.; Khoo, E.S.; Uday, D.; Tear, C.B., "Design, analysis, and implementation of analog complex filter for low-IF Wireless LAN application", in *17th International Conference on VLSI Design, 2004*, pp. 416–421, 2004.

[22] Jantzi, S.; Martin, K.; Sedra, A.S., “The effects of Mismatch in Complex Bandpass $\sum\Delta$ Modulators”, in *Proc. IEEE Intl. Symp. on Circuits and Systems (ISCAS)*, pp. 227–230, May 1996.

[23] Gil, G.-T.; Kim, Y.-D.; Lee, Y.-H., “Non-Data-Aided Approach to I/Q Mismatch Compensation in Low-IF Receivers”, in *IEEE Transactions on Signal Processing*, Vol. 55, No. 7, pp. 3360–3365, Jul. 2007,

[24] Adiseno; Ismail, M.; Olsson, H., “A wide-band RF front-end for multiband multistandard high-linearity low-IF wireless receivers”, in *IEEE Journal of Solid-State Circuits*, Vol. 37, Issue 9, pp. 1162–1168, 2002.

[25] Carta, C.; Vogt, R.; Bachtold, W., “Multiband monolithic BiCMOS low-power low-IF WLAN receivers”, in *IEEE Microwave and Wireless Components Letters*, Vol. 15, Issue 9, pp. 543–545, 2005.

[26] Rudell, J.C.; Ou, J.; Cho, T.B.; Chien, G.; Brianti, F.; Weldon, J.A.; Gray, P.R., “A 1.9-GHz Wide-Band IF Double Conversion CMOS Receiver for Cordless Telephone Applications”, in *IEEE Journal of Solid-State Circuits*, Vol. 32, Issue 12, pp. 2071–2088, Dec. 1997.

[27] Parssinen, A., *Direct Conversion Receivers in Wide-band Systems*, Kluwer Academic Pub, Sep. 2007.

[28] Kitsunezuka, M.; Tokairin, T.; Maeda, T.; Fukaishi, M., “A Low-IF/Zero-IF Reconfigurable Analog Baseband IC With an I/Q Imbalance Cancellation Scheme”, in *IEEE Journal of Solid-State Circuits*, Vol.46, No.3, pp.572–582, Mar. 2011.

[29] Sun, C.; Cheng, J.; and Ohira, T., *Handbook on Advancements in Smart Antenna Technologies for Wireless Networks*, IGI 2008.

[30] Zeman, J.; Nagle, H.T., "A High-Speed Microprogrammable Digital Signal Processor Employing Distributed Arithmetic", in *Proc. IEEE Journal of Solid-State Circuits*, Vol. 15, Issue 1, pp. 70–80, 1980.

[31] Chen, C.K.; Tseng, P.C.; Chang, Y.C.; Chen, L.G., "A digital signal processor with programmable correlator array architecture for third generation wireless communication system", in *Proc. IEEE Transactions on Circuits and Systems II: Analog and Digital Signal Processing*, Vol. 48, Issue 12, pp. 1110–1120, 2001.

[32] Ranganathan, R.; Yang, T.T.; Mikhael, W.B., "Optimum Block Adaptive ICA for Separation of Real and Complex Signals With Known Source Distributions in Dynamic Flat Fading Environments", in *Journal of Circuits Systems and Computers (JCSC)*, Vol. 19, Issue 2, pp. 367–379, Apr. 2010.

[33] Liu, Y.; Ranganathan, R.; Hunter, M.T.; Mikhael, W.B., "Conjugate Gradient Based Complex Block LMS Employing Time-Varying Optimally Derived Stepsizes", in *IEEE Midwest Symposium on Circuits and Systems, Cancun, Mexico*, pp. 590–593, August 2-5, 2009.

[34] Dash, P.K.; Hasan, S.; Panigrahi, B.K., "Adaptive complex unscented Kalman filter for frequency estimation of time-varying signals", in *IET Science, Measurement & Technology*, Vol. 4, Issue 2, pp. 93–103, 2010.

[35] Took, C.C.; Mandic, D.P., "Adaptive IIR Filtering of Noncircular Complex Signals", in *IEEE Transactions on Signal Processing*, Vol. 57, Issue 10, pp. 4111–4118, 1999.

[36] Rivet, F.; Deval, Y.; Begueret, J.-B.; Dallet, D.; Cathelin, P.; Belot, D., "A Disruptive Receiver Architecture Dedicated to Software-Defined Radio", in *IEEE Transactions on Circuits and Systems II*, Vol. 55, Issue 4, pp. 344–348, 2008.

[37] Buracchini, E., "The software radio concept", in *IEEE Communications Magazine*, Vol. 38, Issue 9, pp. 138–143, 2000.

[38] Ting, L.-K.; Woods, R.; Cowan, C.F.N., "Virtex FPGA Implementation of a Pipelined Adaptive LMS Predictor for Electronic Support Measures Receivers", in *IEEE Transactions on Very Large Scale Integration (VLSI) Systems*, Vol. 13, Issue 1, pp. 86–95, 2005.

[39] Bahai, A.R.S.; Saltzberg, B.R.; Ergen, M., *Multi-carrier digital communications: Theory and Applications of OFDM*, Springer, 2004.

[40] Mahattanakul, J., "The Effect of I/Q Imbalance and Complex Filter Component Mismatch in Low-IF Receivers", in *IEEE Transactions on Circuits and Systems I*, Vol. 53, Issue 2, pp. 247–253, Feb. 2006.

[41] Tse, D.; Viswanath, P, *Fundamentals of Wireless Communication*, Cambridge University Press, 2005.

[42] Widrow, B.; Steams, S.D., *Adaptive Signal Processing*, Eagle-wood Cliffs, NJ: Prentice-Hall, 1985.

[43] Widrow, B.; McCool, J.M.; Larimore, M.G.; Johnson, C.R., Jr., "Stationary and nonstationary learning characteristics of the LMS adaptive filter", in *Proceedings of the IEEE*, Vol.64, No.8, pp. 1151–1162, Aug. 1976.

[44] Widrow, B.; Glover, J.R., Jr.; McCool, J.M.; Kaunitz, J.; Williams, C.S.; Hearn, R.H.; Zeidler, J.R.; Dong, E., Jr.; Goodlin, R.C., "Adaptive noise cancelling: Principles and applications", in *Proceedings of the IEEE* , Vol.63, No.12, pp. 1692–1716, Dec. 1975.

[45] Widrow, B.; Mantey, P.E.; Griffiths, L.J.; Goode, B.B., "Adaptive antenna systems", in *Proceedings of the IEEE*, Vol.55, No.12, pp. 2143–2159, Dec. 1967.

[46] Godavarti, M.; Hero, A.O., III, "Partial update LMS algorithms", in *IEEE Transactions on Signal Processing*, Vol.53, No.7, pp. 2382–2399, July 2005.

[47] Vicen-Bueno, R.; Martinez-Leira, A.; Gil-Pita, R.; Rosa-Zurera, M., "Modified LMS-Based Feedback-Reduction Subsystems in Digital Hearing Aids Based on WOLA Filter Bank", in *IEEE Transactions on Instrumentation and Measurement*, Vol.58, No.9, pp.3177–3190, Sep. 2009.

[48] Mikhael, W.; Wu, F.; Kazovsky, L.; Kang, G.; Fransen, L., "Adaptive filters with individual adaptation of parameters", in *IEEE Transactions on Circuits and Systems*, Vol.33, No.7, pp. 677–686, Jul. 1986.

[49] Ranganathan, R., Mikhael, W.B.: "Complex Adaptive FIR Digital Filtering Algorithm with Time-Varying Independent Convergence Factors", in *Signal Processing*, Vol. 88, Issue 7, pp. 1889–1893, July 2008.

[50] Wu, F.H., "Time-varying gradient algorithms for block implementation of adaptive digital filters", *Ph.D. dissertation*, West Virginia University, Morgantown, WV, Jun, 1987.

[51] Mikhael, W.B.; Ranganathan, R, "Complex FIR block adaptive algorithm employing optimal time-varying convergence factors", in *2008 Joint 6th International IEEE*

Northeast Workshop on Circuits and Systems and TAISA Conference, 2008. NEWCAS-TAISA 2008, pp.61–64, Jun. 22–25, 2008.

[52] Clark, G.; Mitra, S.; Parker, S., "Block implementation of adaptive digital filters", in *IEEE Transactions on Circuits and Systems*, Vol.28, No.6, pp. 584–592, Jun, 1981.

[53] Cattivelli, F.S.; Sayed, A.H., "Analysis of Spatial and Incremental LMS Processing for Distributed Estimation", in *IEEE Transactions on Signal Processing*, Vol.59, No.4, pp.1465–1480, Apr. 2011.

[54] Faddeev, D. K.; Faddeeva, V. N., *Computational Methods of Linear Algebra*, San Francisco, CA: Freeman, 1963.

[55] Lee, J.C.; Un, C.K., "A reduced structure of the frequency-domain block LMS adaptive digital filter", in *Proceedings of the IEEE*, Vol.72, No.12, pp. 1816–1818, Dec. 1984.

[56] Ferrara, E., "Fast implementations of LMS adaptive filters", in *IEEE Transactions on Acoustics, Speech and Signal Processing*, Vol.28, No.4, pp. 474–475, Aug. 1980.

[57] Widrow, B.; McCool, J.; Ball, M., "The complex LMS algorithm", in *Proceedings of the IEEE*, Vol.63, No.4, pp. 719–720, April 1975.

[58] Baghel, S.; Shaik, R., "Low power and less complex implementation of fast block LMS adaptive filter using distributed arithmetic", in *Students' Technology Symposium (TechSym), 2011 IEEE*, pp. 214–219, Jan. 14–16, 2011.

[59] Fisher, B.; Bershad, N., "The complex LMS adaptive algorithm--Transient weight mean and covariance with applications to the ALE", in *IEEE Transactions on Acoustics, Speech and Signal processing*, Vol. 31, No. 1, pp. 34–44, Feb. 1983.

[60] Haykin, S.; Widrow, B., *Least-Mean-Square Adaptive Filters*, Wiley-Interscience, Hoboken, NJ, 2003.

[61] Sayed, A., *Adaptive Filter*, Ch. 11, pp. 178–182., Wiley-IEEE Press, 2008.

[62] Florian, S.; Bershad, N.J., "A weighted normalized frequency domain LMS adaptive algorithm", in *IEEE Transactions on Acoustics, Speech and Signal Processing*, Vol.36, No.7, pp.1002–1007, Jul 1988.

[63] Gelfand, S.B.; Wei, Y.; Krogmeier, J.V., "The stability of variable step-size LMS algorithms", in *IEEE Transactions on Signal Processing*, Vol.47, No.12, pp.3277–3288, Dec 1999.

[64] Gupta, A.; Joshi, S., "Variable Step-Size LMS Algorithm for Fractal Signals", in *IEEE Transactions on Signal Processing*, Vol.56, No.4, pp.1411–1420, Apr. 2008.

[65] Saad, Y., *Iterative methods for sparse linear systems*, SIAM, 2003.

[66] Shewchuk, J. R., "An Introduction to the Conjugate Gradient Method Without the Agonizing Pain", in *Technical Report: CS-94-125*, Carnegie Mellon University, 1994.

[67] Ahmad, N. A., "A Globally Convergent Stochastic Pairwise Conjugate Gradient-Based Algorithm for Adaptive Filtering", in *IEEE Signal Processing Letters*, Vol. 15, pp. 914–917, 2008.

[68] Erhel, J.; Guyomarc'h, F., "An augmented Conjugate Gradient method for solving consecutive symmetric positive definite systems", in *SIAM Journal on Matrix Analysis and Applications*, Vol. 21, No. 4, pp. 1279–1299, 2000.

[69] Torii, M.; Hagan, M. T., “Stability of steepest descent with momentum for quadratic functions”, in *IEEE Transaction on Neural Networks*, Vol. 13, Issue 3, pp. 752–756, May, 2002.

[70] Liu, Y.; Mikhael, W.B., “A Fast-Converging Adaptive FIR Technique for Channel Equalization”, in *IEEE Midwest Symposium on Circuits and Systems*, Boise, Idaho, pp. 828–831, August 5–8, 2012.

[71] Liu, Y.; Mikhael, W.B., “A Unified Conjugate Gradient Based Approach for Optimal Complex Block FIR Filtering”, submitted to *Circuits, Systems, and Signal Processing*.

[72] Liu, Y.; Ranganathan, R.; Hunter, M. T.; Mikhael, W. B., “Fast-converging conjugate-gradient adaptive algorithm for complex channel estimation” , in *Electronics Letters*, Vol. 46, Issue 2, pp. 180–182, Jan 21, 2010.

[73] Liu, Y.; Ranganathan, R.; Hunter, M.T.; Mikhael, W.B., “Complex Adaptive LMS Algorithm Employing the Conjugate Gradient Principle for Channel Estimation and Equalization”, in *Circuits, Systems, and Signal Processing*, pp. 1–21, doi: 10.1007/ s00034-011- 9368- 8, Nov. 22 2011.

[74] Liu, Y.; Mikhael, W.B., “A Simplified Approach for Complex Block Conjugate Gradient LMS with Individual Adaptation”, under preparation for *IEEE Midwest Symposium on Circuits and Systems*, Columbus, Ohio, August 4–7, 2013.

[75] Apolinario, J., Jr.; Campos, M.L.R.; Diniz, P.S.R., “Convergence analysis of the binormalized data-reusing LMS algorithm”, in *IEEE Transactions on Signal Processing*, Vol.48, No.11, pp. 3235–3242, Nov. 2000.

[76] Zhang, L.; Liu, W.; Langley, R.J., “A Class of Constrained Adaptive Beamforming Algorithms Based on Uniform Linear Arrays”, in *IEEE Transactions on Signal Processing*, Vol.58, No.7, pp.3916–3922, July 2010.

[77] Tong, Y.; Tennant, A., “A Two-Channel Time Modulated Linear Array With Adaptive Beamforming”, in *IEEE Transactions on Antennas and Propagation*, Vol. 60, No.1, pp.141–147, Jan. 2012.

[78] Li, J.; Stoica, P., *Robust Adaptive Beamforming*, John Wiley & Sons, New York, NY, 2005.

[79] Huang, X.; Guo, Y.J.; Bunton, J.D., “A hybrid adaptive antenna array”, in *IEEE Transactions on Wireless Communications*, Vol.9, No.5, pp.1770–1779, May 2010.

[80] Srar, J.A.; Chung, K.-S.; Mansour, A., “Adaptive Array Beamforming Using a Combined LMS-LMS Algorithm”, in *IEEE Transactions on Antennas and Propagation*, Vol.58, No.11, pp.3545–3557, Nov. 2010.

[81] Huang, F.; Sheng. W.; Ma, X., “Efficient parallel adaptive array beamforming algorithm”, in *Journal of Systems Engineering and Electronics*, Vol.20, No.6, pp.1221–1226, Dec. 2009.

[82] Vía, J.; Ramírez, D.; Santamaría, I., “Properness and Widely Linear Processing of Quaternion Random Vectors”, in *IEEE Transactions on Information Theory*, Vol.56, No.7, pp.3502–3515, July 2010.

[83] Ollila, E., “On the Circularity of a Complex Random Variable”, in *IEEE Signal Processing Letters*, Vol.15, pp.841–844, 2008.

[84] Picinbono, B., “On circularity”, in *IEEE Transactions on Signal Processing*, Vol. 42, No. 12, pp. 3473–3482, Dec. 1994.

[85] Schreier, P. J.; Scharf, L. L., “Second-order analysis of improper complex random vectors and processes”, in *IEEE Transactions on Signal Processing*, Vol. 51, No. 3, pp. 714–725, Mar. 2003.

[86] Eriksson, J.; Koivunen, V., “Complex random vectors and ICA models: Identifiability, uniqueness and seperability”, in *IEEE Transactions on Information Theory*, Vol. 52, No. 3, pp. 1017–1029, Mar. 2006.

[87] Abeida, H.; Delmas, J.-P., “MUSIC-like estimation of direction of arrival for noncircular sources”, in *IEEE Transactions on Signal Processing*, Vol. 54, No. 7, pp. 2678–2690, Jul. 2006.

[88] Douglas, S. C., “Fixed-point algorithms for the blind separation of arbitrary complex-valued non-Gaussian signal mixtures”, in *EURASIP Journal on Advances in Signal Process*ing, pp. 83, 2007.

[89] Anttila, L.; Valkama, M.; Renfors, M., “Blind compensation of frequency-selective I/Q Imbalances in Quadrature Radio Receivers: Circularity-based Approach”, in *IEEE ICASSP*, Honolulu, HI, pp. III245–III248, Apr. 2007.

[90] Anttila, L.; Valkama, M.; Renfors, M., “Circularity-based I/Q imbalance compensation in wideband direct-conversion receivers”, in *IEEE Transactions on Vehicular Technology*, Vol.57, No.4, pp.2099–2113, July 2008.

[91] Liu, Y.; Ranganathan, R.; Hunter, M.T.; Mikhael, W.B.; Yang, T.T., "Optimal Block Adaptive I/Q Mismatch Compensation Based on Circularity", in *IEEE Midwest Symposium on Circuits and Systems,* Aug., 2010, pp. 320–323.

[92] Liu, Y.; Yang, T.T.; Mikhael, W.B., "A Non-Data-Aided Frequency-dependent I/Q Mismatch Compensation Approach and Performance Analysis", submitted to *Eurasip Signal Processing*.

[93] Liu, Y.; Yang, W.B., "An Adaptive Filtering Algorithm to Compensate for Frequency-dependent Image Interference in Practical Wireless Receivers", submitted to *J. Circuit Syst. Comp.*

[94] Garcia, J.C.F.; Kalenatic, D.; Bello, C.A.L., "An evolutionary approach for imputing missing data in time series", in *J. Circuit Syst. Comp.* Vol. 19, pp. 107–121, 2010.

[95] Mendieta, F.J.; Trevino, A.; Martinez, C.A., "Complementary sequence correlations with applications to reflectometry studies", in *Instrumentation and Development*, Vol.3, No.6, pp. 37–46, 1996.

[96] Proakis, J.G., *Digital Communications*, 3rd ed. New York: McGraw-Hill, 1995.

[97] Zheng, B; Bapat, R. B., "Generalized inverse $A^{(2)}_{T,S}$ and a rank equation", in *Applied Mathematics and Computation*, Vol. 155, pp. 407–415, 2004,

[98] Yang, T.T.; Mikhael, W.B., "Baseband digital image-suppression in low-IF receivers by complex-valued ICA", in *2003 IEEE 46th Midwest Symposium on Circuits and Systems*, Vol. 3, pp. 1287–1290, Dec. 27–30, 2003.

[99] Lee, J.; Ha, Y.; Shin, B.-S.; Kim, S.; Kim, B.-M.; Chung, W., “Novel Pilot Scheme for Transmitter IQ Mismatch Compensation in CO-OFDM System”, in IEEE Photonics Technology Letters, Vol.24, No.17, pp.1543-1545, Sept.1, 2012.

[100] Egashira, Y.; Tanabe, Y.; Sato, K., “A novel IQ imbalance compensation method with pilot-signals for OFDM system”, in *2006 IEEE 64th Vehicular Technology Conference*, pp.1–5, Sept. 25–28, 2006.

[101] Gao, J.; Zhu, X.; Lin, H.; Nandi, A.K., “Independent component analysis based semi-blind I/Q imbalance compensation for MIMO OFDM systems”, in *IEEE Transactions on Wireless Communications*, Vol.9, No.3, pp.914–920, March 2010.

[102] Tsai, Y.; Yen, C.; Wang, X., “Blind frequency-dependent I/Q imbalance compensation for direct-conversion receivers”, in *IEEE Transactions on Wireless Communications*, Vol.9, No.6, pp.1976–1986, June 2010.

[103] Matsui, M.; Nakagawa, T.; Kudo, R.; Ishihara, K.; Mizoguchi, M., “Blind frequency-dependent IQ imbalance compensation scheme using CMA for OFDM system”, in *IEEE 22nd International Symposium on Personal Indoor and Mobile Radio Communications (PIMRC), 2011*, pp.1386-1390, Sep. 11–14, 2011.

[104] Chakraborty, M.; Sakai, H., “Convergence analysis of a complex LMS algorithm with tonal reference signals”, in *IEEE Transactions on Speech and Audio Processing*, Vol. 13, Issue. 2, pp. 286–292, 2005.

[105] Zhou, Y.; Guan, Y.; Law, C., “Modified Phase-Only Correlator with Kurtosis-Based Amplified-Noise Suppression”, in *IEEE Transactions on Wireless Communications*, Vol. 9, Issue. 11, pp. 3341–3345, 2010.

[106] Park, H.; Oh, S.; Lee, S., “Adaptive noise cancelling based on independent component analysis”, in *Electronics Letters*, Vol. 38, Issue 15, pp. 832–833, 2002.

[107] Zhang, Z.; Etoh, M., “ICA-based Noise Reduction for Mobile Phone Speech Communication”, in *Proceedings of 16th International Conference on Computer Communications and Networks*, 2007, pp. 470–473, 2007.

[108] Bharitkar, S.; Kyriakakis, C., “Selective signal cancellation for multiple-listener audio applications: an information theory approach”, in *IEEE International Conference on Multimedia and Expo, 2000, ICME 2000*, Vol.1, pp. 245–248, 2000.

[109] Wada, T.S.; Juang, B., “Acoustic echo cancellation based on independent component analysis and integrated residual echo enhancement”, in *2009 IEEE Workshop on Applications of Signal Processing to Audio and Acoustics*, pp. 205–208, New Paltz, NY, October 18–21, 2009.

[110] Liu, Y; Yang, T.T.; Mikhael, W.B., “Effect of signals' probabilistic distributions on performance of adaptive noise canceling algorithms”, in *IEEE 54th International Midwest Symposium on Circuits and Systems (MWSCAS), 2011*, pp.1–4, Aug. 7–10, 2011.

[111] Hyvarinen, A.; Karhunen, J., Oja, E, *Independent Component Analysis*, John Wiley & Sons, Inc. 2001.

[112] Hyvarinen, A., “Survey on Independent Component Analysis”, in *Neural Computing*, Vol.2, pp.94–128, 1999.

[113] Bell A.J.; Sejnowski, T.J., “An information-maximization approach to blind separation and blind deconvolution”, in *Neural Computation*, Vol. 7, pp. 1129–1159, 1995.

[114] Oja, E., “The nonlinear PCA learning rule in independent component analysis”, in *Neuro-computing*, Vol. 17, pp. 25–46, 1997.

[115] Anttila, L.; Valkama, M.; Renfors, M., “Frequency-Selective I/Q Mismatch Calibration of Wideband Direct-Conversion Transmitters”, in *IEEE Transactions on Circuits and Systems-II: Express Briefs*, Vol. 55, Issue 4, pp. 359–363, Apr. 2008.